A THESIS

entitled

KINETIC STUDIES BY STOPPED-FLOW PULSE FOURIER TRANSFORM NUCLEAR MAGNETIC RESONANCE SPECTROSCOPY

by

ALAN JOHNSON BROWN, B.Sc., M.Sc.

Submitted to the University of Warwick in fulfilment of the requirements for the award of the degree of Doctor of Philosophy

September, 1977.

INDEX

ACKNOWLEDGEMENTS

I wish to express my sincere thanks to Drs. O.W. Howarth and P. Moore of this department for their constant advice and encouragement throughout the course of this work.

I am also indebted to Mr. E. Burgess, of the School of Molecular Sciences Glassblowing Workshops, for his invaluable help in the design of the variable temperature stopped-flow NMR attachment.

Use of the Algol programs WLSAPROG and ACTPAR of Dr. P. Moore, the Fortran program LAME8 of Dr. W.J.E. Parr of this department, and the Bruker-Nicolet program DISKFT, written by Dr. D.A. Couch, also of this department, are gratefully acknowledged, as is the gift of the tricarbonyl(tropylium)tungsten(0) and molybdenum(0) fluoroborate complexes from Dr. P. Powell of the Department of Chemistry, Royal Holloway College, Egham, Surrey.

I wish to further acknowledge Dr. W.J.E. Parr of this department for his collaboration with the work described in Chapter 4, and Dr P. Powell who collaborated with the work described in Chapter 5.

The work described in this thesis was carried out in the School of Molecular Sciences between October, 1975 and September, 1977, the facilities of which and a Science Research Award are also gratefully acknowledged.

Parts of the work contained in this thesis have been published in the scientific literature, with the following references:-

A.J. Brown, D.A. Couch, O.W. Howarth, P. Moore, J. Magnet. Reson., 1976, 21, 503-505.

A.J. Brown, O.W. Howarth, P. Moore, W.J.E. Parr, J. Chem. Soc. Chem. Comm., 1977, 586-587.

A.J. Brown, O.W. Howarth, P. Moore, J. Amer. Chem. Soc., in press.

..... TO MY FATHER .....

'Spectator, this machine you see here is one of the most perfect constructed by the infernal gods for the mathematical destruction of the mortal !'

Jean Cocteau
The Infernal Machine

SUMMARY

A variable temperature stopped-flow NMR attachment has been developed for use with a commercial Fourier transform NMR spectrometer (a Bruker WH90). The attachment is capable of kinetic measurements over the temperature range 200 to 343 K within an accuracy of ±0.5 K and has been used to investigate three different types of chemical reaction in solution, these being:-

(i) electrophilic attack at co-ordinated ligands,

(ii) solvent exchange and ligand substitution reactions, and

(iii) nucleophilic attack at co-ordinated ligands.

In the case of (i), the reaction mechanism for the reaction between N-chlorosuccinimide and some tris-(pentane-2,4-dionato) metal complexes {$[M(acacH)_3]$ ($M = Co^{III}$, Rh^{III}, Ir^{III}, Ga^{III}, Al^{III})} was investigated, as was the solvent dependence of these reaction rates, and for some of the complexes the effect of subsitution by chloro- and nitro- groups at the C3-position of a non-reacting acetylacetone ring. A minor free-radical reaction was observed when the metal was Co(III) and the solvent was chloroform by the detection of transient CIDNP enhanced ^1H NMR resonances. However, the otherwise normal kinetics of these reactions indicate a simple electrophilic (S_E2) reaction mechanism in most cases.

In (ii) the solvent exchange rate and some ligand substitution reactions of the hexakis(dimethyl sulphoxide)aluminium(III) ion {$[Al^{III}(DMSO)_6]^{3+}$} with neutral ligands in deuterionitromethane solution were investigated. The ligands pyridine, 1,10-phenanthroline, 2,2'-bipyridine and 2,2':6'2''-terpyridine all showed an unusually high outer sphere formation constant (K_o) for the first stage of their reactions with the $[Al^{III}(DMSO)_6]^{3+}$ ion as did the aliphatic amine tert-butylamine. The nature of this effect was investigated for the aromatic ligands studied, and attributed to electrostatic dipole-dipole interactions between the incoming ligand and the polar solvent molecules of the inner-sphere, and direct ion-dipole interactions between the incoming ligand and the effective positive charge of the Al(III) ion. In the case of tert-butylamine, however, it may be that the unusually

high value of K_o observed is due to a strong hydrogen bonding interaction between the highly basic amine and the acidic protons of the co-ordinated DMSO molecule in the outer-sphere complex. During the reactions of the ligands 2, 2'-bipyridine and 2, 2':6'2''-terpyridine, direct evidence for a rate determining chelate-ring closure mechanism was observed, and the enthalpies and entropies of activation for each stage of these multistage reactions were measured.

In (iii) the nature of the transient intermediates involved in the reactions between tricarbonyl(tropylium)tungsten(0) and molybdenum(0) fluoroborates and the iodide ion was investigated. A previous UV-visible stopped-flow investigation of these reactions failed to yield any information as to the structure of these intermediates involved. In the SFPFTNMR study described in Chapter 5, however, the structures of the transient species was established. A mechanism is proposed in which initial nucleophilic attack of the iodide ion at the metal centre of the complex is followed by transfer of the nucleophile to the tropylium ring of the complex (forming exocyclic and endocyclic isomers of the second transient species), decomposition of which results in the transfer of the nucleophile back to the metal centre of the complex with the loss of a carbonyl group forming the final product of the reaction.

LIST OF ABBREVIATIONS

ARP	Adiabatic rapid passage.
CF	Continuous flow
CIDNP	Chemically induced dynamic nuclear polarization
CW	Continuous wave
^{o}C	Degrees Celsius
ESR	Electron spin resonance
FID	Free induction decay
K	Degrees Kelvin
NMR	Nuclear magnetic resonance
ORD	Optical rotatory dispersion
RF	Radio frequency
SF	Stopped-flow
SFPFTNMR	Stopped-flow pulse Fourier transform nuclear magnetic resonance
S/N	Signal to noise ratio
T_1	Longitudinal spin lattice relaxation time (s)
T_2	Transverse spin lattice relaxation time (s)
TMS	Tetramethylsilane
UV	Ultra violet
VT	Variable temperature
$\Delta H^{\ddagger}$	Enthalpy of activation (kJ mol^{-1})
$\Delta S^{\ddagger}$	Entropy of activation (J K^{-1} mol^{-1})
acacH	2, 4-pentanedione
acacBr	3-bromo-2, 4-pentanedione
acacCl	3-chloro-2, 4-pentanedione
acacD	3-deuterio-2, 4-pentanedione
acacMe	3-methyl-2, 4-pentanedione
acacMe.Cl	3-methyl-3-chloro-2, 4-pentanedione
acacNO_2	3-nitro-2, 4-pentanedione

bipy	2, 2'-bipyridine
en	1, 2-diaminoethane
phen	1, 10-phenanthroline
terpy	2, 2':6'2''-terpyridine
$[Al^{III}(DMSO)_6](ClO_4)_3$	Hexakis(dimethyl sulphoxide)aluminium(III) perchlorate
$[Cr^{III}(DMSO)_6](ClO_4)_3$	Hexakis(dimethyl sulphoxide)chromium(III) perchlorate
$[(C_7H_7)Mo(CO)_3](BF_4)$	Tricarbonyl(tropylium)molybdenum(0) fluoroborate
$[(C_7H_7)W(CO)_3](BF_4)$	Tricarbonyl(tropylium)tungsten(0) fluoroborate
$(^nBu)_3P$	Tri-^{n}butylphosphine
RNCl	B-chlorosuccinimide
RNBr	N-bromosuccinimide
RNH	Succinimide
$(C_7H_7)^+$	Tropylium cation

All other abbreviations are consistent with the IUPAC system of nomenclature.

LIST OF FIGURES

following page

LIST OF PLATES

LIST OF TABLES

CHAPTER 1

INTRODUCTION.

1.1 Introduction

During the past decade, the use of rapid reaction techniques for studying reaction mechanisms in solution has become commonplace. A broad range of techniques is now available to the mechanistic chemist which can be grouped into four sections: rapid-mixing, relaxation, irradiation and magnetic resonance methods. The relevant time scales for some of these techniques are shown in Figure 1.1.

Nuclear magnetic resonance (NMR) spectroscopy is a very diagnostic technique, and line-broadening studies by NMR are commonly used to investigate reactions in solution. However, studies of this type can only be used to investigate systems at equilibrium, and very slow chemical reactions. Therefore a new technique has been developed to investigate chemical reactions on a moderately fast time scale by NMR (see Figure 1.1). This stopped-flow pulse Fourier transform NMR (SFPFTNMR) method utilizes a rapid mixing technique, and can be applied to a variety of types of chemical reactions, some of which can not be investigated by any other means.

The following sections of this chapter discuss the continuous-flow and stopped-flow methods of measuring rapid reaction rates in solution, their development, and the development of the SFPFTNMR technique. Because of the large differences in the types of reaction which have been studied by the SFPFTNMR method, the chemistry of each system will be discussed at the beginnings of the relevant chapters.

1.2 The continuous-flow and stopped-flow techniques and their development

Until 1923 there existed no direct, generally applicable method for measuring the rates of chemical reactions in solution with half-lives of less than about 10 s. In that year Hartridge and Roughton extended the observable time range by a factor of 10^4, by the development of the continuous-flow (CF) method of monitoring rapid reactions on the millisecond timescale.[1] The principle of their CF technique was that the two solutions which were to react were placed in separate containers (usually

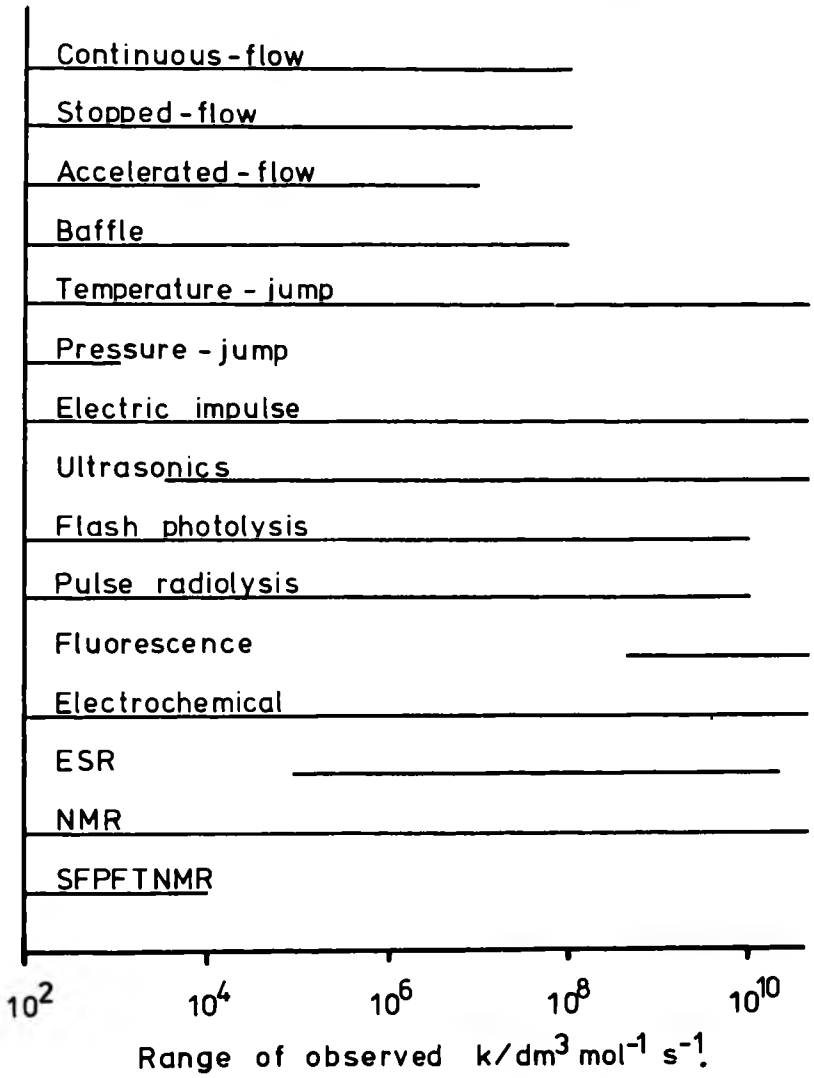

Figure 1.1

Characteristics of some rapid reaction methods.

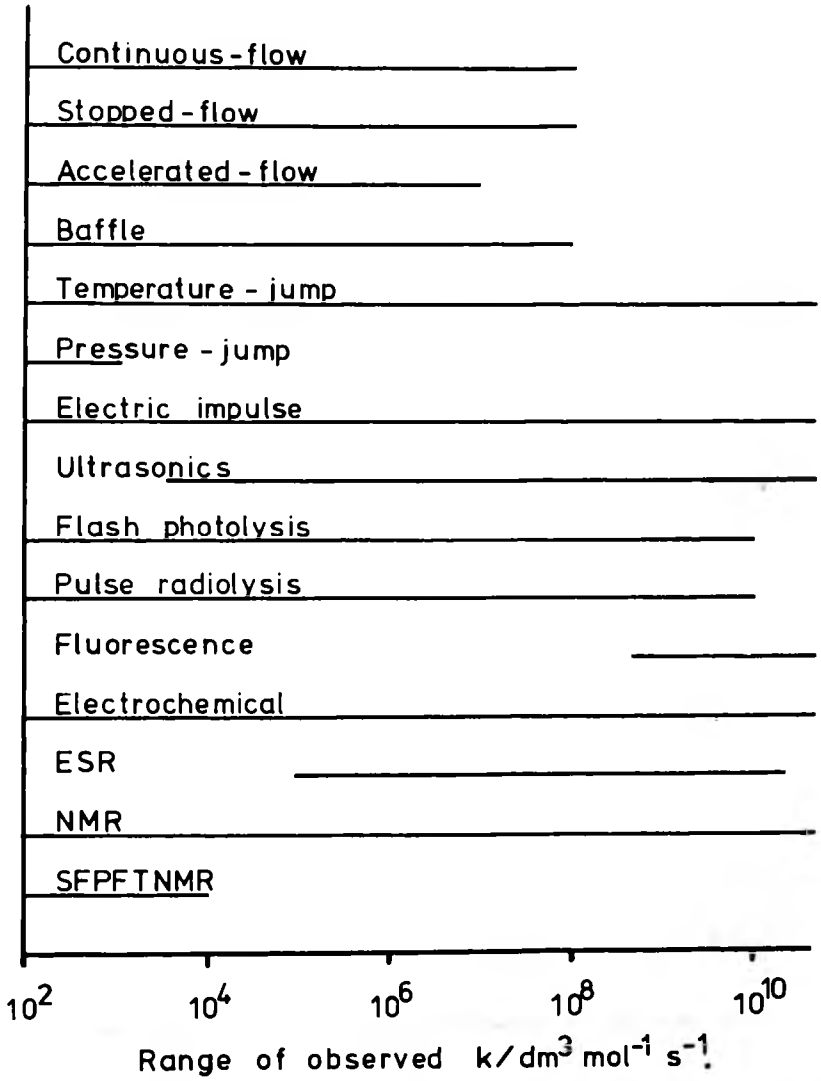

Figure 1.1

Characteristics of some rapid reaction methods.

syringes) and driven together through a special mixing chamber, which allowed rapid and efficient mixing in approximately 10^{-3} s. The emerging mixed fluid passed down an observation tube, and at various cross sections down the tube the composition of the flowing liquid was determined by a physical technique (usually UV-visible spectrophotometry). If d is the distance in centimetres between the mixing chamber and the cross section under investigation, and $\bar{u}$ the average linear velocity in cms^{-1} of the flowing liquid, then $d/\bar{u}$ gives the extent of reaction in seconds at the observation point. From observation at five or more cross sections, a typical concentration vs time curve can be plotted and the rate of reaction determined.

The CF technique has one major drawback in that it requires large volumes of each reactant solution to determine a number of points on a concentration versus time graph. These volumes can be reduced by continuously accelerating the flow through the observation tube as described by Chance,[2] or by stopping the flow in the observation tube and following the course of the reaction by an optical or other suitable technique. The latter of these two methods, the stopped-flow (SF) method, was originally described by Chance in 1940[2] and later improved by Gibson.[3,7]

With the development of rapid response electronic detectors, the SF method has become one of the most widely used techniques for the investigation of rates and mechanisms of rapid reactions taking place in solution.[4-6] It has some intrinsic advantages over the CF method,[7] these being:-

(i) It is independent of the rate and character of flow down the observation tube.

(ii) A permanent record can be obtained of the progress of the reaction over a period starting at a few milliseconds after mixing and extending as long as desired.

(iii) The volume of reagents required is minimal.

Most CF and SF apparatuses utilize UV-visible spectrophotometry as a detection technique[4, 5, 8-10] but despite the sensitivity of UV-visible spectroscopy, it suffers from the severe disadvantage of being very nondiagnostic. As a result of this, many workers have attempted to couple less sensitive, but more diagnostic detection techniques to the basic CF or SF experiment, in order to gain more detailed information about the rates and mechanisms of rapid reactions taking place in solution.

Meier et al.[11] in 1957 developed a CF apparatus which permitted glass electrode pH measurements to be taken 10^{-2} s after mixing of the two reactant solutions. This flow-pH technique was used to determine the acidity constant of carbonic acid (H_2CO_3) by mixing potassium bicarbonate in one solution with hydrochloric acid in the other reactant solution. The rate of dehydration of carbonic acid was obtained from these experiments. More recently, a CF system has been developed which utilizes liquid membrane ion-selective electrodes as sensors.[12] This system is also capable of measuring reactions on the 10 ms time scale, and has been used to determine the rates of complex formation of Ca^{2+}, Mg^{2+} and Be^{2+} metal ions to biologically important ligands.

Prince, in 1958, published a method of studying rapid reactions by conductivity.[13] This apparatus could be used in either a CF or SF mode. By means of his flow-conductivity technique, Prince was able to measure the rate of hydrolysis of triphenylchlorosilane in aqueous acetone mixtures, reactions which do not give rise to a measurable UV-visible spectral change.[13]

Fluorimetry has been successfully combined with the SF technique.[7, 14] This has proved to be a very useful combination for following biochemical reactions, such as the glutamate dehydrogenase catalysed reduction of α-ketoglutarate in the presence of NADH and ammonium chloride.[14] The reaction is followed by the rate of disappearance of NADH fluorescence.

With the development of electron spin resonance spectroscopy (ESR) came the construction of a CF ESR apparatus for the investigation of free radicals produced during rapid reactions.[15] Bielski and Saito were

the first workers to publish the CF ESR technique;[16, 17] they investigated the mechanism of oxidation of hydrogen peroxide with cerium(IV) sulphate by the detection of $HO_2^{\cdot}$ radicals produced as a transient species during the oxidation. The basic CF ESR experiment has been further developed to allow double mixing experiments,[18] which have been used to study the formation and exchange reactions of peroxy complexes of different cations,[19] as well as reactions between alcohols and alcoholic radicals.[20]

SF-calorimetry has been developed[21] along with thermocouples which have response times in the submillisecond range.[22] This adaptation of the SF method was constructed specifically for the investigation of thermal changes produced as a consequence of rapid biological reactions such as the heats associated with haemolysis of red blood cells.[21]

Anson and Bayley have recently reported a SF-circular dichroism system,[23] which was also developed to investigate kinetic processes in biological macromolecules. Both the interaction between the symmetrical triphenylmethane dye crystal violet and highly polymerised calf-thymus DNA, and the binding of dicarboxylate substrate analogues to aspartate aminotransferase have been successfully followed on the millisecond timescale by this method.[24]

SF-polarimetric studies have been described by Goodall and Cross,[25] which allow optical rotatory dispersion (ORD) changes in reacting systems to be measured on the millisecond timescale. This apparatus is capable of detecting millidegree changes in optical rotation and absorbance changes at wavelengths between 230 and 800 nm, and can be used to study the dynamics of conformational changes in macromolecules as well as interactions between proteins and coenzymes.

The infra-red absorptions of a compound can be readily assigned to particular functional groups within the compound, and the frequency (in wave numbers) of these absorptions can give detailed information as regards molecular structure. Rudolph et al.[26] and Brady et al.[27] have

both described SF infra-red sensitive apparatus which is capable of monitoring reactions on the millisecond timescale. Brady et al. found it necessary to use rapid response photoconductive infra-red (IR) detectors and high speed radiation choppers to be able to monitor reactions with half-lives of ca. 10 ms; by means of several single wavenumber kinetic determinations followed by subtracting the IR transmissions due to the product, he was able to construct infra-red spectra of transient complexes which can not be detected by any other technique.[27]

Many attempts have been made to improve on the basic CF and SF experiments to allow faster reactions to be observed, such as the development of highly efficient multijet mixers,[28] diaphragm syringes[27] and the use of high drive pressures.[28] Anaerobic SF equipment has been developed to study reactions of air-sensitive compounds on the millisecond timescale[10] and various low temperature UV-visible SF equipment has been described which can operate between +55 to -120° C.[4,8] SF has even been combined with the temperature-jump technique to facilitate the measurement of reaction rates on the submillisecond timescale.[29]

The one limitation of all CF and SF techniques that utilize single wavelength spectroscopic detectors is the lack of information that can be gained per flow experiment.[27] However, with the development of rapid scanning UV-visible spectrometers, it is now possible to obtain complete UV-visible spectra, during a SF experiment, every few milliseconds.[30] The introduction of pulse Fourier transform (FT) infra-red spectrometers has permitted the development of SF pulse FT infra-red experiments, where complete IR spectra (3600 to 600 cm^{-1}) can be collected and stored on a magnetic disk during the course of a chemical reaction.[31] However, due to the long scan and repetition times associated with this technique (1 s and 3.5 s respectively), only reactions with a half-life of greater than 10 s can be measured.

1.3 Continuous-flow and stopped-flow continuous wave NMR and the application of pulse Fourier transform NMR techniques to flow methods

High resolution nuclear magnetic resonance (NMR) spectroscopy, although a relatively insensitive technique, is very diagnostic for systems at equilibrium and is probably the most widely used technique for the characterization of unknown organic, inorganic and organometallic compounds;[32] NMR is also widely used to study exchange reactions in chemical and biochemical systems at equilibrium.[33]

The development of continuous wave (CW) NMR spectrometers brought about the first flow-NMR kinetic measurements.[34-36] By tuning to the frequency of a resonance of interest and activating the drive syringes of a SF attachment, an NMR transient signal can be recorded (similar to those obtained from conventional SF/UV-visible spectrophotometry). This transient signal represents the rate of decay (or growth) of the resonance under investigation with time. With this SFCWNMR technique, Grimaldi and Sykes[36] have successfully investigated the conformational changes induced in concanavalin A by the binding of Mn^{2+}, Ca^{2+} and α-methyl-D-mannoside at pH 5.28. Although SF CWNMR allows reactions to be followed on the millisecond timescale, it does have some basic drawbacks which may lead to errors. For example:-

(i) Any magnet or electronic fluctuations will cause unreliable transients to be recorded.

(ii) The resonance being monitored will be broad as the sample can not be spun to average out magnetic field inhomogenieties.

(iii) Spin-saturation may occur during the reaction which will also lead to false transients being recorded.

(iv) No information can be gained about other resonances in the NMR spectrum.

The first limitation was largely removed by the development of magnet lock channels[36] which prevent field drift during data acquisitions.

Richards and Evans developed a CF electrolysis cell used in conjunction with a CW ^{1}H NMR spectrometer.[37] This apparatus employed a spinning 5 mm NMR tube so helping to improve the spectral resolution, and the whole ^{1}H NMR spectrum was scanned under CF conditions, hence gaining maximum information about the system under investigation. But, by virtue of using a CF technique, theysuffered loss of signal to noise ratio (S/N) and resolution due to the nuclei not becoming fully magnetically equilibrated.

The problem of spin-saturation can be removed by the addition of an inert paramagnetic relaxing agent (e.g. [Cr(acacH)$_3$] to one or both of the solutions being mixed;[38] this also helps the problem of pre-magnetic equilibration as the longitudinal spin-lattice relaxation times (T_1's) of the nuclei are greatly reduced. Hence the time required to reach magnetic equilibration (ca. 5 T_1) is also greatly reduced, although the addition of a relaxing agent does lead to paramagnetic line broadening and some loss of resolution.

Full NMR spectra can be collected during a flow-NMR experiment by one of two means:-

(1) During a CF experiment the whole ^{1}H NMR spectrum can be scanned. This technique, however, requires large volumes of each reactant solution, and many repeat runs to build up a concentration/time profile for the reaction under investigation.

(2) Pulse Fourier transform techniques can be employed in conjunction with a SF experiment. Here full NMR spectra can be collected in the form of free induction decays (FID's) during the course of the reaction, and stored on a magnetic disk. Very little of each reactant solution is required and in the case of ^{1}H NMR measurements, deuterated solvents can be used to remove unwanted solvent resonances from the ^{1}H NMR spectrum, and to avoid saturation of the receiver amplifier.

1.3.1 The CF ^{1}H NMR technique

The method of CF NMR for the detection of transient species produced during rapid reactions has been developed by Fyfe *et al.*[39] His apparatus uses a modified Varian V 4331 ^{1}H NMR probe with a 15 inch Varian magnet.

By taking advantage of the fact that the magnetic field does not drop off rapidly from the centre of the pole faces of his magnet, and winding coils of polythene tubing leading from the drive syringes to the mixer inside the probe head, he achieves pre-magnetic equilibration of both reactant solutions. Rapid and efficient mixing is produced by a 4 jet Teflon mixing chamber situated at the top of the probe in place of the spinner block. The mixed solution then passes down through a static 5 mm NMR tube past the detection coils in the probe, and out at the bottom of the probe to a collection vessel. The reactant solutions are held in two 100 cm^3 syringes which are driven in unison by an electric motor. The minimum 'dead-time' between mixing and observation with this technique is ca. 100 ms; no problems of magnetic equilibration and spin-saturation occur and complete ^1H NMR spectra can be obtained at any time after the 'dead-time' by simply varying the flow rate and scanning the flowing liquid. By means of a special capillary delivery tube from the mixer block to the detector coils of the spectrometer, Fyfe et al. have recently been able to reduce the 'dead-time' of their technique to 40 ms.[40]

The CF NMR technique, however, does have some disadvantages. Firstly, line broadening does occur due to the use of a static tube (line-widths are typically 2 Hz), and secondly, because of the large volume of solutions required, deuterated solvents can not be used. Instead, Fyfe has developed an adiabatic rapid passage (ARP) spin-saturation technique[41] to specifically invert the solvent ^1H NMR resonance in one of the reactant solutions prior to mixing and observation. This has the effect of nulling the solvent resonance from the observed ^1H NMR spectrum, but can only be used during the detection of relatively fast reactions as the spin-polarization induced by ARP techniques decays over a period of 3 T_1's.

Despite its limitations, much useful mechanistic information has been gained by this technique, including the detection of tetrahedral intermediates in the addition reactions of hydroxylamine,[42-45] the study of transient and stable species formed by the attack of alkoxide ions on substituted benzenes,[46-48] and the investigation of intermediates formed during the bromination of phenols.[40]

1.3.2 The stopped-flow pulse Fourier transform ^{1}H NMR technique

Three different types of SF pulse FT ^{1}H NMR kinetics equipment have been reported.[49-51] These will be described individually and their failings discussed.

(i) Robinson and Rosenfeld reported a stopped-flow pulse Fourier transform NMR (SFPFTNMR) system[49] in which they used an unmodified Bruker WH 90 10 mm probe head. By using a wide bore probe head; they are able to operate their spectrometer in a locked mode during kinetic runs, the mixed reactants are directed into a 5 mm NMR tube concentrically positioned inside a 10 mm tube with deuteriochloroform ($CDCl_3$) as an eternal lock sample in the annular gap. They are able to spin the sample tube to gain maximum spectral resolution, and collect full 10 ppm 4K FID's every 2 s. The FID's are stored individually as a magnetic disk for processing later. The reactant solutions are stored in two manually driven syringes which are as close as possible to the highfield of the Bruker WH90 spectrometer, and mixed in a simple T-mixer. The 'dead-time' of this technique is approximately 4 s and is governed by the low efficiency mixer, the lack of full pre-magnetic equilibration, and the considerable distance between mixing and observation.

Due to the large 'dead-time' of this method and the loss of signal to noise ratio (S/N) inherent in using a 10 mm probe, only moderately fast reactions can be studied (half-lives in the order of 20 to 30 s). A further disadvantage is that the T-mixer requires cleaning after each run.

(ii) Grimaldi and Sykes[50] in their SFPFTNMR apparatus employ a more conventional SF system with drive and stopping syringes. They use a modified Varian V-4331 probe, fitted with a rapid mixing cell and stopping syringe block. The drive syringes are activated by means of a pneumatic piston and the stopping syringe triggers the start of the NOVA 1220 12K computer controlled data acquisition cycle. By using high drive pressures, a 'dead'time' of 1 ms can readily be obtained. However, due to the problems associated with spin-saturation, and loss of S/N ratio as a result of having a static sample tube, the repetition time for data

1.3.2 The stopped-flow pulse Fourier transform ^{1}H NMR technique

Three different types of SF pulse FT ^{1}H NMR kinetics equipment have been reported.[49-51] These will be described individually and their failings discussed.

(i) Robinson and Rosenfeld reported a stopped-flow pulse Fourier transform NMR (SFPFTNMR) system[49] in which they used an unmodified Bruker WH 90 10 mm probe head. By using a wide bore probe head; they are able to operate their spectrometer in a locked mode during kinetic runs, the mixed reactants are directed into a 5 mm NMR tube concentrically positioned inside a 10 mm tube with deuteriochloroform ($CDCl_3$) as an eternal lock sample in the annular gap. They are able to spin the sample tube to gain maximum spectral resolution, and collect full 10 ppm 4K FID's every 2 s. The FID's are stored individually as a magnetic disk for processing later. The reactant solutions are stored in two manually driven syringes which are as close as possible to the highfield of the Bruker WH90 spectrometer, and mixed in a simple T-mixer. The 'dead-time' of this technique is approximately 4 s and is governed by the low efficiency mixer, the lack of full pre-magnetic equilibration, and the considerable distance between mixing and observation.

Due to the large 'dead-time' of this method and the loss of signal to noise ratio (S/N) inherent in using a 10 mm probe, only moderately fast reactions can be studied (half-lives in the order of 20 to 30 s). A further disadvantage is that the T-mixer requires cleaning after each run.

(ii) Grimaldi and Sykes[50] in their SFPFTNMR apparatus employ a more conventional SF system with drive and stopping syringes. They use a modified Varian V-4331 probe, fitted with a rapid mixing cell and stopping syringe block. The drive syringes are activated by means of a pneumatic piston and the stopping syringe triggers the start of the NOVA 1220 12K computer controlled data acquisition cycle. By using high drive pressures, a 'dead'time' of 1 ms can readily be obtained. However, due to the problems associated with spin-saturation, and loss of S/N ratio as a result of having a static sample tube, the repetition time for data

accumulation can be as high as 4 s. This technique does give very reproducible spectra and the problem of lack of S/N ratio can be eased by digitally adding FID's from different kinetic runs, which improves the repetition time sufficiently to allow reactions with half-lives of the order of 0.1 to 0.2 s to be measured. However, this type of rapid pulsing and multiple kinetic-run data accumulation, coupled with field drift problems,(the spectrometer is unlocked), can cause the spectral resolution to be as poor as 10 Hz.

As with the method of Robinson and Rosenfeld,[49] FID's are computer stored during each kinetic run and are processed at the end of the data accumulation.

(iii) Couch et al.[51] have described an attachment for a commercially available Bruker WH90 pulse FTNMR spectrometer. This technique employs a spinning 5 mm sample tube for maximum spectral resolution and a capillary mixing system fed from two drive syringes positioned as near the pole faces of the magnet as possible. The relatively short 'dead-time' of 0.3 s together with rapid and efficient mixing (less than 30 ms) and a repetition rate of ca. 0.6 s allows reactions with half-lives of 0.5 s or greater to be measured. Because of the small volume of solutions required, deuterated solvents are used, which permit locking of the spectrometer in slower kinetic runs. Single or multipulse FID's are collected, using 1 k or up to 8 k data points depending on the reaction rate, and are stored by a Bruker-Nicolet BNC-12 computer on a standard magnetic disk and processed at the end of each kinetic run.

The SFPFTNMR method of Couch et al.[51] which enables high resolution (linewidths less than 1 Hz) ^{1}H NMR spectra to be collected on a moderately fast time scale was used in the following work, and a new variable temperature version has been developed (see chapter 2) to enable reactions which are too rapid to measure at room temperature to be investigated at low temperatures. Activation parameters of the reactions under investigation can also be obtained from studies over a wide temperature range.

1.4 The scope of the stopped-flow pulse Fourier transform NMR method of measuring reaction rates

Many different types of chemical reactions can be studied by the SFPFTNMR method, some of which can not be investigated by any other technique. For example, it is possible to work in solvents that absorb strongly in the UV[38] (e.g. nitromethane) solvents which make UV stopped-flow experiments impossible. It is also possible to study hydrogen-deuterium exchange reactions by this method[51] as well as metal ion solvent exchange reactions.[38] (These types of reaction do not give rise to changes in the UV or visible spectral regions). The technique has also proved to be very useful in detecting transient intermediates formed in rapid reactions.[49,52]

Some classes of reactions which have been investigated by the SFPFTNMR method are listed below:-

(i) The hydrolysis reactions of enzymes.[50]

(ii) Hydrogen-deuterium exchange reactions.[51]

(iii) Solvent exchange reactions of labile metal ions[38] (see chapter 4).

(iv) Ligand substitution reactions (see chapter 4).

(v) Electrophilic attack at co-ordinated ligands[52] (see chapter 3), and

(vi) Nucleophilic attack at co-ordinated ligands (see chapter 5).

It can be seen therefore that this method of studying moderately rapid reactions overlaps with flow techniques already available, and in many instances can yield information about the rates and mechanisms of reactions occurring in solution that can be gained by no other means.

1.4 The scope of the stopped-flow pulse Fourier transform NMR method of measuring reaction rates

Many different types of chemical reactions can be studied by the SFPFTNMR method, some of which can not be investigated by any other technique. For example, it is possible to work in solvents that absorb strongly in the UV[38] (e.g. nitromethane) solvents which make UV stopped-flow experiments impossible. It is also possible to study hydrogen-deuterium exchange reactions by this method[51] as well as metal ion solvent exchange reactions.[38] (These types of reaction do not give rise to changes in the UV or visible spectral regions). The technique has also proved to be very useful in detecting transient intermediates formed in rapid reactions.[49, 52]

Some classes of reactions which have been investigated by the SFPFTNMR method are listed below:-

(i) The hydrolysis reactions of enzymes.[50]

(ii) Hydrogen-deuterium exchange reactions.[51]

(iii) Solvent exchange reactions of labile metal ions[38] (see chapter 4).

(iv) Ligand substitution reactions (see chapter 4).

(v) Electrophilic attack at co-ordinated ligands[52] (see chapter 3), and

(vi) Nucleophilic attack at co-ordinated ligands (see chapter 5).

It can be seen therefore that this method of studying moderately rapid reactions overlaps with flow techniques already available, and in many instances can yield information about the rates and mechanisms of reactions occurring in solution that can be gained by no other means.

CHAPTER 2

INSTRUMENTATION

2.1 The Prototype Stopped-Flow N M R Attachment

A prototype SF attachment for use with a standard Bruker WH 90 pulse Fourier transform NMR spectrometer was developed by Couch et al.[51] To avoid distortion of the magnetic field of the spectrometer the attachment (see Figure 2.1) was built entirely of non-magnetic materials (brass, aluminium alloy, stainless steel, glass and plastics). The two reactant solutions are introduced into the two horizontally mounted 2 cm^3 all-glass drive syringes, A, which are rigidly held to the aluminium platform, B, by means of the fixing clamps, C. The syringes are filled prior to bolting the stopped-flow attachment to the probe arm, D, of the Bruker WH 90 spectrometer, using the fixing bolts, E. Care is taken during the filling procedure to eliminate bubbles in each flow line and to ensure that premixing of the reactant solutions does not occur. Once filled, the glass pistons of the drive syringes are held by a slotted plate, F, which prevents creeping of the pistons and also connects the glass plungers to the pneumatic drive piston, G. The solutions are driven from the syringes using drive pressures of 1.0 to 1.5 atmospheres. The solutions pass from each syringe through 2 mm bore glass capillary tubes. The capillary tubes bend down towards the probe head and have a further bend near the spinner block. The tubes at this point are fused together before being drawn out into the two thin-walled capillary tubes (0.5 mm bore), H, which are bent down at right angles and fit inside the shortened spinning 5 mm outside diameter ^1H NMR tube, J, without touching the sides. Reservoir bulbs, K, are blown into each of the glass capillary tubes prior to the forming of the thin walled capillaries, H. These serve as pre-magnetic equilibration bulbs (see section 3 of this chapter) as they hold ca. 0.2 cm^3 of solution (ca. 0.15 cm^3 is injected for each kinetic run) and are situated well inside the edge of the magnet pole faces, R. Fixed equal volumes of each solution (ca. 0.15 cm^3) are injected from the glass capillary tubes, H,

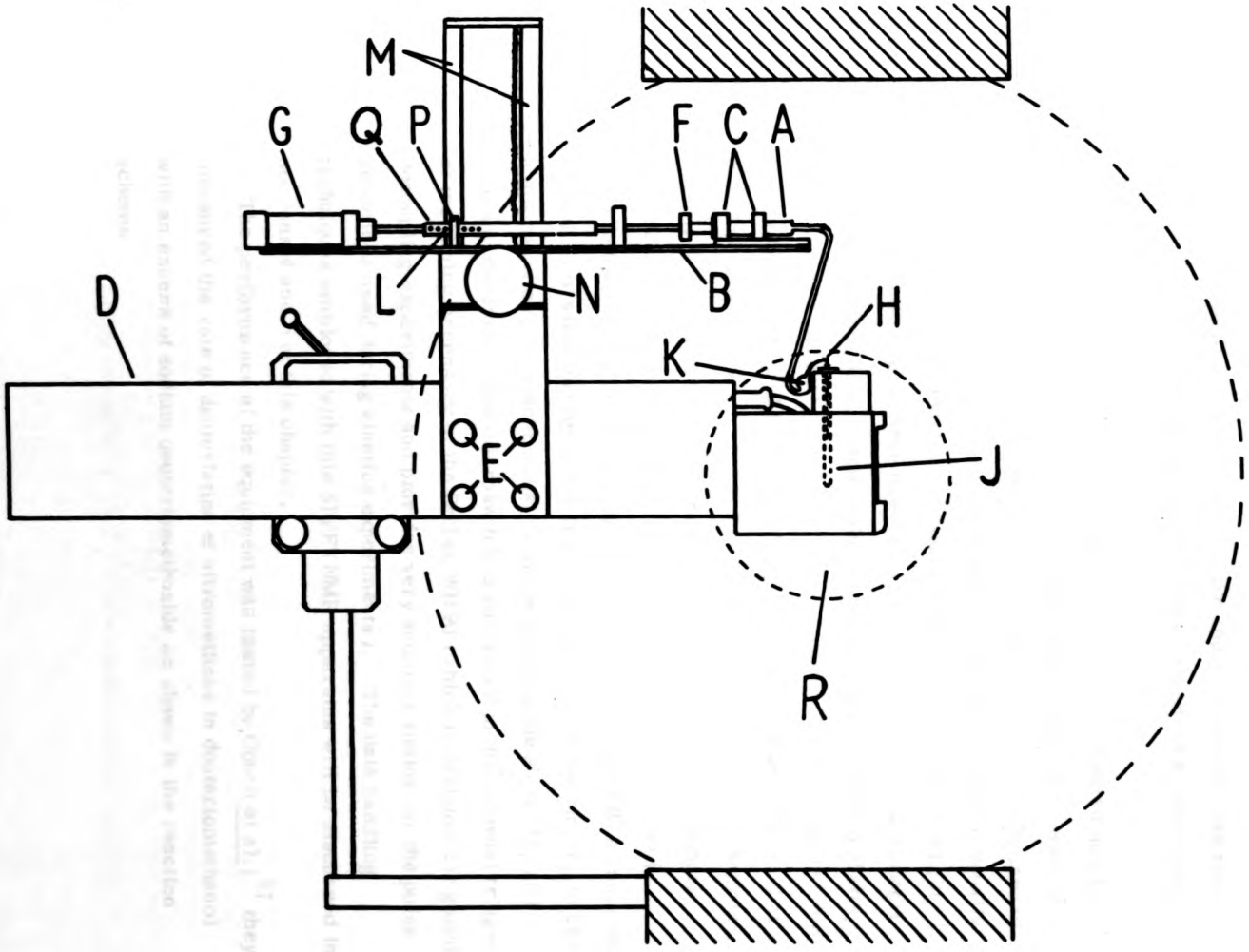

Figure 2.1

Schematic diagram of the prototype SFNMR attachment.

into the empty spinning NMR tube where mixing occurs. The ends of the glass capillaries are positioned ca. 30 mm above the bottom of the NMR tube. The mixing arrangement is similar in principle to that described by Thompson and Gordon[53] for mixing two solutions inside a 1 cm pathlength cuvette of a UV-visible spectrometer in less than 30 ms. The efficiency of mixing and measurement of a 'dead-time' is discussed in section 3 of this chapter.

To stop the flow and limit the volume of solution injected into the NMR tube to ca. 0.3 cm^3 total volume per kinetic run, the piston of the pneumatic ram, G, is connected to the syringe yoke, F, by means of a hollow section, Q, through both sides of which a series of equally spaced holes (3 mm apart) have been drilled. A stainless steel pin, L, is inserted into one of these holes so as to permit 3 mm of horizontal travel before the pin (L) strikes the nearer of the two vertical shafts, M, which also support a rack and pinion. The rack and pinion is used to vertically raise and lower the plate, B, using the wheel, N, so that the NMR tube can be emptied and cleaned between injections. Approximately 6-8 runs are possible from one filling of the drive syringes. The procedure for setting up the spectrometer for a kinetic run is described in section 4 of this chapter. Recording of the FID's commences immediately after mixing and is triggered by allowing the pin, L, to close a microswitch, P, synchronously with its striking the shaft, M, and stopping the flow. The microswitch is connected to the external trigger of the timing accessory of the Bruker WH90 (which is designed for gated decoupling experiments and provides very accurate timing for the pulse sequences used during kinetics experiments). The data handling techniques employed with this SFPFTNMR apparatus will be discussed in sections 4 and 5 of this chapter.

The performance of the equipment was tested by Couch et al.;[51] they measured the rate of deuteriation of nitromethane in deuteriomethanol with an excess of sodium deuteriomethoxide as shown in the reaction scheme

$$CH_3NO_2 + [OCD_3]^- \xrightarrow{k_1} [CH_2NO_2]^- + CD_3OH \qquad (2.1)$$

$$[CH_2NO_2]^- + 2CD_3OD \xrightarrow{k_2} [CD_2NO_2]^- + 2CD_3OH \qquad (2.2)$$

With an excess of sodium deuteriomethoxide ($Na^+[OCD_3]^-$) reaction (2.1) is too fast to measure by the SFPFTNMR method, but can be measured by stopped-flow UV-spectrophotometry.[54] The subsequent deuteriation reaction (2.2) can be readily monitored by the SFPFTNMR method and Couch et al. measured a pseudo-first-order rate constant for this reaction of 0.18 s^{-1} at 297 K,[51] ($[CD_3O^-]$ = 0.055 mol dm^{-3}), which is in good agreement with the second-order rate constant obtained by Caldin and Gold[55] ($k/dm^3\ mol^{-1}\ s^{-1}$ = 2.8).

The prototype stopped-flow attachment did however have some limitations. Firstly, the drive syringes could not be filled with the attachment bolted in place on the probe arm of the spectrometer, and secondly, no means of temperature control was possible. This meant that all kinetic runs had to be carried out at the ambient temperature of the magnet cavity (297 ± 1 K). However, it was found that the technique gave very reproducible results from day to day since the instrument is situated in a temperature controlled room. This stopped-flow attachment was used for the majority of the work described in chapter 3, and led to the development of a variable-temperature stopped-flow NMR attachment also for use with a Bruker WH 90 Fourier transform NMR spectrometer.

2.2 The variable temperature (VT) stopped-flow FTNMR attachment

This attachment was designed specifically for the measurement of rate constants at reduced and elevated temperatures. The basic attachment is shown in Figure 2.2 and is similar to that of the prototype. The pneumatic ram, A, and syringe piston retaining block, Y, is mounted at the front of a box section beam, B. A pivot, C, allows the beam to be tilted backwards to facilitate filling of the all-glass 2 cm^3 drive syringes, D, while the attachment is bolted on the probe arm of the spectrometer, E; a brass counterweight, F, and locking clip, G, have also been added to ease the filling procedure. A 1 mm pitch tapped brass stopping

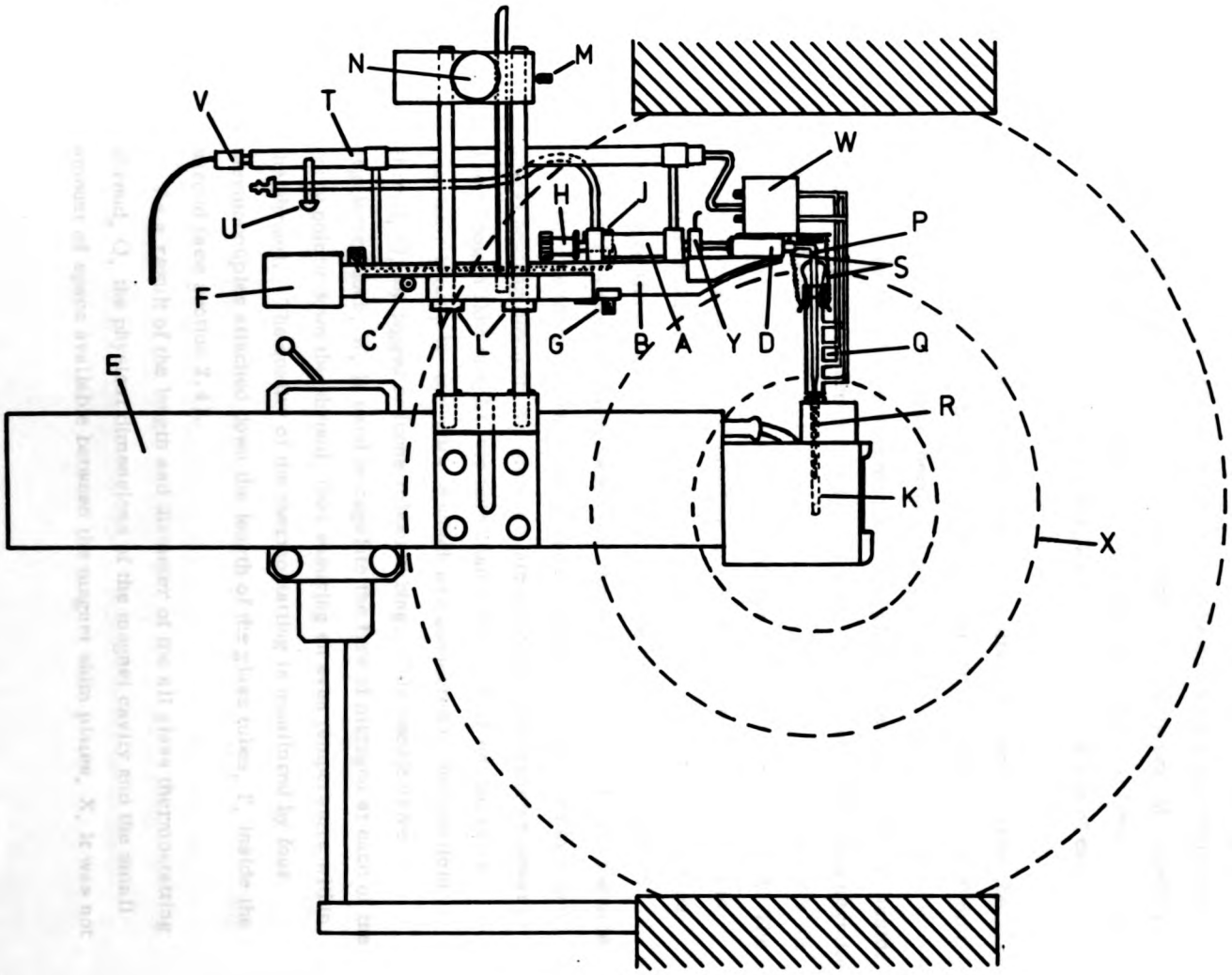

Figure 2.2

Schematic diagram of the variable temperature SFNMR attachment.

collar, H, screwed on to the rear of the pneumatic ram, is used to stop the flow and trigger the microswitch, J, which commences recording of the FID's during the kinetic run. The collar is turned back three times to allow a 3 mm travel of the pneumatic piston, delivering as before ca. 0.15 cm^3 of each solution into the spinning 5 mm NMR tube, K. Locking collars, L, and a spring loaded retaining pin, M, together with the rack and pinion assembly, N, allow the horizontal beam, B, to be raised and lowered to empty the NMR tube, K, at the end of each experiment.

The flow line of the 1.0 mm bore glass tubes, P, leading from the drive syringes, D, has been simplified to permit the addition of a 20 mm outside diameter all-glass thermostatting shroud, Q, for variable temperature kinetic measurements. The glass reservoir tubes, P, inside the shroud (3.0 mm bore) holed ca. 0.4 cm^3 of each solution; this permits efficient thermostatting prior to injection of the reactant solutions into the empty spinning NMR tube, K, via the drawn out glass capillaries, R. The efficiency of mixing and 'dead-time' for this apparatus is described in section 3 of this chapter. The glass shroud, Q, is detachable to ease cleaning of the glassware and is held in place by two spring clips, S. Dry, cold, gaseous nitrogen is fed into the transfer dewar, T, via the side arm, U; the temperature of the gaseous nitrogen is regulated by a long spiral heating element, V, inserted into the end of the transfer dewar. The nitrogen flow is split into four channels by a four needle valve regulator block, W, the exits of which are connected to the manifold shroud, Q, by lagged silicone rubber tubing. This needle valve regulator block, W, is used to regulate the flow of nitrogen at each of the entry points down the shroud, thus ensuring an even temperature within the shroud. The quality of the thermostatting is monitored by four thermocouples attached down the length of the glass tubes, P, inside the shroud (see section 2.4).

As a result of the length and diameter of the all glass thermostatting shroud, Q, the physical dimensions of the magnet cavity and the small amount of space available between the magnet shim plates, X, it was not

possible to include magnetic equilibration bulbs in the design. The effect of this on the 'dead-time' of this attachment is discussed in section 3 of this chapter.

The accuracy of variable temperature measurements obtained by this technique was checked by measuring the activation parameters of the dimethylsulphoxide(DMSO) solvent exchange rate of hexakis(dimethylsulphoxide)aluminium(III) perchlorate $[Al^{III}[DMSO]_6](ClO_4)_3$ in deuterionitromethane. Thomas and Reynolds, by means of ^1H NMR line broadening studies, previously measured the enthalpy ($\Delta H^{\ddagger}$) and entropy ($\Delta S^{\ddagger}$) of activation for this process over the temperature range 40 to 65 C;[56] they obtained values of 84.10 ± 3.34 kJ mol^{-1} and 13.31 ± 10.25 JK^{-1} mol^{-1} respectively for $\Delta H^{\ddagger}$ and $\Delta S^{\ddagger}$. Variable temperature measurements by the SFPFTNMR method over the temperature range -11 to +24°C (see chapter 4) gave values of 79.15 ± 6.40 kJ mol^{-1} and -5.47 ± 22.77 JK^{-1} mol^{-1} respectively for $\Delta H^{\ddagger}$ and $\Delta S^{\ddagger}$, which are in good agreement (within the errors) to the values determined by Thomas and Reynolds.

With this apparatus it has been found possible to carry out stopped-flow ^1H NMR measurements over the temperature range -60 to +70°C, with an accuracy of ± 0.5°C for any single kinetic measurement within that range. This variable temperature stopped-flow NMR attachment was used for all variable temperature kinetic measurements described in chapters, 3, 4 and 5.

2.3 The efficiency of mixing and measurement of the instrument 'dead-times'.

The principle of mixing used in both the SFPFTNMR attachments which have been described has been shown by Thompson and Gordon to give efficient mixing in less than 30 ms, when solutions are injected into a 1 cm pathlength cuvette of a UV-visible spectrophotometer.[53] Mixing inside a spinning NMR tube was shown to be efficient and complete for both SFNMR attachments in less than 1 s by visually observing the disappearance of an indicator colour (phenolphthalein), when dilute

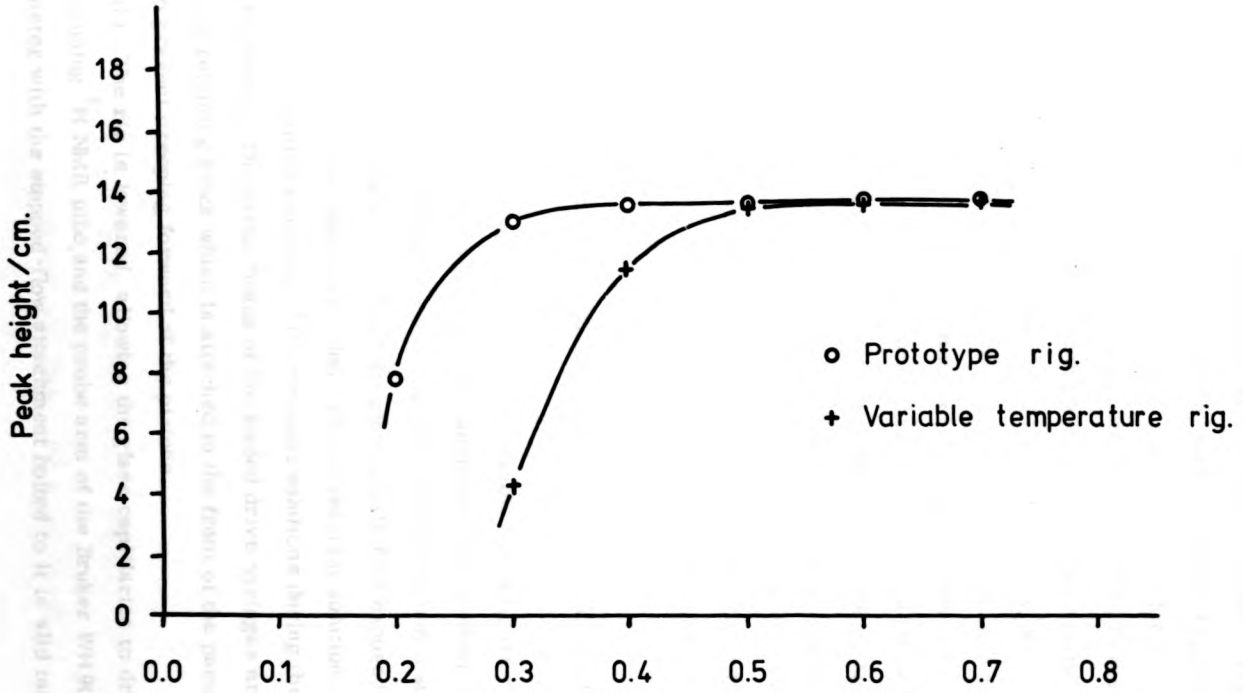

Figure 2.3

'Dead-time' callibration curves for the two SFNMR attachments.

sodium hydroxide was mixed with an excess of dilute nitric acid. A further test of the efficiency of mixing was carried out as follows: dimethylsulphoxide was injected from both drive syringes and the initial delay before collecting the first FID was varied. The signal height, after Fourier transformation, was then plotted against initial delay in seconds (see Figure 2.3). The time taken for the sample to reach magnetic equilibration (or constant peak height) is then a measure of the 'dead-time' of the technique. From Figure 2.3 it can be seen that the prototype SFPFTNMR attachment, with its pre-magnetic equilibration bulbs, has a 'dead-time' of ca. 0.3 - 0.45 s, whereas the variable temperature version has a 'dead-time' of ca. 0.5 s. Since the peak height does drop off more rapidly as the initial delay is reduced for the variable temperature rig, the inclusion of magnetic equilibration reservoirs in the prototype does improve upon the problem of pre-magnetic equilibration. In fact, reliable peak heights can be gained from the prototype attachment 0.3 s after mixing,[51] whereas 0.5 s is the minimum initial delay possible with the variable temperature apparatus.

2.4 The procedure for using the variable temperature SFPFTNMR attachment

The procedure for carrying out a variable temperature kinetic run via the stopped-flow pulse Fourier transform NMR method, using the attachment described in section 2.2, can be split up into 5 subsections.

(i) With the rig elevated and the glass capillaries exposed (see plate 2.1) the drive syringes are filled with the reactant solutions, care being taken to avoid pre-mixing of the reactant solutions during the filling procedure. The piston heads of the loaded drive syringes are then held by a retaining block which is attached to the front of the pneumatic ram to prevent creeping forward of the pistons.

(ii) The rig is lowered, allowing the glass capillaries to drop inside the spinning ^{1}H NMR tube, and the probe arm of the Bruker WH 90 spectrometer with the stopped-flow attachment bolted to it is slid into the magnet

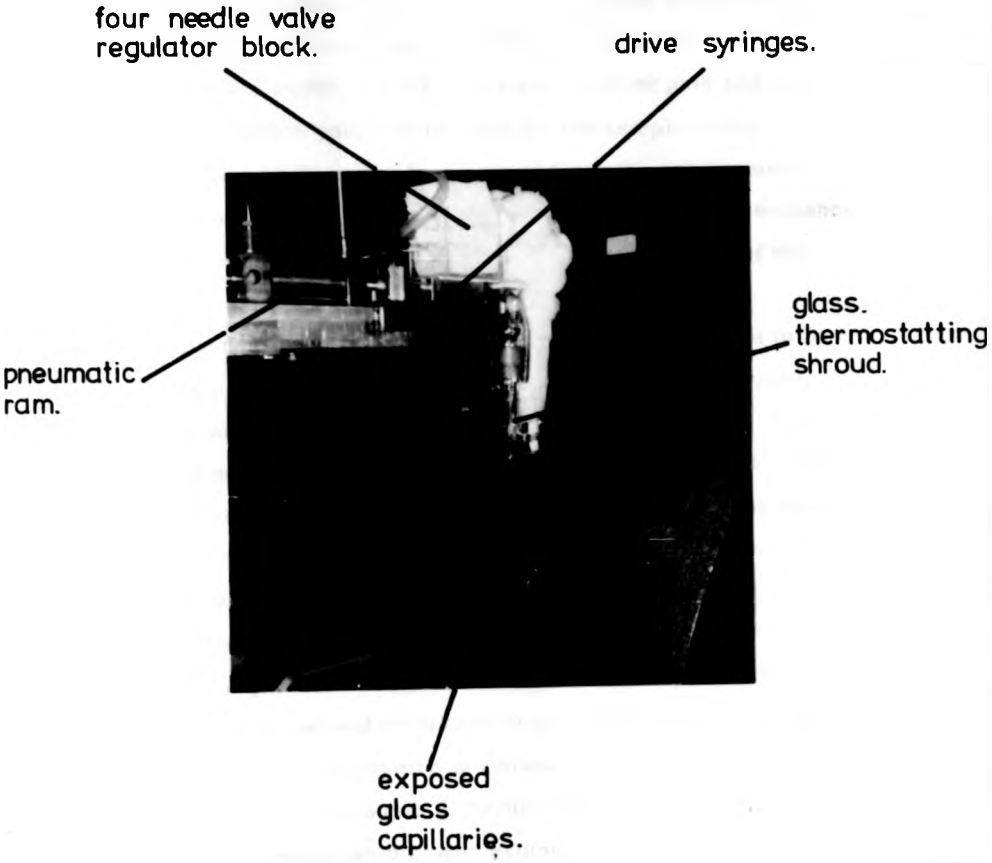

Plate 2.1

SFPFTNMR attachment raised to allow filling of the drive syringes.

and clamped in place. At this point ca. 0.15 cm^3 of each reactant solution is injected into the empty spinning NMR tube (3 mm horizontal travel on the pneumatic ram); this enables adjustments to the magnetic field homogeneity to be made along with adjustments to the radio-frequency (RF) pulse length, the RF receiver amplifier gain and the number of data collection points to be used for the sample under investigation. Also at this point in the procedure, the spectrometer field drift is minimized, by means of observing the deuterium resonance of the deuterated solvent used, via the deuterium lock channel of the spectrometer.

(iii) Having selected the temperature at which the experiment is to be carried out, the probe of the Bruker WH90 spectrometer is thermostatted to that temperature by means of a cold nitrogen blower, A, in plate 2.2, and the standard Bruker variable temperature unit, B. The thermostatting shroud of the SF attachment is then brought to the same temperature as the probe by means of the auxiliary cold nitrogen blower, C, and a second variable temperature unit, D. By means of a temperature offset dial, E, on the variable temperature unit, D, the temperature of the gaseous nitrogen entering the four needle-valve regulator block can be set and stabilized to any value within the range -100 to + 100 C. This temperature is constantly monitored by means of a copper/constantan thermocouple in the nitrogen flow line and a Comark series 3000 copper/constantan digital thermometer, F. The needle valve regulator block is then used to adjust the flow of thermostatted nitrogen into the glass thermostatting shroud, to give an even temperature within the shroud. The temperature inside the shroud, and thus of the solutions to be injected into the NMR tube is monitored by means of a Comark type 1605 chrome/aluminium battery thermometer, G, which is connected to four chrome/aluminium thermocouples evenly spaced down the length of the shroud and attached to the glass reservoir tubes (see plate 2.3). Thermostatting by this procedure thus ensures that the spectrometer probe, NMR tube and the reactant solutions to be injected are all at the same temperature, within an accuracy of ± 0.5 K.

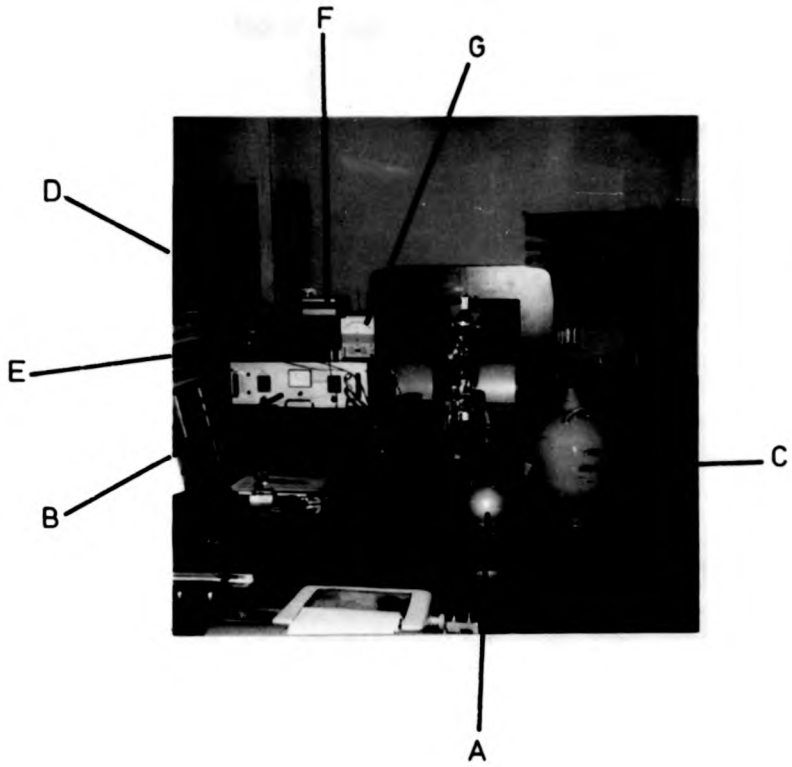

Plate 2.2

The assembled SFPFTNMR attchment.

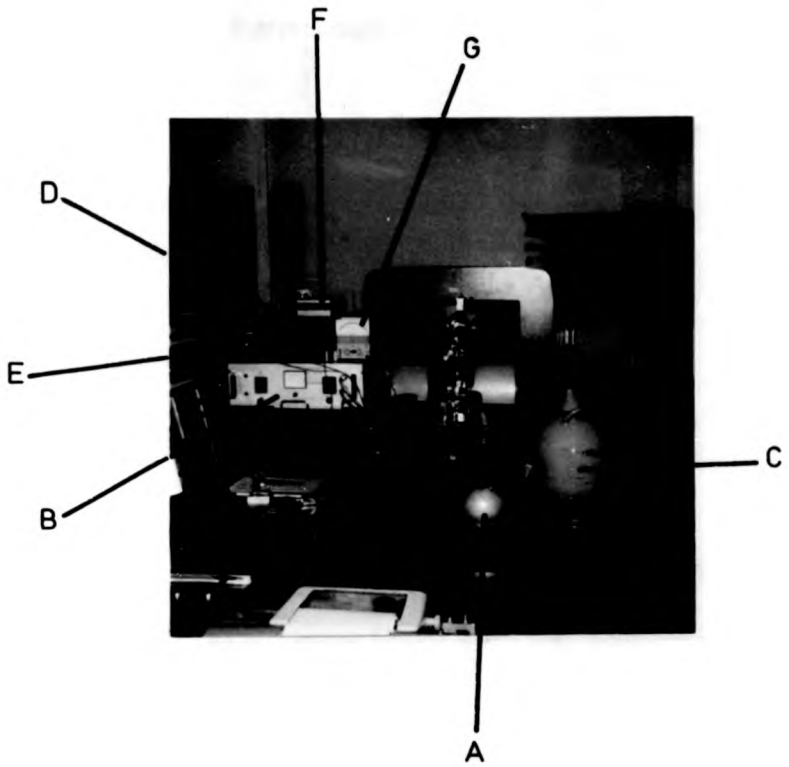

Plate 2.2

The assembled SFPFTNMR attchment.

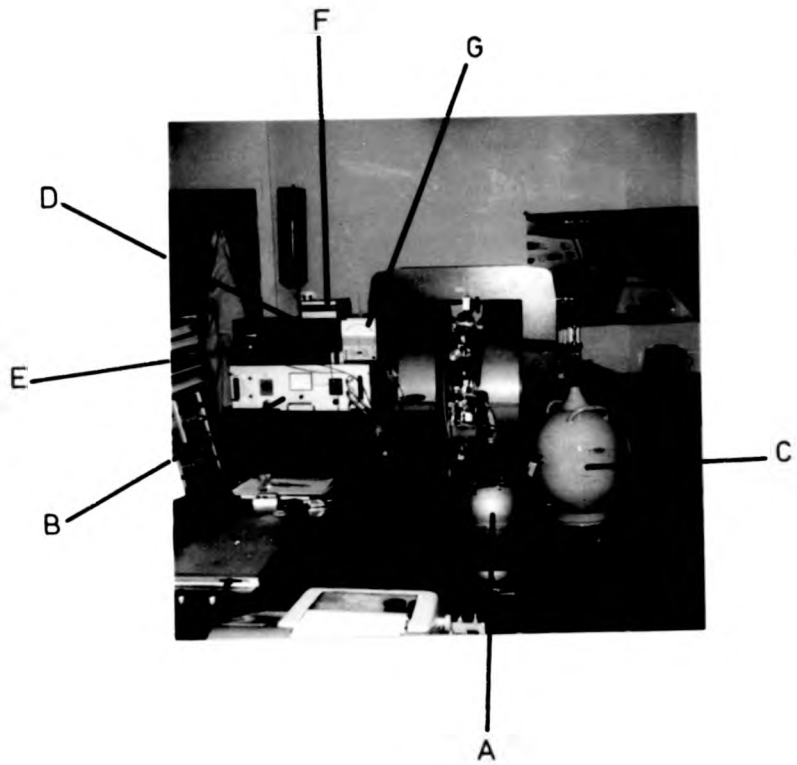

Plate 2.2

The assembled SFPFTNMR attchment.

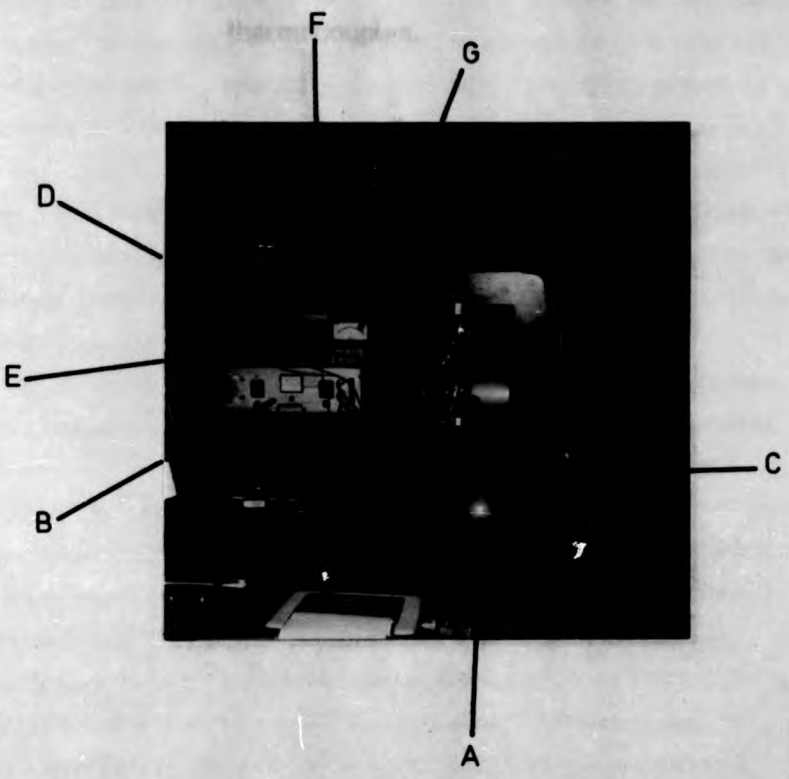

Plate 2.2

The assembled SFPFTNMR attchment.

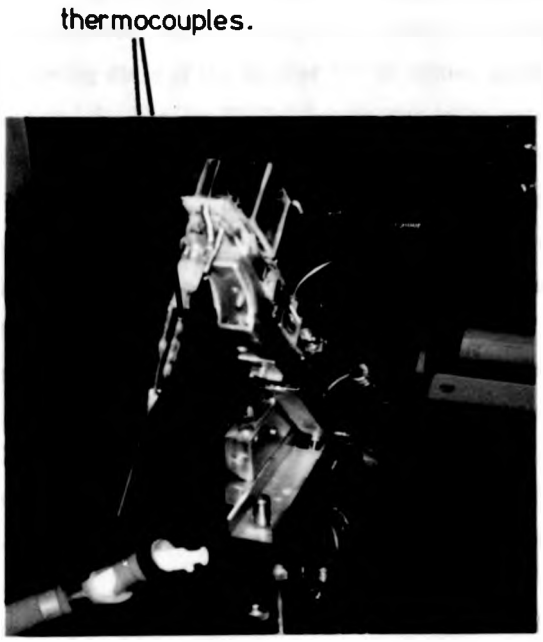

Plate 2.3

Attachment of the Cr/Al thermocouples to the glass reservoir tubes inside the thermostatting shroud.

Plate 2.3

Attachment of the Cr/Al thermocouples to the glass reservoir tubes inside the thermostatting shroud.

thermocouples.

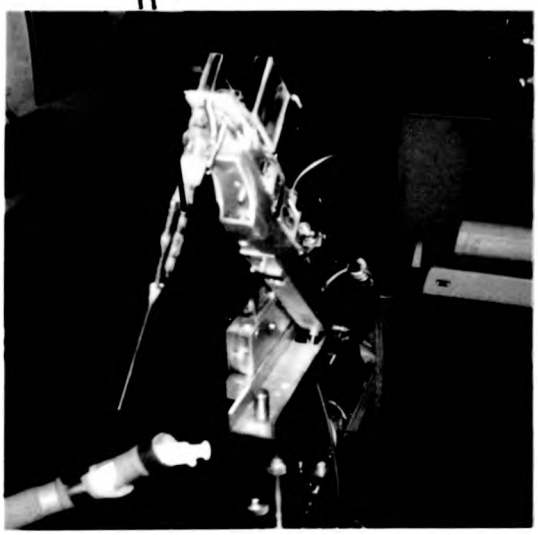

Plate 2.3

Attachment of the Cr/Al thermocouples to the glass reservoir tubes inside the thermostatting shroud.

Plate 2.3

Attachment of the Cr/Al thermocouples to the glass reservoir tubes inside the thermostatting shroud.

(iv) Having achieved satisfactory thermostatting, the initial delay (D1, time in seconds between mixing and the first spectrum) and repetition time (D2, the total repetition time in seconds between spectra, including the data acquisition time of the spectrometer) are selected on the appropriate timing dials of the Bruker WH 90 timing accessory. With this accessory and the Nicolet BNC-12 computer in an external timing mode, both D1 and D2 can be varied from 0.1 s to 99.9 s in steps of as little as 0.1 s. For slower reactions, the delays required can be entered into the Nicolet BNC-12 computer via a teletype; in such circumstances the computer is operated in an internal timing mode and the spectrometer timing accessory becomes redundant.

When monitoring rapid reactions, single pulse FID's are recorded by the computer and stored on a standard magnetic disk interfaced to the BNC-12, the number of these FID's per kinetics experiment being entered to the Nicolet computer before the commencement of the experiment. The spectrometer, for these rapid reactions, is operated in an unlocked mode with the field sweep turned off. However, when monitoring slower reactions, the spectrometer can be locked and multiple pulses can be signal-averaged for each point in time during the reaction. The resultant FID's are stored on the magnetic disk. Under these conditions, a long initial delay is usually set (20 s), which allows sufficient time to lock the spectrometer on the deuterium resonance of the deuterated solvent used, before commencement of the first signal-averaging data accumulation. At this point the brass stopping collar of the pneumatic ram is rotated three times anticlockwise to open the microswitch connected to the timing accessory of the spectrometer, and allow 3 mm of travel on the pneumatic ram when it is next activated. Thus, having decided the number of RF pulses per experiment or spectra (KN), and the number of experiments per kinetic run (NE), along with the desired delays D1 and D2, the Nicolet BNC-12 computer is given a 'kinetics-go' (KG) command, at which point it awaits closure of the microswitch on the kinetics rig before starting its data accumulation cycle.

(v) The NMR tube containing the dead solution in the spectrometer probe is changed for an empty tube by sliding the probe arm out of the magnet, and raising the glass capillaries of the SF attachment out of the NMR tube. Thus, with an empty NMR tube in place, the probe arm back in the magnet, and the computer set up for data accumulation, the quality of the thermostatting can be finally checked. When this is satisfactory, the pneumatic ram is activated with compressed air at drive pressures between 1.0 to 1.5 atmospheres, causing injection of the reactant solutions into the empty spinning NMR tube and triggering of the computer when the flow is stopped via the closure of the micro-switch on the rig. The FID's generated during the reaction are stored on a standard magnetic disk interfaced to the Nicolet BNC-12. As a ^{1}H 1k FID can be stored on disk in ca. 0.03 s, and the minimum time required for a 1k data point accumulation is 0.2 s, with a typical spectrometer sweep width of 1200 Hz, it can be seen that there is negligible delay to data acquisition caused by the data storage process.

Although a Bruker WH90 pulse FTNMR spectrometer is capable of multinuclear facilities, and no modifications to the SF attachment would be required to carry out kinetic measurements by, say, ^{13}C, ^{31}P or even ^{27}Al NMR, all the ensuing work was all carried out with the ^{1}H probe (the most sensitive NMR nucleus).

2.5 Data processing and the kinetics Nicolet BNC-12 computer program

A new computer program (DISKFT) was written for the Nicolet BNC-12 spectrometer computer to handle the rapid accumulation of data during kinetic runs.[51] This program acts interactively with a standard magnetic disk interfaced to the BNC-12, and as data in the form of FID's is collected during a kinetic run, the program stores them on magnetic disk, under a file name specified at the commencement of the run. The FID's thus stored are processed and re-stored in the form of NMR spectra at the end of the kinetic run, to give an 'action replay' of the chemical reaction under investigation. DISKFT also has facilities for listing the heights of any resonance observed during the course of a chemical

reaction, and allows selected regions of each spectra stored on disk to be plotted in the form of a kinetic plot (see chapters 3, 4 and 5). A listing of the commands available with DISKFT is given in Appendix 1.

As a result of possible variations in spectrometer pulse length and computer normalization, the kinetic data from each run (in the form of decaying or growing ^{1}H NMR resonance heights) are normalized to a resonance which remains unchanged throughout the chemical reaction. This is usually the residual ^{1}H NMR resonance of the deuterated solvent used, or could be an inert compound doped into one or both of the reactant solutions specifically for the purpose of normalization. The treatment of kinetic data and the measurement of rate constants for the individual systems investigated by the SFPFTNMR method is discussed as these systems are described (see chapters 3, 4 and 5).

CHAPTER 3

ELECTROPHILIC ATTACK AT CO-ORDINATED LIGANDS. A STOPPED-FLOW PULSE FT ^{1}H NMR INVESTIGATION OF THE RATES OF CHLORINATION OF METAL ACETYLACETONATES BY N-CHLOROSUCCINIMIDE

3.1 Introduction

The chemistry of metal β-diketonates has been extensively studied and well reviewed.[57-62, 97] The pseudo-aromatic character of these compounds has also been given much attention. According to Collman[63] and other workers,[64] each chelate ring in metal acetylacetonates [M(acacH)$_3$] (M = trivalent metal ion; [acacH]$^-$ = $CH_3COCHC(O^-)CH_3$), has a cyclic π-orbital, formed by overlap of a vacant d-orbital of the central metal atom with the 6π-electron orbital of the ligand, whereas Lloyd and Marshall[65] have suggested an acyclic conjugated π-electron system with little delocalization through the metal-oxygen (M-O) bonds, and Holm and Cotton[66] have even expressed doubts over such aromaticity in these compounds. Metal acetylacetonates, however, have been found to undergo typical electrophilic substitution reactions of the hydrogen atom bonded to the sp^2 hybridized carbon atom in the 3-position of the ligand, and have, therefore, been termed pseudo-aromatic.

Replacement of the methine proton of [acacH]$^-$ in metal tris acetylacetonate complexes by a wide range of substituents (X) to give [M(acacX)$_3$] can be acheived by the use of electrophilic reagents such as N-halogenosuccinimides (halogenation reactions),[67] or metal nitrates in acetic anhydride (nitration reactions).[68] Thiocyanogenation,[69,70] formylation,[71] diazotization[72] and Friedel-Crafts reactions[73] of metal acetylacetonates have also been reported, although the mechanism of these various substitution reactions has not been extensively studied.

N-halogensuccinimides are the best reagents for halogenation of [M(acacH)$_3$] complexes,[67] the rate of bromination being much faster than that of iodination and chlorination. Three reaction mechanisms may be put forward to explain these halogenation reactions:-

(i) An ionic (S_E2) mechanism involving a tetrahedral intermediate[67] [reaction (3.1)].

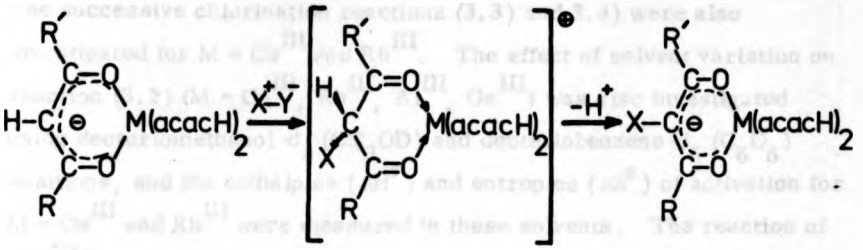

(3.1)

(ii) A free radical mechanism.[74]

or

(iii) A mechanism involving small concentrations of molecular halogen produced in solution.[40]

In this study the kinetics and mechanisms of the chlorination reactions of metal acetylacetonates have been investigated by the stopped-flow pulse Fourier transform ^{1}H NMR (SFPFTNMR) method described in Chapter 2. This technique is particularly suitable for reactions of this type since it gives a much more detailed picture of the reaction mechanisms involved than is possible by UV-visible spectrophotometry. In fact, most of the reactions studied here do not give rise to measurable UV-visible changes. Substitution at the periphery of a metal complex does not usually bring about a marked change in its UV-visible spectrum since the donor-atoms themselves have not changed, whereas ^{1}H NMR is much more indicative of the structural changes involved and can also readily detect minor side-reactions as the following work will show.

The rates of mono-chlorination of the acetylacetonate complexes of the Co^{III}, Rh^{III}, Ir^{III}, Al^{III}, Ga^{III} and Be^{II} metal ions with N-chloro-succinimide (RNCl) have been investigated in deuteriochloroform ($CDCl_3$) at 297 K (reaction (3.2), RNH = succinimide).

$$[M(acacH)_3] + RNCl \xrightarrow{k_1} [M(acacH)_2(acacCl)] + RNH \qquad (3.2)$$

$$[M(acacH)_2(acacCl)] + RNCl \xrightarrow{k_2} [M(acacH)(acacCl)_2] + RNH \qquad (3.3)$$

$$[M(acacH)(acacCl)_2] + RNCl \xrightarrow{k_3} [M(acacCl)_3] + RNH \qquad (3.4)$$

The successive chlorination reactions (3.3) and 3.4) were also investigated for M = Co^{III} and Rh^{III}. The effect of solvent variation on reaction (3.2) (M = Co^{III}, Rh^{III}, Al^{III}, Ga^{III}) was also investigated using deuteriomethanol-d_4 (CD_3OD) and deuteriobenzene-d_6 (C_6D_6) solutions, and the enthalpies ($\Delta H^{\ddagger}$) and entropies ($\Delta S^{\ddagger}$) of activation for M = Co^{III} and Rh^{III} were measured in these solvents. The reaction of $[Co^{III}(acacD)_3]$ with N-chlorosuccinimide was investigated in $CDCl_3$ and CD_3OD for comparison with the rates of reaction of $[Co^{III}(acacH)_3]$ in these solvents. The relative electron-withdrawing abilities of nitro-(NO_2-) and chloro(Cl-) 3-substituents was established by comparing the rates of mono-chlorination of $[Co^{III}(acacH)_2(acacNO_2)]$, $[M(acacH)_2$-(acacCl)] and $[M(acacH)(acacCl)_2]$ (M = Co^{III} and Rh^{III}). Finally, the chlorination reactions of some metal acetylacetonate complexes of the type $[Co^{III}(acacH)_2(acacMe)]$ and $[M(acacMe)_3]$ (M = Co^{III}, Rh^{III}; $acacMe^- = CH_3COC(CH_3)C(O^-)CH_3$) were investigated. Some new synthetic routes to these complexes of acacMe were devised.

3.2 Experimental

3.2.1 Materials and Methods

Deuteriated solvents ($CDCl_3$, CD_3OD, C_6D_6) were obtained from Merck, Sharp and Dohme, Ltd. and reclaimed by vacuum distillation after use. N-chlorosuccinimide (B.D.H. Chemicals) was recrystallised from chloroform before use. The tris-(pentane-2,4-dionato) complexes $[M(acacH)_3]$ (where M = Co^{III}, Rh^{III}, Ir^{III}, Al^{III}, Ga^{III}) were prepared by published methods[75-77] using redistilled acetylacetone and the highest purity metal salts available (rhodium and iridium trichloride were on loan from Johnson Matthey, Ltd.), and recrystallised from 40:60 toluene-petroleum ether before use. These complexes were shown to be pure by ^1H NMR (Table 3.1) and by mass spectrometery (Table 3.2).

M	Unchlorinated [M(acacH)$_3$] CH	Unchlorinated [M(acacH)$_3$] CH_3	Monochlorinated [M(acacH)$_2$(acacCl)] CH	Monochlorinated [M(acacH)$_2$(acacCl)] CH_3	Dichlorinated [M(acacH)(acacCl)$_2$] CH	Dichlorinated [M(acacH)(acacCl)$_2$] CH_3	Trichlorinated [M(acacCl)$_3$] CH_3
Co^{III}	5.51	2.16	5.52	2.38 2.19 2.16	5.54	2.42 2.39 2.18	2.46
Rh^{III}	5.47	2.14	5.49	2.41 2.16 2.15	5.50	2.41 2.40 2.16	2.42
Ir^{III}	5.46	1.99	5.47	2.23 2.01 1.99	5.48	2.25 2.24 2.02	2.26
Al^{III}	5.49	1.99	5.47	2.245 1.99[a]	5.51	2.25[b] 1.99	
Ga^{III}	5.41	1.99	5.43	2.26 1.99[a]			
Be^{II} [c]	5.60	2.06	5.61	2.30 2.06	–	2.32	

a Methyls of unchlorinated (acacH) rings unresolved.
b Methyls of chlorinated (acacCl) rings unresolved.
c [Be^{II}(acacH)$_2$].

TABLE 3.1

^1H NMR chemical shifts in ppm of [M(acacH)$_3$] complexes studied and their 3-chloro derivatives (δ/ppm relative to $CHCl_3$ at δ 7.25 ppm).

Complex	Formula	Relative Molecular Mass	Observed molecular ions (m/e) [a]	
			M^+	MH^+
$[Co^{III}(acacH)_3]$	$C_{15}H_{21}O_6Co$	356.02	356	357
$[Co^{III}(acacCl)_3]$	$C_{15}H_{18}O_6Cl_3Co$	459.37	459[b] 461[c] 463[d]	460[b] 462[c] 464[d]
$[Cr^{III}(acacCl)_3]$	$C_{15}H_{18}O_6Cl_3Cr$	452.43	452[b] 454[c] 456[d]	453[b] 455[c] 457[d]
$[Be^{II}(acacH)_2]$	$C_{10}H_{14}O_4Be$	207.07	207	208
$[Be^{II}(acacH)(acacCl)]$	$C_{10}H_{13}O_4ClBe$	241.52	242[e] 244[f]	243[e] 245[f]
$[Be^{II}(acacCl)_2]$	$C_{10}H_{12}O_4Cl_2Be$	275.97	276[e] 278[f]	277[e] 279[f]
$[Co^{III}(acacH)_2(acacCH_3)]$	$C_{16}H_{23}O_6Co$	370.03	370	371
$[Co^{III}(acacCH_3)_3]$	$C_{18}H_{27}O_6Co$	398.05	398	399
$[Rh^{III}(acacCH_3)_3]$	$C_{18}H_{27}O_6Rh$	442.02	442	443

a Reference to $Re_2(CO)_{10}$.

b Ion from ^{35}Cl, ^{35}Cl, ^{35}Cl isotopes.

c Ion from ^{35}Cl, ^{35}Cl, ^{37}Cl isotopes.

d Ion from ^{35}Cl, ^{37}Cl, ^{37}Cl isotopes.

e Ion from ^{35}Cl, ^{35}Cl isotopes.

f Ion from ^{35}Cl, ^{37}Cl isotopes.

TABLE 3.2

Mass spectral molecular ion data of some of the metal acetylacetonates studied.

Complex	Formula	Relative Molecular Mass	Observed molecular ions (m/e) [a]	
			M^+	MH^+
$[Co^{III}(acacH)_3]$	$C_{15}H_{21}O_6Co$	356.02	356	357
$[Co^{III}(acacCl)_3]$	$C_{15}H_{18}O_6Cl_3Co$	459.37	459[b] 461[c] 463[d]	460[b] 462[c] 464[d]
$[Cr^{III}(acacCl)_3]$	$C_{15}H_{18}O_6Cl_3Cr$	452.43	452[b] 454[c] 456[d]	453[b] 455[c] 457[d]
$[Be^{II}(acacH)_2]$	$C_{10}H_{14}O_4Be$	207.07	207	208
$[Be^{II}(acacH)(acacCl)]$	$C_{10}H_{13}O_4ClBe$	241.52	242[e] 244[f]	243[e] 245[f]
$[Be^{II}(acacCl)_2]$	$C_{10}H_{12}O_4Cl_2Be$	275.97	276[e] 278[f]	277[e] 279[f]
$[Co^{III}(acacH)_2(acacCH_3)]$	$C_{16}H_{23}O_6Co$	370.03	370	371
$[Co^{III}(acacCH_3)_3]$	$C_{18}H_{27}O_6Co$	398.05	398	399
$[Rh^{III}(acacCH_3)_3]$	$C_{18}H_{27}O_6Rh$	442.02	442	443

a Reference to $Re_2(CO)_{10}$.
b Ion from ^{35}Cl, ^{35}Cl, ^{35}Cl isotopes.
c Ion from ^{35}Cl, ^{35}Cl, ^{37}Cl isotopes.
d Ion from ^{35}Cl, ^{37}Cl, ^{37}Cl isotopes.
e Ion from ^{35}Cl, ^{35}Cl isotopes.
f Ion from ^{35}Cl, ^{37}Cl isotopes.

TABLE 3.2

Mass spectral molecular ion data of some of the metal acetylacetonates studied.

Mixed complexes of the type $[M(acacCl)_n(acacH)_{3-n}]$ (n = 1 or 2 and M = Co^{III} or Rh^{III}) were prepared by the reaction of approximately one or two moles of N-chlorosuccinimide (RNCl) with the desired $[M(acacH)_3]$ complex in toluene. The mixtures of products obtained by this process were separated by preparative thin layer chromatography on neutral aluminium oxide [Merck 60 PF_{254} (type E)] with toluene as a developing solvent; the R_F values were as follows:-

	$[M(acacCl)_n(acacH)_{3-n}]$			
M	n = 0	n = 1	n = 2	n = 3
Co^{III}	0.27	0.43	0.55	0.69
Rh^{III}	0.20	0.33	0.54	0.71
Ir^{III}	0.18	0.43	0.59	0.78

These complexes were shown to be pure after recrystallisation from 40:60 toluene:petroleum ether by ^1H NMR (see Table 3.1). Fully assigned ^1H NMR spectra of the complexes $[Co^{III}(acacCl)_n(acacH)_{3-n}]$ (n = 0, 1, 2 and 3) are shown in Figures 3.1 to 3.4.

$[Cr^{III}(acacCl)_3]$ for use as an inert paramagnetic relaxing agent was prepared by the above method using an excess of RNCl. The purity of this complex was verified by thin layer chromatography and mass spectrometry (see Table 3.2).

$[Co^{III}(acacH)_2(acacNO_2)]$ was prepared by the reaction of approximately one mole of copper nitrate in acetic anhydride with one mole of $[Co^{III}(acacH)_3]$[68], purified by thin layer chromatograpy and shown to be pure by ^1H NMR (see Table 3.3).

$[Co^{III}(acacMe)(acacH)_2]$ was prepared via the $[Co^{III}(CO_3)_3]^{3-}$ ion as follows: to $CoCl_2 \cdot 6H_2O$ (5.95 g) in water (12.5 cm^3) was added hydrogen peroxide (4 cm^3, 10 vol). This solution was then added to an ice-cold slurry of $KHCO_3$ (16.3 g) in water (20 cm^3) with stirring. To the resulting green solution of $[Co^{III}(CO_3)_3]^{3-}$ was added acetylacetone (5 cm^3) and the mixture was heated with stirring at 60°C for 1 hour. The resulting solution was chloroform extracted to remove

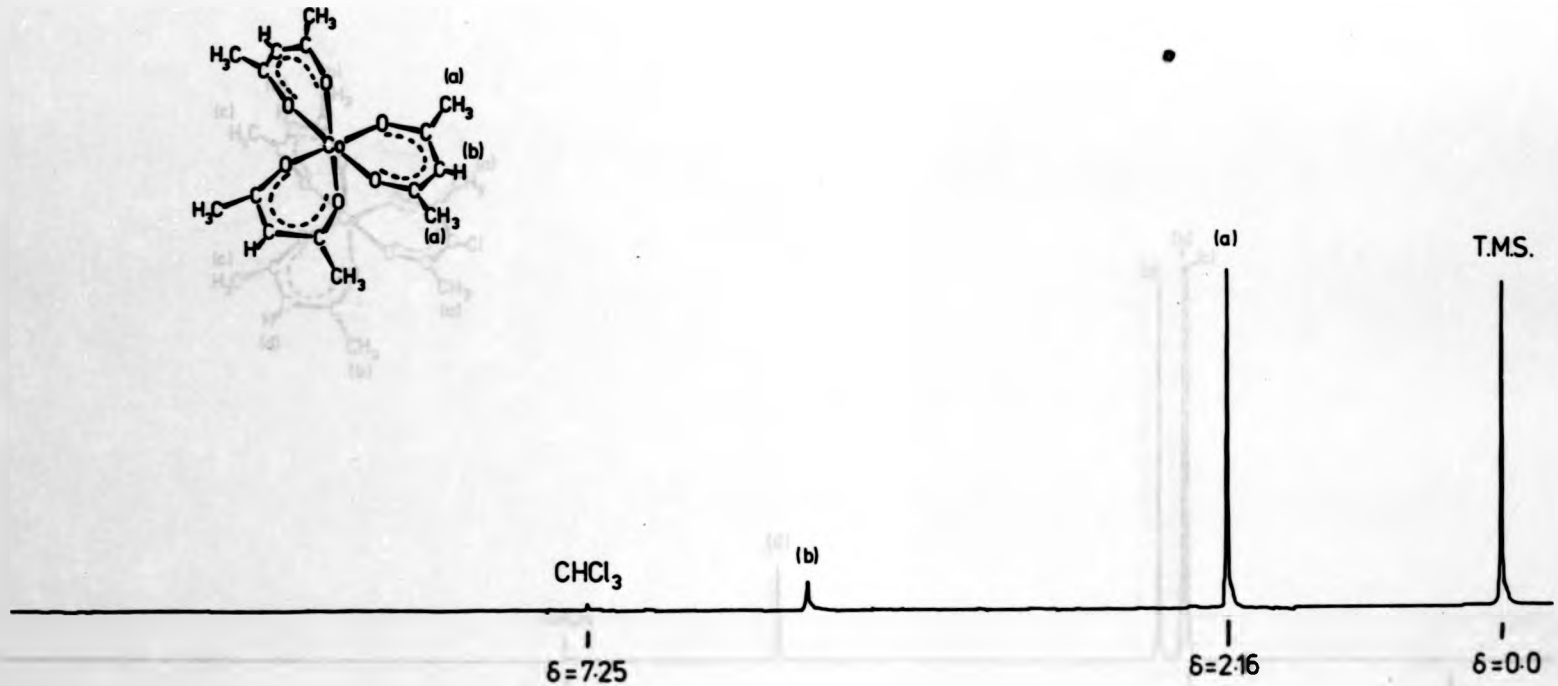

Figure 3.1

^{1}H NMR spectrum of $[Co^{III}(acacH)_3]$ in $CDCl_3$ at 297K.

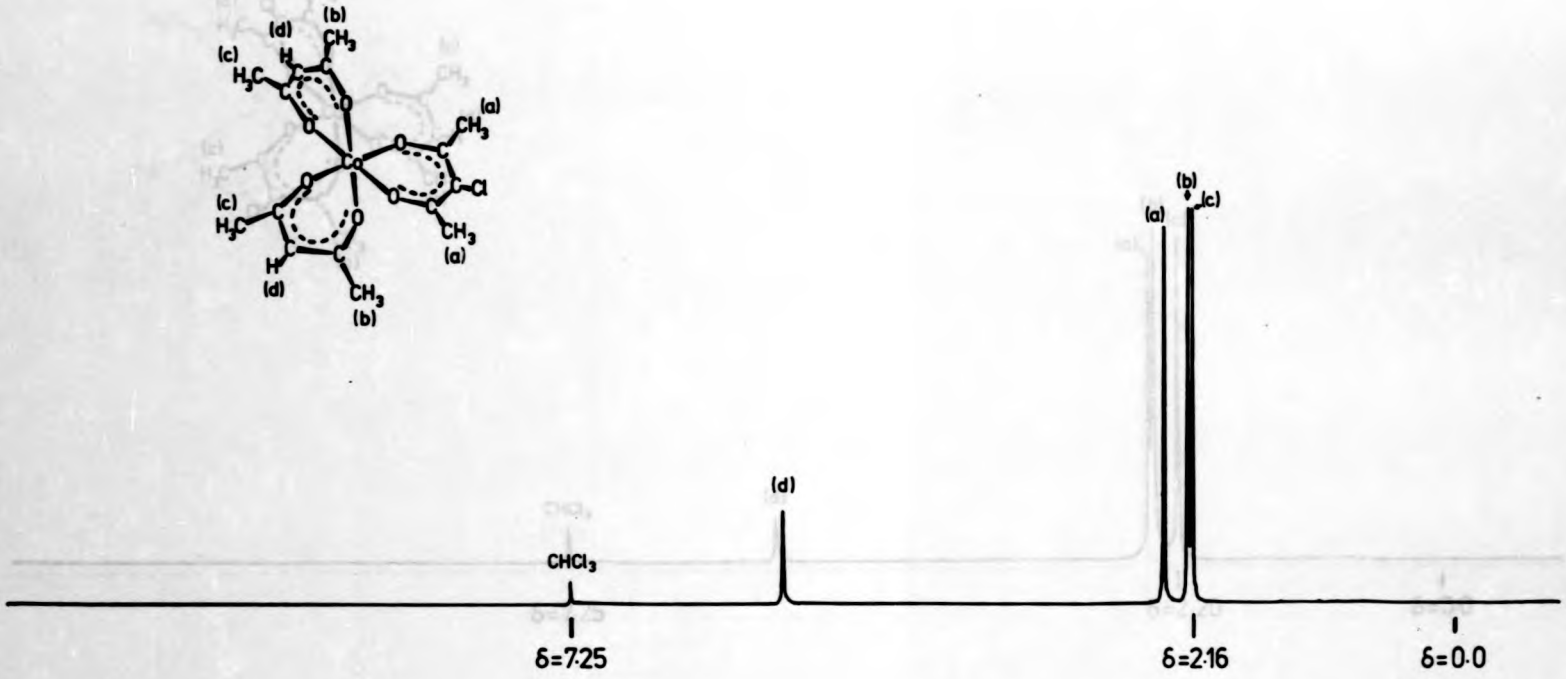

Figure 3.2

^{1}H NMR spectrum of $[Co^{III}(acacH)_2(acacCl)]$ in $CDCl_3$ at 297K.

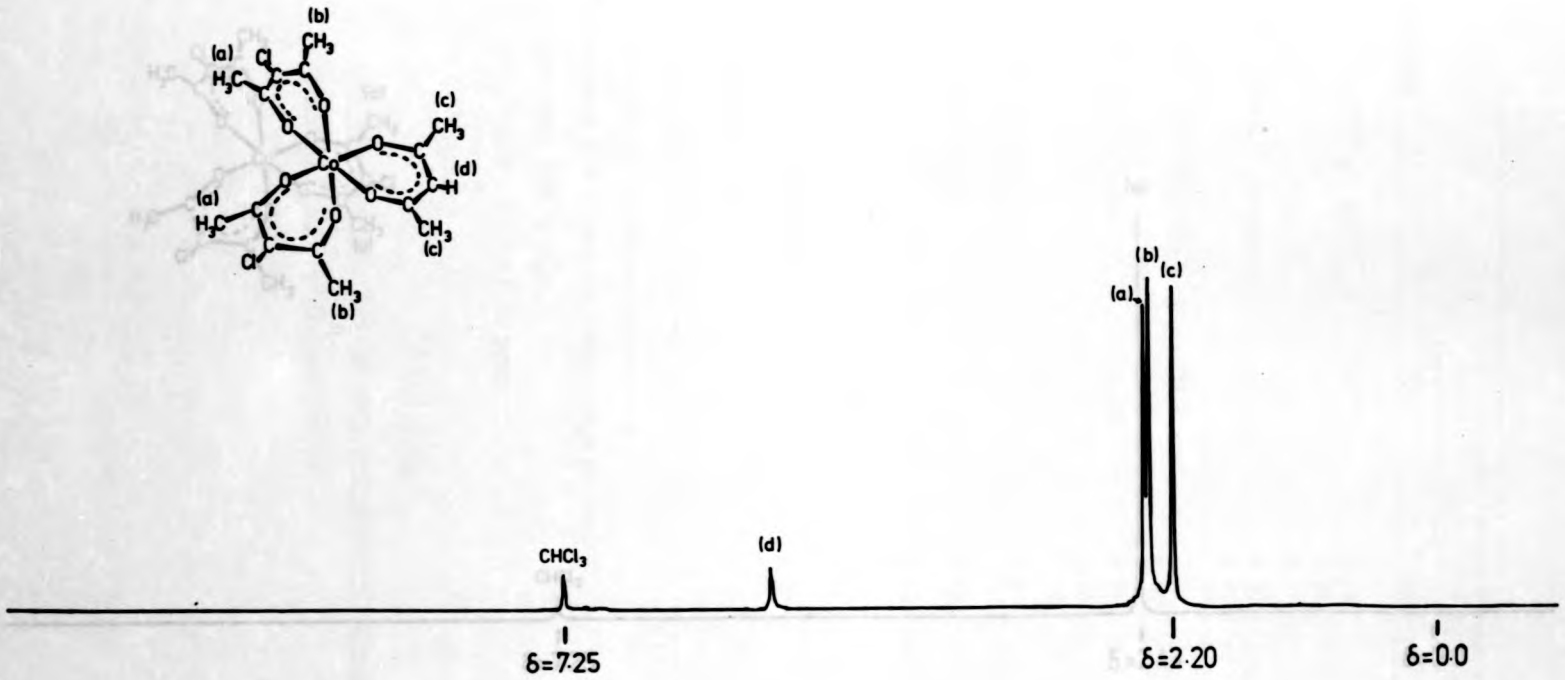

Figure 3.3

^1H NMR spectrum of $[Co^{III}(acacH)(acacCl)_2]$ in $CDCl_3$ at 297K.

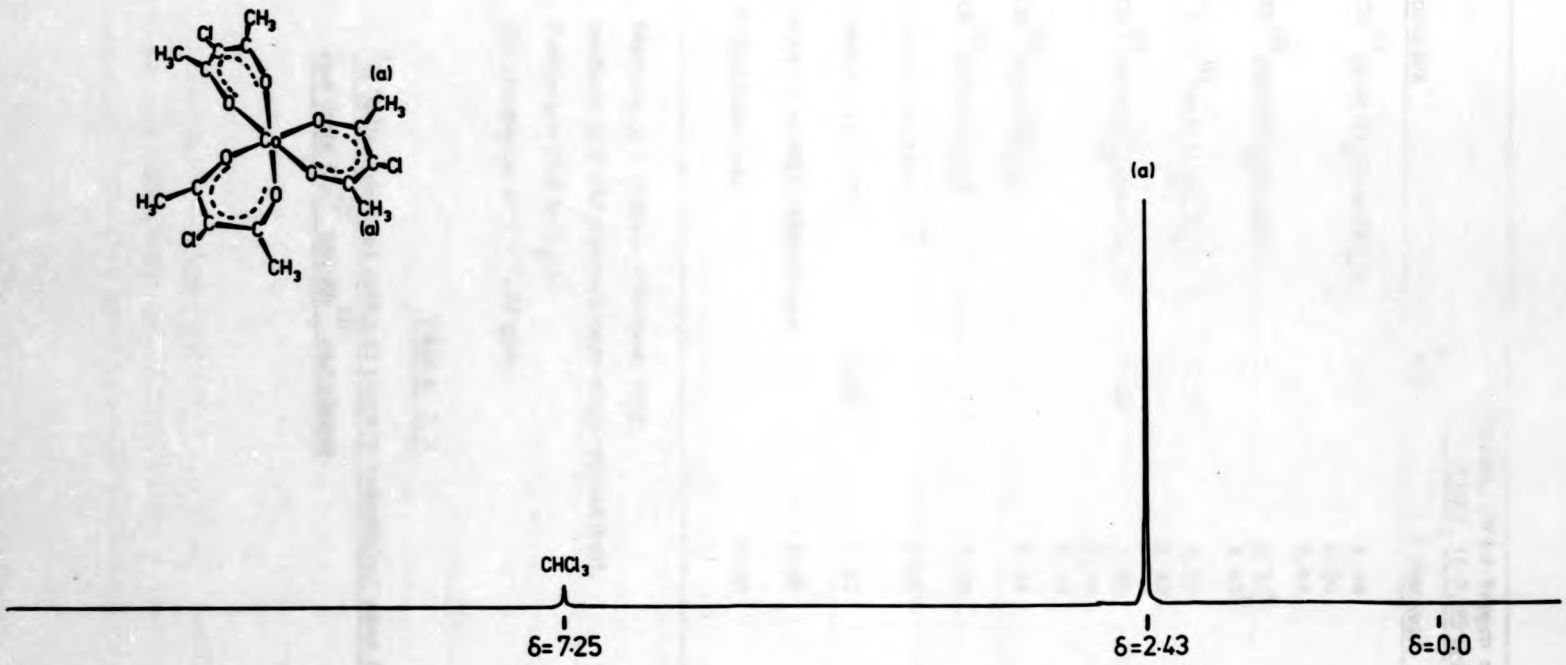

Figure 3.4

^1H NMR spectrum of $[Co^{III}(acacCl)_3]$ in $CDCl_3$ at 297K.

Complex	Chemical shifts δ/ppm relative to $CHCl_3$ (δ 7.25 ppm)		
	CH	1.5 methyls	3-methyl
$[Co^{III}(acacH)_2(acacNO_2)]$	5.57	2.44 2.26 2.18	
$[Rh^{III}(acacCl)_2(acacBr)]$		2.51 [a] 2.42 [b]	
$K^+[Co^{III}(acacH)_2(CO_3)]^-$ [c]	5.88	2.29 2.22	
$[Co^{III}(acacH)_2(acacCH_3)]$	5.49	2.25 2.16 2.14	1.92
$[Co^{III}(acacCH_3)_3]$		2.21	1.90
$[Rh^{III}(acacCH_3)_3]$		2.19	1.94
3-methyl-acac(enol) [d]		2.05	1.74
3-methyl-acac(keto)	3.60	2.12	1.24
3-chloro 3-methyl-acac(keto)		2.26	1.66
3,3-dichloro-acac		2.46	

a Methyls of 3-brominated-acac ring.

b Methyls of 3-chlorinated-acac rings unresolved.

c Reference DSS in D_2O.

d OH resonance at δ = 7.52 ppm.

TABLE 3.3

^1H NMR chemical shifts of some 3-substituted-acac ligands and their Co^{III} and Rh^{III} complexes.

any $[Co^{III}(acacH)_3]$, and the aqueous layer then passed down a column of DOWEX-1 anion exchange resin (1 x 8-50) in the chloride form. Elution with water gave a green solution of the $[Co^{III}(acacH)_2CO_3]^-$ ion, leaving a green band of the $[Co^{III}(acacH)(CO_3)_2]^{2-}$ ion on the resin. The solution of $[Co^{III}(acacH)_2(CO_3)]^-$ ion was concentrated to 20-30 cm^3 by rotary evaporation and 5 cm^3 of 3-methylpentane-2,4-dione (acacMe) was added to give a green precipitate of $[Co^{III}(acacH)_2(acacMe)]$. This was collected by filtration after 10 minutes and recrystallised from 40:60 toluene:petroleum ether. Anal. ($C_{16}H_{23}O_6Co$) Calculated: C, 51.89%, H, 6.26%; Found: C, 51.42%, H, 6.19%.

$[M(acacMe)_3]$ (M = Co^{III}, Rh^{III}) complexes were prepared by standard methods[76,77] substituting (acacMe) for (acacH). Anal. ($C_{18}H_{27}O_6Co$) Calculated: C, 54.27, H, 6.83%; Found: C, 53.89, H, 6.78%. ($C_{18}H_{27}O_6Rh$) Calculated: C, 48.88, H, 6.15%; Found: C, 48.85, H, 6.17%. These 3-methylacetylacetone complexes were also characterised by mass spectroscopy and ^1H NMR (see Tables 3.2 and 3.3).

3,3-dideuteriopentane-2,4-dione (acacD) was prepared by stirring (acacH) (6 cm^3) with D_2O (30 cm^3) overnight, then extracting the aqueous solution with dichloromethane, repeating the deuteration with a further 30 cm^3 of D_2O, extracting and fractionally distilling off the (acacD). This ligand was shown to be 99% deuteriated at the methine (3-) position by ^1H NMR.

$[Co^{III}(acacD)_3]$ was prepared by the published method for $[Co^{III}(acacH)_3]$[76] substituting acacD for acacH and D_2O_2 for H_2O_2. (D_2O_2 was prepared from Na_2O_2 and DCl/D_2O). The recrystallised $[Co^{III}(acacD)_3]$ was shown to be 99% deuterated by ^1H NMR. The use of H_2O_2 instead of D_2O_2 in this preparation gave a product which was only ca. 60% deuteriated.

3-methylpentatne-2,4-dione (acacMe) was prepared by the action of 1 mole of methyliodide and 1 mole of sodium pentane-2,4-dione ion in ethanol.[78] The pure ligand was fractionally distilled at 435 ± 1 K

(1 atmosphere) and was shown to be pure by ^{1}H and ^{13}C NMR [^{1}H NMR shifts in Table 3.3: ^{13}C NMR shifts relative to TMS at δ 12.54, 28.86, 61.36 and 205.13 (keto-form), and at 21.32, 23.27, 105.03 and 190.63 ppm (enol-form).

All ^{1}H NMR chemical shift measurements are quoted to ± 0.01 ppm (either relative to TMS, or the residual ^{1}H NMR resonance of the deuteriated solvent used), and were recorded on a Bruker WH 90 Fourier transform NMR spectrometer.

Mass spectral measurements were recorded with V.G. Micromass 12 mass spectrometer.

3.2.2 Kinetics

The reactions in this chapter (apart from the variable temperature measurements) were studied at 297 ± 0.5 K in deuteriated solvents using the SFPFTNMR attachments described in Chapter 2. Complete ^{1}H NMR spectra were recorded as FID's every few seconds after mixing, and after Fourier transformation the decaying N-chloro-succinimide ^{1}H NMR resonance (at δ = 2.90 ppm) was used to obtain the rate constants. Most reactions were studied under pseudo-first-order conditions with a 10:1 ratio of metal complex to N-chlorosuccinimide. The pseudo-first-order rate constants (k) were obtained by least squares analysis (with the Algol program WLSAPROG) from the slopes of plots of ln[(RNCl peak height or integral)/(solvent peak height or integral)] versus time (see Figure 3.5). Because of solubility problems, a few reactions were studied under second-order conditions with [Complex] = [RNCl]; second-order rate constants were then obtained from least squares analysis of the slopes of plots of [(RNCl peak height)/(solvent peak height)]$^{-1}$ versus time (see Figure 3.6 and Appendix 2 for the derivation of these plots).

3.3 Results

3.3.1 The main reaction

A 'kinetic plot' of the highfield region of the observed ^{1}H NMR spectra for the mono-chlorination of [$Co^{III}(acacH)_3$] by N-chlorosuccinimide

(1 atmosphere) and was shown to be pure by ^{1}H and ^{13}C NMR [^{1}H NMR shifts in Table 3.3: ^{13}C NMR shifts relative to TMS at δ 12.54, 28.86, 61.36 and 205.13 (keto-form), and at 21.32, 23.27, 105.03 and 190.63 ppm (enol-form).

All ^{1}H NMR chemical shift measurements are quoted to ± 0.01 ppm (either relative to TMS, or the residual ^{1}H NMR resonance of the deuteriated solvent used), and were recorded on a Bruker WH 90 Fourier transform NMR spectrometer.

Mass spectral measurements were recorded with V.G. Micromass 12 mass spectrometer.

3.2.2 Kinetics

The reactions in this chapter (apart from the variable temperature measurements) were studied at 297 ± 0.5 K in deuteriated solvents using the SFPFTNMR attachments described in Chapter 2. Complete ^{1}H NMR spectra were recorded as FID's every few seconds after mixing, and after Fourier transformation the decaying N-chloro-succinimide ^{1}H NMR resonance (at δ = 2.90 ppm) was used to obtain the rate constants. Most reactions were studied under pseudo-first-order conditions with a 10:1 ratio of metal complex to N-chlorosuccinimide. The pseudo-first-order rate constants (k) were obtained by least squares analysis (with the Algol program WLSAPROG) from the slopes of plots of ln[(RNCl peak height or integral)/(solvent peak height or integral)] versus time (see Figure 3.5). Because of solubility problems, a few reactions were studied under second-order conditions with [Complex] = [RNCl]; second-order rate constants were then obtained from least squares analysis of the slopes of plots of [(RNCl peak height)/(solvent peak height)]$^{-1}$ versus time (see Figure 3.6 and Appendix 2 for the derivation of these plots).

3.3 Results

3.3.1 The main reaction

A 'kinetic plot' of the highfield region of the observed ^{1}H NMR spectra for the mono-chlorination of [$Co^{III}(acacH)_3$] by N-chlorosuccinimide

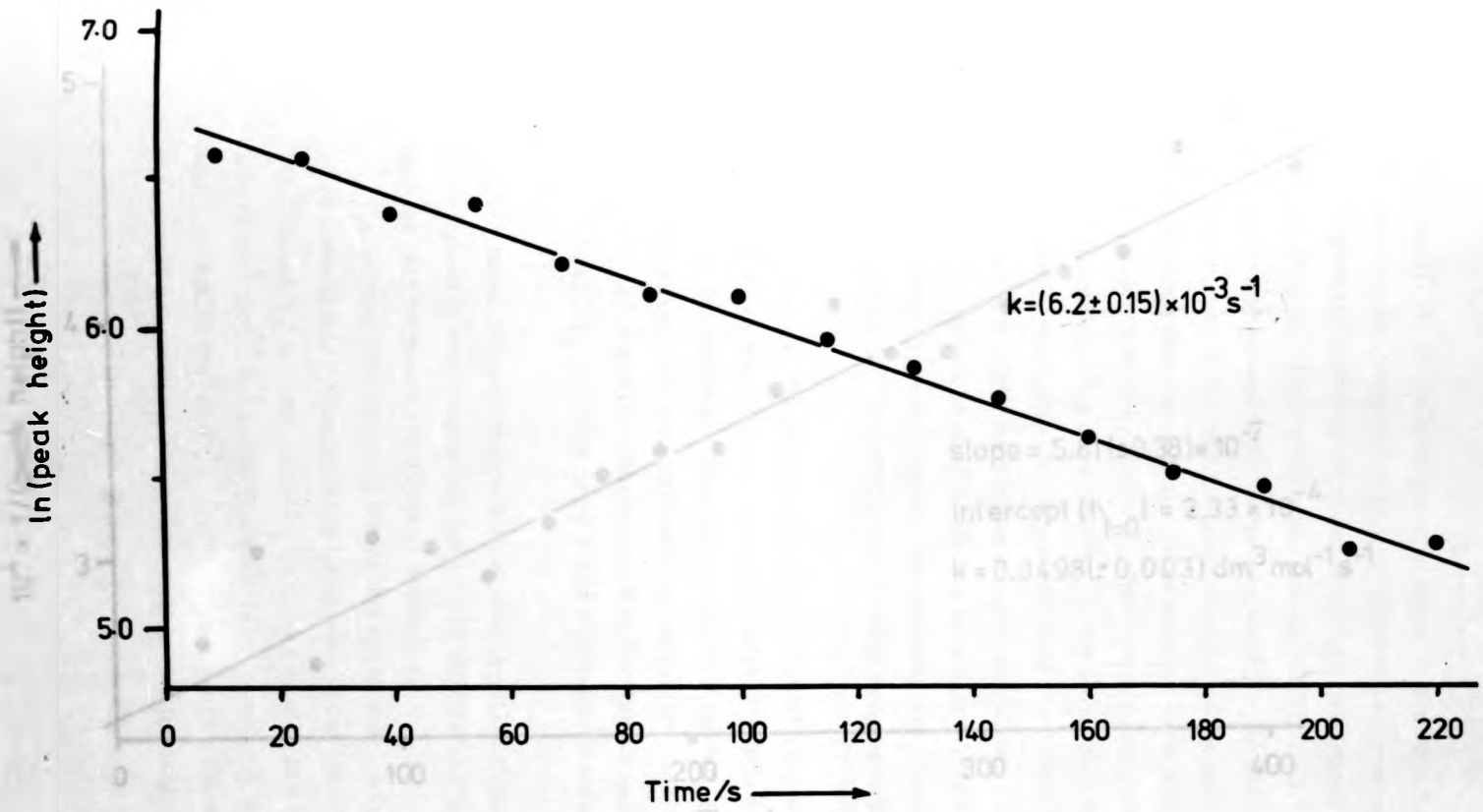

Figure 3.5

Pseudo-first-order rate plot for the reaction between $[Co(acacH)_3]$ (0·1 mol dm^{-3}) and N-chlorosuccinimide (0·01 mol dm^{-3}), in C_6D_6 at 297 K.

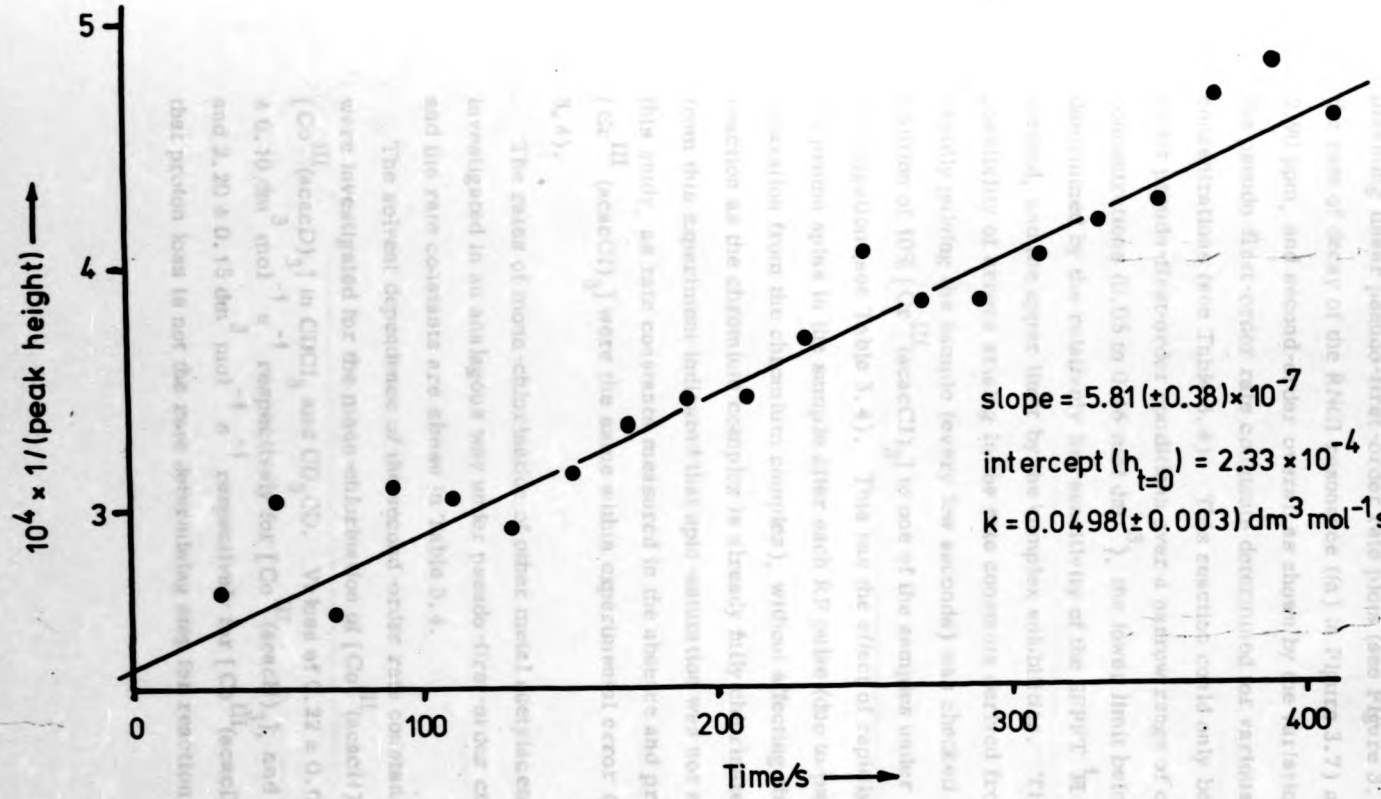

Figure 3.6

Second-order rate plot for the reaction between $[Rh^{III}(acacH)_3]$ (0.05 mol dm^{-3}) and RNCl (0.05 mol dm^{-3}) in C_6D_6 at 334.9 K.

(reaction (3.2)) in $CDCl_3$ at 297 K is shown in Figure 3.7. This reaction was demonstrated to be first order in both reactants by obtaining linear pseudo-first-order rate plots (see Figure 3.5) from the rate of decay of the RNCl resonance ((a) in Figure 3.7) at δ = 2.90 ppm, and second-order overall as shown by the variation of the pseudo-first-order rate constants determined for various complex concentrations (see Table 3.4). This reaction could only be studied under pseudo-first-order conditions over a narrow range of complex concentrations (0.05 to 0.16 mol dm^{-3}), the lower limit being determined by the relatively low sensitivity of the SFPFT ^1H NMR method, and the upper limit by the complex solubilities. The possibility of errors arising in the rate constants derived from rapidly pulsing the sample (every few seconds) was checked by the addition of 10% $[Cr^{III}(acacCl)_3]$ to one of the samples under investigation (see Table 3.4). This has the effect of rapidly relaxing the proton spins in the sample after each RF pulse (due to paramagnetic relaxation from the chromium complex), without affecting the rate of reaction as the chromium complex is already fully chlorinated. Results from this experiment indicated that spin-saturation was not a problem in this study, as rate constants measured in the absence and presence of $[Cr^{III}(acacCl)_3]$ were the same within experimental error (see Table 3.4).

The rates of mono-chlorination of other metal acetylacetonates were investigated in an analagous way under pseudo-first-order conditions, and the rate constants are shown in Table 3.4.

The solvent dependence of the second-order rate constants, k_1, were investigated for the mono-chlorination of $[Co^{III}(acacH)_3]$ and $[Co^{III}(acacD)_3]$ in $CDCl_3$ and CD_3OD. Values of 0.22 ± 0.02 and 2.05 ± 0.10 $dm^3\ mol^{-1}\ s^{-1}$ respectively for $[Co^{III}(acacH)_3]$, and 0.21 ± 0.02 and 2.20 ± 0.15 $dm^3\ mol^{-1}\ s^{-1}$ respectively for $[Co^{III}(acacD)_3]$ indicate that proton loss is not the rate determining step for reaction (3.2).

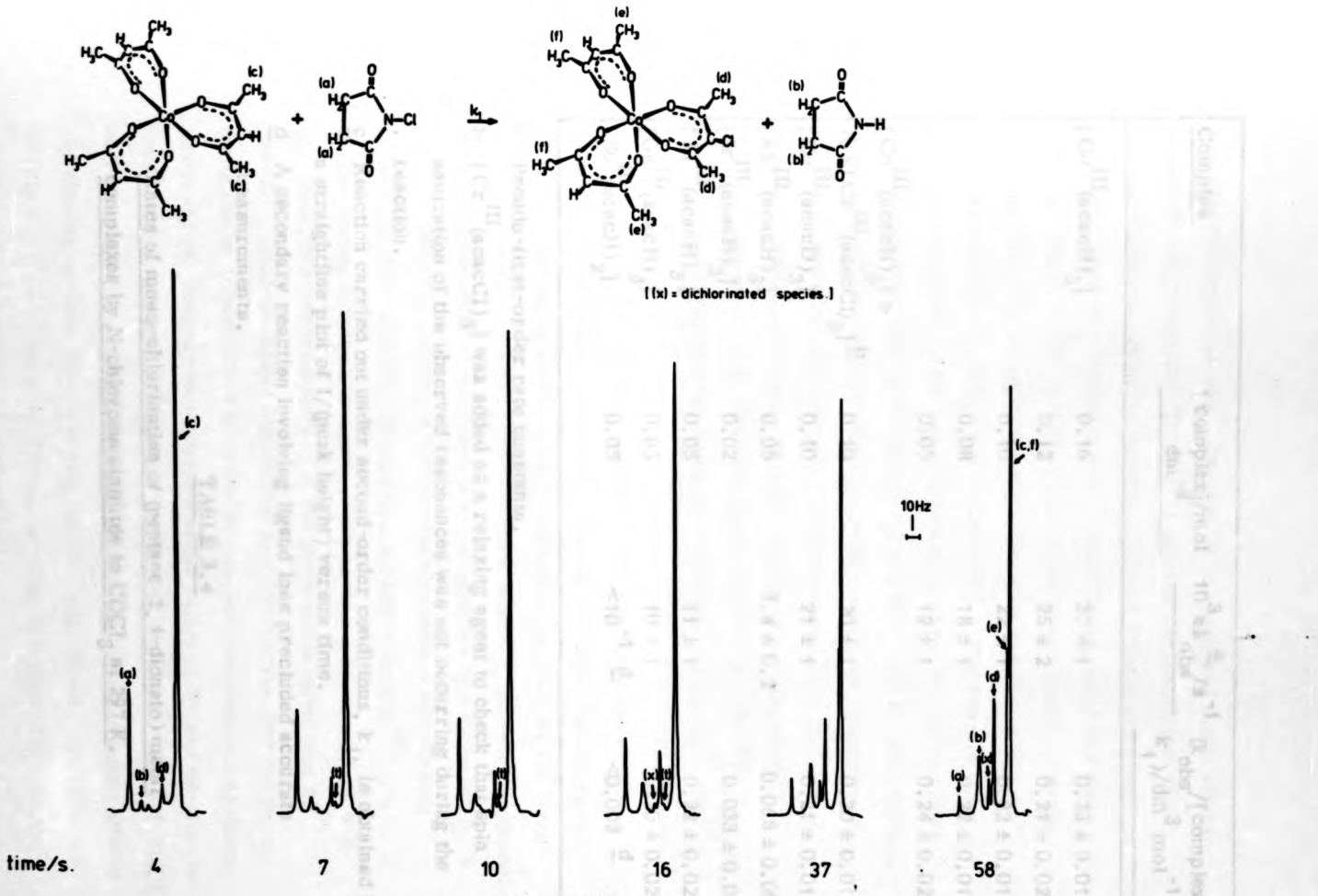

Figure 3.7

A 'kinetic plot' of the high field region of the observed ^{1}H NMR spectra during the reaction of $[Co^{III}(acacH)_2]$ (0.1 mol dm^{-3}) with RNCl (0.1 mol dm^{-3}) in $CDCl_3$ at 297K.

Complex	[complex]/mol dm^{-3}	$10^3 \times k_{obs}$ [a] /s^{-1}	(k_{obs}/[complex] = k_1)/dm^3 mol^{-1} s^{-1}
[$Co^{III}(acacH)_3$]	0.16	37 ± 1	0.23 ± 0.01
"	0.12	25 ± 2	0.21 ± 0.02
"	0.10	22 ± 1	0.22 ± 0.01
"	0.08	18 ± 1	0.22 ± 0.01
"	0.05	12 ± 1	0.24 ± 0.02
[$Co^{III}(acacH)_3$] + 10%[$Cr^{III}(acacCl)_3$] [b]	0.10	20 ± 1	0.20 ± 0.01
[$Co^{III}(acacD)_3$]	0.10	21 ± 1	0.21 ± 0.01
[$Rh^{III}(acacH)_3$]	0.05	3.4 ± 0.2	0.068 ± 0.004
[$Ir^{III}(acacH)_3$]	0.02		0.033 ± 0.001 [c]
[$Al^{III}(acacH)_3$]	0.05	11 ± 1	0.22 ± 0.02
[$Ga^{III}(acacH)_3$]	0.05	10 ± 1	0.20 ± 0.02
[$Be^{II}(acacH)_2$]	0.05	<10^{-1} [d]	<0.002 [d]

a Pseudo-first-order rate constants.

b [$Cr^{III}(acacCl)_3$] was added as a relaxing agent to check that spin saturation of the observed resonances was not occurring during the reaction.

c Reaction carried out under second-order conditions, k_1, is obtained from a straightline plot of 1/(peak height) versus time.

d A secondary reaction involving ligand loss precluded accurate measurements.

TABLE 3.4

Rates of mono-chlorination of (pentane-2, 4-dionato) metal complexes by N-chlorosuccinimide in $CDCl_3$ at 297 K.

The solvent variations of k_1 observed for a variety of metal acetylacetonate complexes (see Table 3.5) support the postulation of an S_E2 mechanism as shown in equation (3.1) for all these reactions, as an enhancement of reaction rate (k_1) would be expected in a more polar solvent (i.e. CD_3OD) if an electrophilic mechanism prevails.

The effect on k of replacing a non-reacting $acacH^-$ by an $acacX^-$ ligand (where X = Cl, NO_2) was investigated. Figures 3.8 and 3.9 show 'kinetic plots' of the high field regions of the second and third chlorination reactions of $[Co(acacH)_3]$ in $CDCl_3$ 297 K, starting with pure mono-chlorinated and di-chlorinated complexes respectively. Pseudo-first-order rate constants (k) determined from the rate of decay of the RNCl resonance in these reactions and the rates of chlorination per mole of available ligand (acacH) (k') for the successive chlorination reactions of $[M(acacH)_3]$ (M = Co^{III}, Rh^{III}) and the mono-chlorination of $[Co^{III}(acacH)_2(acacNO_2)]$ are given in Table 3.6. From this data it can be seen that successive substitutions of $acacCl^-$ for $acacH^-$ reduces the rate of chlorination of the complex at an $acacH^-$ ring by factors of ca. 2.5 for Co^{III} and ca. 4 for Rh^{III}. However, substitution of $acacNO_2$ for acacH reduces the subsequent rate of chlorination of the complex by a factor of ca. 5 for Co^{III} which is consistent with the known electron withdrawing capacities of Cl- and NO_2-groups in aromatic systems.[85] The corresponding substitution experiments could not be carried out with tris-acetylacetonate complexes of the more labile metal ions Al^{III} and Ga^{III}, because ligand scrambling on these metals does not permit the isolation of partially 3-substituted tris-acetylacetonato complexes. However, qualitative measurements of the ratios of di- and tri-chlorinated species produced through the reaction of $[Al^{III}(acacH)_3]$ with RNCl, under second order conditions, indicate that the Cl-substitutent effects are similar to those for the analagous Co^{III} complexes. The greater lability of $[Ga^{III}(acacH)_3]$ precluded even this type of qualitative measurement for the $[Ga^{III}(acacH)_3]$ complex.

Solvent	$k_1/dm^3mol^{-1}s^{-1}$					
	Al^{III}	Ga^{III}	Co^{III}	Rh^{III}	Ir^{III}	Be^{II}
CD_3OD [a]	13.5 ± 0.5	78.0 ± 1.0	2.0 ± 0.1	0.71 ± 0.01	–	0.90 ± 0.01
$CDCl_3$	0.22 ± 0.02	0.20 ± 0.02	0.22 ± 0.01	$(6.8 \pm 0.4) \times 10^{-2}$	$(3.3 \pm 0.1) \times 10^{-2}$	$< 2 \times 10^{-3}$
C_6D_6	$(6.3 \pm 0.1) \times 10^{-3}$	$(1.6 \pm 0.1) \times 10^{-2}$	$(6.2 \pm 0.2) \times 10^{-2}$	$(9.0 \pm 0.1) \times 10^{-3}$	–	[b]

[a] For comparison, the rate of chlorination of Na(acacH) in CD_3OD was too fast to measure ($k_1 \gg 100\ dm^3mol^{-1}s^{-1}$).

[b] Reaction rate too slow to measure.

TABLE 3.5

The solvent dependence of the rates of mono-chlorination of some metal acetylacetonates

Figure 3.8

A 'kinetic plot' of the high field region of the observed ^1H NMR spectra during the reaction of $[Co^{III}(acacH)_2(acac)Cl]$ (0.1 mol dm^{-3}) with RNCl (0.1 mol dm^{-3}) in $CDCl_3$ at 297K.

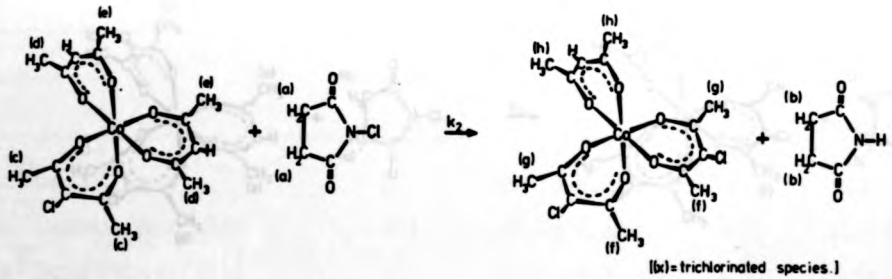

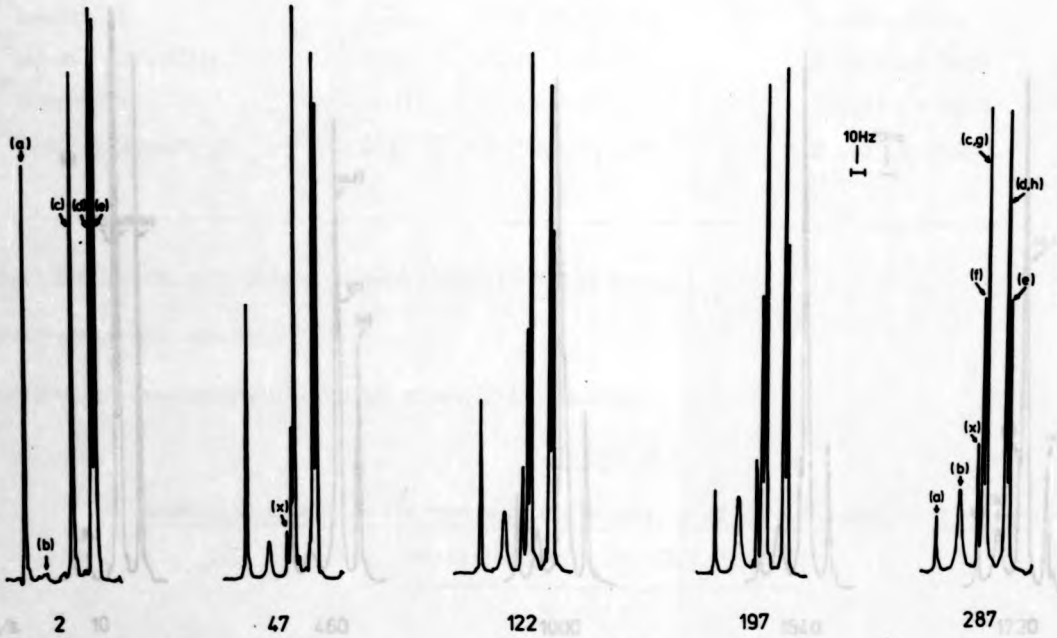

Figure 3.8

A 'kinetic plot' of the high field region of the observed ^{1}H NMR spectra during the reaction of $[Co^{III}(acacH)_2(acacCl)]$ (0.1 mol dm^{-3}) with RNCl (0.1 mol dm^{-3}) in $CDCl_3$ at 297K.

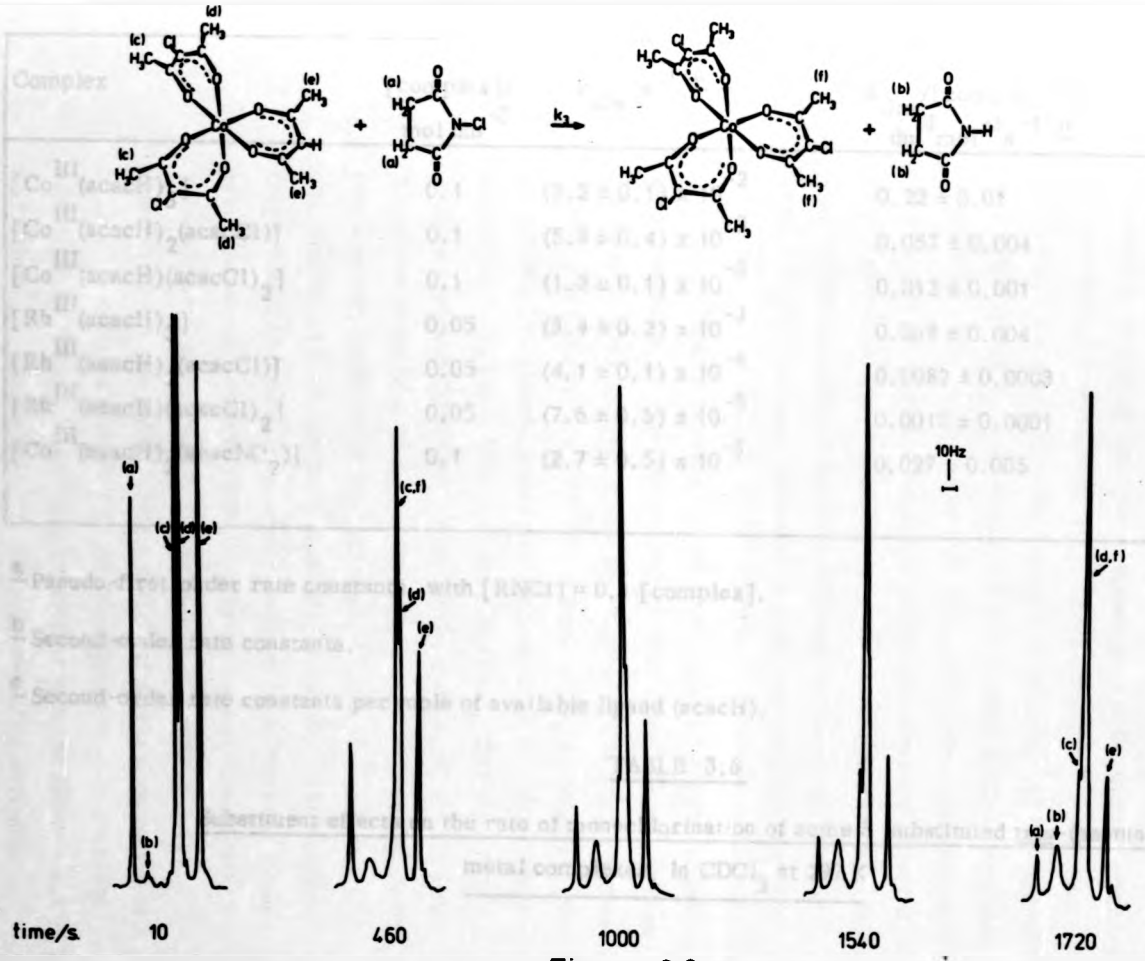

Figure 3.9

A 'kinetic plot' of the high field region of the observed ^1H NMR spectra during the reaction of $[Co^{III}(acacH)(acacCl)_2]$ (0.1 mol dm^{-3}) with RNCl (0.1 mol dm^{-3}) in $CDCl_3$ at 297K.

Complex	[complex]/ mol dm^{-3}	k_{obs}/s^{-1} [a]	$(k_{obs}/[complex]=k)/$ $dm^3 mol^{-1} s^{-1}$ [b]	$k'/dm^3 mol^{-1} s^{-1}$ [c]
$[Co^{III}(acacH)_3]$	0.1	$(2.2 \pm 0.1) \times 10^{-2}$	0.22 ± 0.01	0.07 ± 0.01
$[Co^{III}(acacH)_2(acacCl)]$	0.1	$(5.3 \pm 0.4) \times 10^{-3}$	0.053 ± 0.004	0.026 ± 0.004
$[Co^{III}(acacH)(acacCl)_2]$	0.1	$(1.2 \pm 0.1) \times 10^{-3}$	0.012 ± 0.001	0.012 ± 0.001
$[Rh^{III}(acacH)_3]$	0.05	$(3.4 \pm 0.2) \times 10^{-3}$	0.068 ± 0.004	0.022 ± 0.004
$[Rh^{III}(acacH)_2(acacCl)]$	0.05	$(4.1 \pm 0.1) \times 10^{-4}$	0.0082 ± 0.0003	0.0041 ± 0.0003
$[Rh^{III}(acacH)(acacCl)_2]$	0.05	$(7.6 \pm 0.5) \times 10^{-5}$	0.0015 ± 0.0001	0.0015 ± 0.0001
$[Co^{III}(acacH)_2(acacNO_2)]$	0.1	$(2.7 \pm 0.5) \times 10^{-3}$	0.027 ± 0.005	0.013 ± 0.005

[a] Pseudo-first-order rate constants, with [RNCl] = 0.1 [complex].

[b] Second-order rate constants.

[c] Second-order rate constants per mole of available ligand (acacH).

TABLE 3.6

Substituent effects on the rate of monochlorination of some 3-substituted tris-(pentane-2,4-metal complexes, in $CDCl_3$ at 297 K

As chlorination of an acacH ring in these tris-acetylacetonate complexes produces marked changes in the ^{1}H NMR spectrum of the complex (see Figures 3.1 to 3.4), the reaction rates for the successive chlorination reactions of $[Co^{III}(acacH)_3]$ were further checked by following the rate of appearance of the methyl resonances of chlorinated acetylacetone rings of the complex. A reaction profile for the reaction of equimolar (0.1 mol dm^{-3}) $[Co^{III}(acacH)_3]$ and RNCl in $CDCl_3$ was simulated with a Nicolet BNC-12 program (KINET). The results were then compared to the experimentally determined reaction profile for the same reaction (see Figure 3.10). Good agreement is obtained for the reaction profile simulated from rate constants obtained from the decaying N-chlorosuccinimide (RNCl) resonance (see Table 3.6) and that constructed from the rate of growth of the chlorinated species.

The difference between the rates of bromination (with N-bromosuccinimide) and chlorination (with N-chlorosuccinimide) of metal acetylacetonato complexes was investigated. The least reactive complex to chlorination ($[Rh^{III}(acacH)(acacCl)_2]$), however, was completely brominated within the 'dead-time' of the SFPFTNMR technique (0.3 s) at 0.0125 mol dm^{-3} in $CDCl_3$, 297 K. This implies a pseudo-first-order rate constant of ca. 20 s^{-1} (a half-life of the order of 0.03 s), as the complex $[Rh^{III}(acacH)(acacCl)_2]$ has a pseudo-first-order rate constant of 7.6 x 10^{-5} s^{-1} for chlorination at 0.05 mol dm^{-3} in $CDCl_3$ at 297 K. This implies that the rate of bromination of this complex is at least 10^6 times greater than that of chlorination. The absence of Chemically Induced Dynamic Nuclear Polarisation (CIDNP) effects (see Appendix 3) in this study indicates that the reaction mechanism of N-bromosuccinimide (RNBr) is not free-radical and is probably electrophilic in nature, which is consistent with the observation of Kluiber[96]. The enhancement in rate over that of N-chlorosuccinimide is probably due to the greater lability of the nitrogen-bromine bond in RNBr compared to that of the nitrogen-chlorine bond in RNCl.

Figure 3.10

Reaction profile for the reaction between $[Co^{III}(acacH)_3]$ and RNCl under second-order conditions in $CDCl_3$ at 297K; --- simulated, ○, ● and □ experimentally determined.

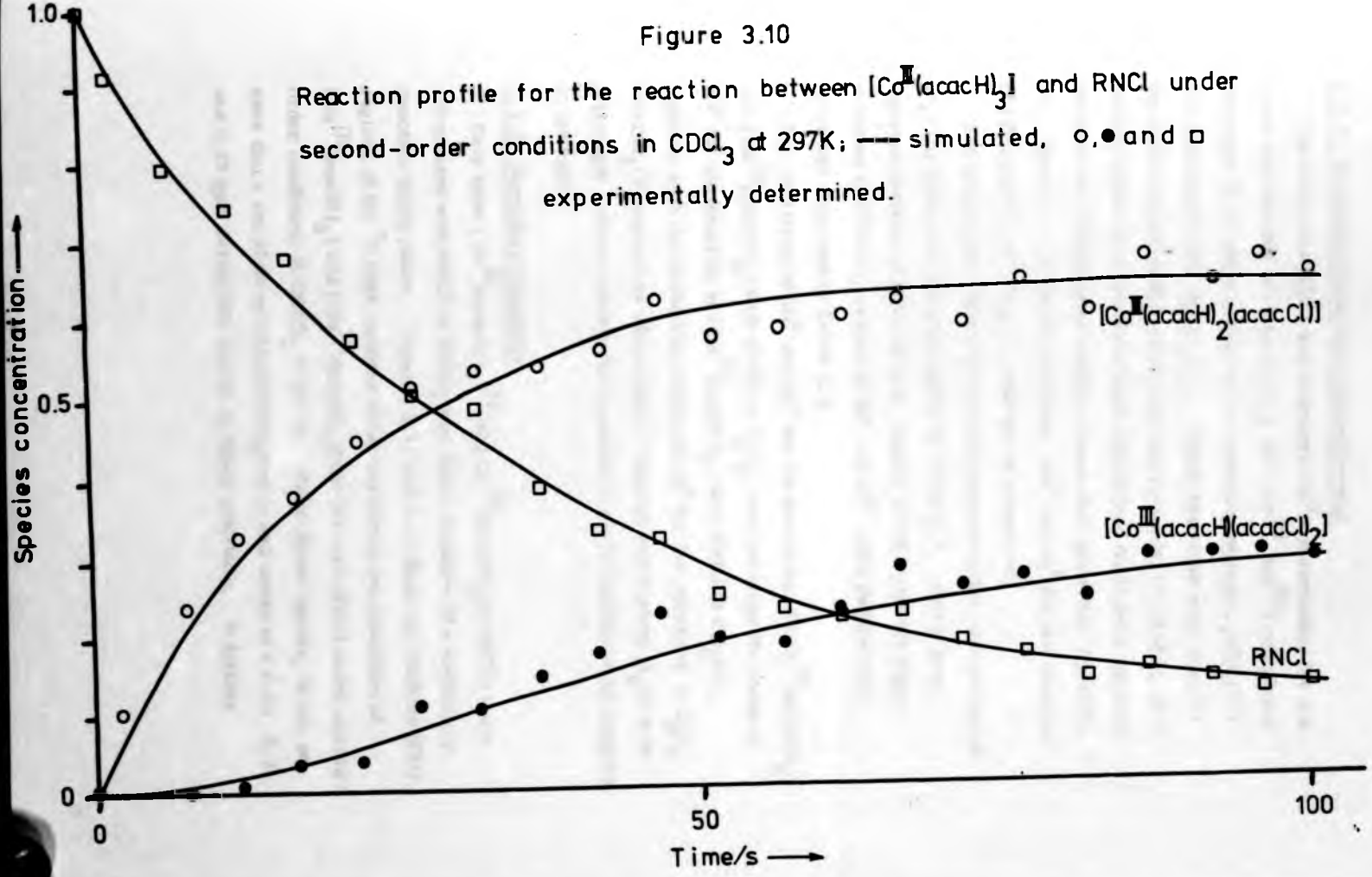

3.3.2 Activation Parameter Measurements

The enthalpies ($\Delta H^{\ddagger}$) and entropies ($\Delta S^{\ddagger}$) of activation for the mono-chlorination of [M(acacH)$_3$] (M = Co^{III}, Rh^{III}) complexes (reaction (3.2)) were measured in deuteriomethanol-d_4(CD_3OD) and deuteriobenzene-d_6 (C_6D_6). These reactions were carried out under second-order conditions with [complex] =[RNCl], and second-order rate constants were determined from least squares analysis of 1/(RNCl peak height) versus time plots (see Appendix 2). Because of solubility problems, $\Delta H^{\ddagger}$ and $\Delta S^{\ddagger}$ for the reaction of [Rh(acacH)$_3$] in CD_3OD could not be measured.

The temperature dependence of the second-order rate constants (k_1) for these reactions are given in Table 3.7. From least squares analysis of plots of ln k_1 versus 1/T(K) with the Algol program (ACTPAR), values of $\Delta H^{\ddagger}$ and $\Delta S^{\ddagger}$ were determined; these are displayed in Table 3.8.

The similarity of $\Delta H^{\ddagger}$ and $\Delta S^{\ddagger}$ for the reactions of [Co^{III}(acacH)$_3$] and [Rh^{III}(acacH)$_3$] with RNCl in C_6D_6, and the large decrease of $\Delta H^{\ddagger}$ for the reaction of [Co^{III}(acacH)$_3$] with RNCl in CD_3OD, together with the dissimilar values of $\Delta S^{\ddagger}$ for the reactions in C_6D_6 and CD_3OD support an electrophilic reaction mechanism (S_E2) with a strongly solvated tetrahedral species as the transition state complex in methanol.

3.3.3 Secondary reactions

Only when [Co^{III}(acacH)$_3$][52] or [Co^{III}(acacH)$_2$(acacCl)] were chlorinated with RNCl in $CDCl_3$ was there evidence of a secondary reaction taking place. Figures 3.11 and 3.12 show the methine (CH) regions of the ^{1}H NMR spectra recorded during the reactions of [Co^{III}(acacH)$_3$] and [Co^{III}(acacH)$_2$(acacCl)] with RNCl under second-order conditions in $CDCl_3$ at 297 K. From these figures, it can be seen that a set of three resonances grow in and decay at δ 6.01, 5.71 and 5.31 ppm during the course of these reactions. A further

Complex	Solvent	T/°C	[complex]/moldm^3	k_1/dm^{3}mol^{-1}s^{-1}
[Co^{III}(acacH)$_3$]	C_6D_6	24.0	0.1	0.062 ± 0.002
"	"	35.9	"	0.17 ± 0.02
"	"	45.4	"	0.29 ± 0.06
"	"	55.8	"	0.65 ± 0.01
[Rh^{III}(acacH)$_3$]	C_6D_6	24.0	0.05	0.0034 ± 0.0002
"	"	35.9	"	0.0065 ± 0.0004
"	"	44.9	"	0.018 ± 0.0019
"	"	55.8	"	0.025 ± 0.0016
"	"	61.7	"	0.049 ± 0.003
[Co^{III}(acacH)$_3$]	CD_3OD	24.0	0.025	2.1 ± 0.1
"	"	15.5	"	1.36 ± 0.1
"	"	5.2	"	0.76 ± 0.08
"	"	-4.5	"	0.45 ± 0.05
"	"	-14.3	"	0.25 ± 0.01

TABLE 3.7

The temperature dependence of the second-order rate constants for the mono-chlorination of tris-acetylacetonato Co^{III} and Rh^{III} complexes in CD_3OD and C_6D_6.

Complex	Solvent	$\Delta H^{\ddagger}$/kJ mol^{-1}	$\Delta S^{\ddagger}$/J K^{-1} mol^{-1}
$[Co^{III}(acacH)_3]$	C_6D_6	+56.5 ± 2.7	-77.7 ± 8.8
$[Rh^{III}(acacH)_3]$	C_6D_6	+55.3 ± 5.5	-106.4 ± 17.4
$[Co^{III}(acacH)_3]$	CD_3OD	+32.9 ± 0.5	-127.9 ± 1.9

TABLE 3.8

Activation parameters for the mono-chlorination reactions of $[M(acacH)_3]$ ($M = Co^{III}$, Rh^{III}) complexes in C_6D_6 and CD_3OD.

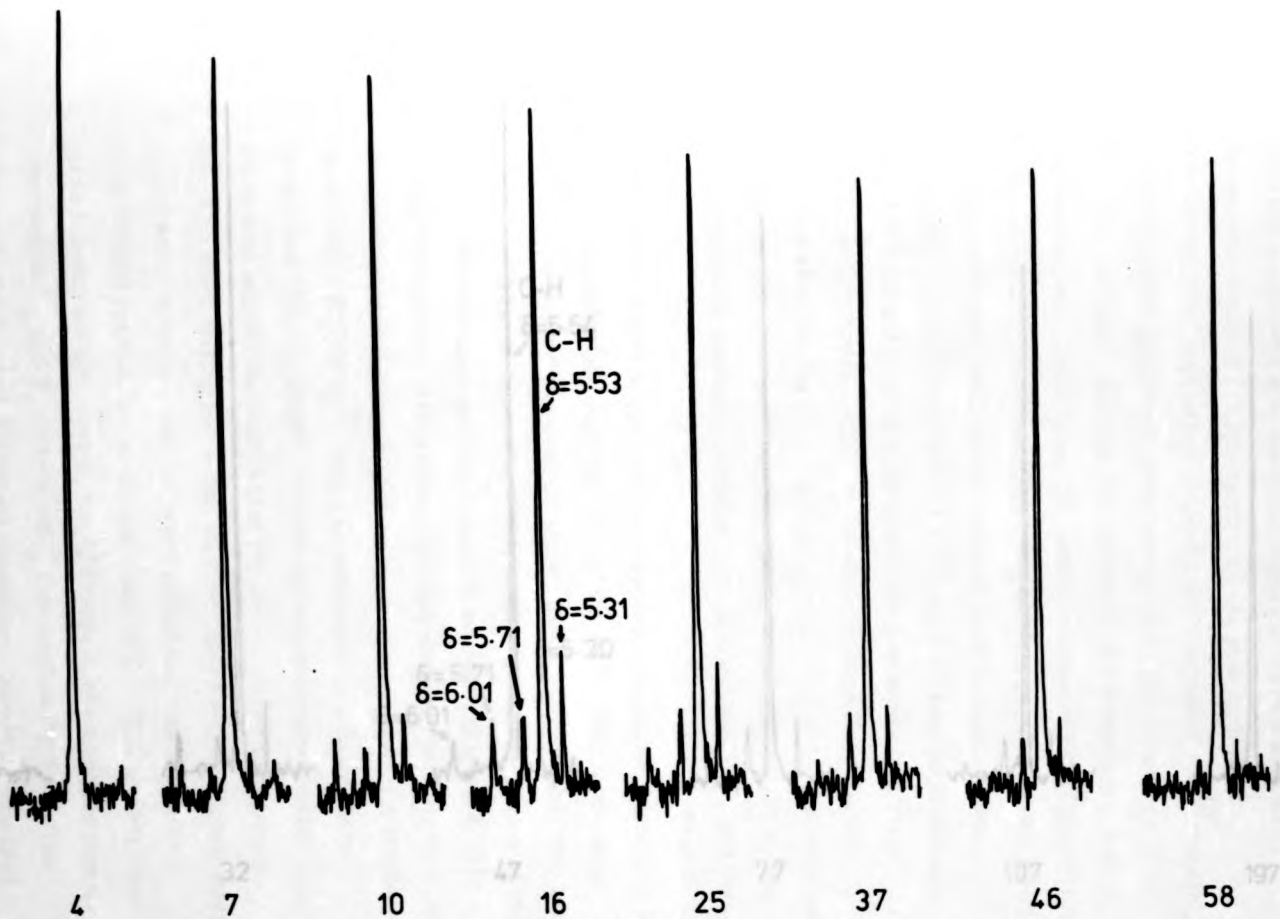

Figure 3.11

A 'kinetic plot' of the methine(C-H) region of the observed ^{1}HNMR spectra during the reaction of $[Co^{III}(acacH)_3]$(0.1 mol dm^{-3}) with RNCl(0.1 mol dm^{-3}) in $CDCl_3$ at 297K.

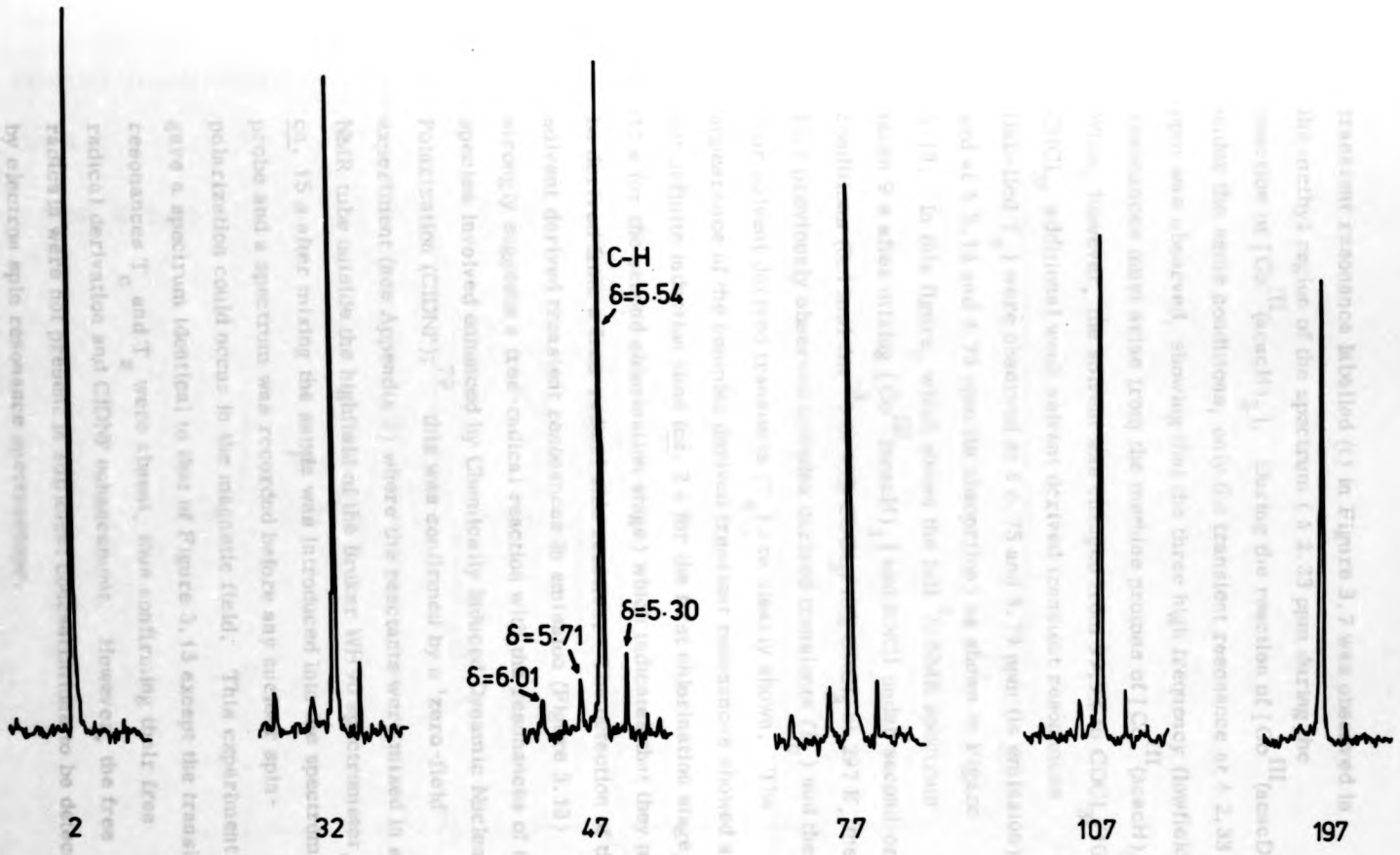

Figure 3.12

A 'kinetic plot' of the methine(C-H) region of the observed ^{1}H NMR spectra during the reaction of $[Co^{III}(acacH)_2(acacCl)]$(0.1 mol dm^{-3}) with RNCl(0.1 mol dm^{-3}) in $CDCl_3$ at 297K.

transient resonance labelled (t) in Figure 3.7 was observed in the methyl region of the spectrum (δ 2.33 ppm during the reaction of $[Co^{III}(acacH)_3]$. During the reaction of $[Co^{III}(acacD)_3]$ under the same conditions, only the transient resonance at δ 2.33 ppm was observed, showing that the three high frequency (lowfield) resonances must arise from the methine protons of $[Co^{III}(acacH)_3]$. When, however, the solvent was changed from 99.9% to $CDCl_3$/10% $CHCl_3$, additional weak solvent derived transient resonances (labelled T_s) were observed at δ 6.75 and 5.79 ppm (in emission) and at δ 5.14 and 4.73 ppm (in absoprtion) as shown in Figure 3.13. In this figure, which shows the full ^1H NMR spectrum taken 9 s after mixing $[Co^{III}(acacH)_3]$ and RNCl under second-order conditions (0.1 mol dm^{-3}) in 90% $CDCl_3$/10% $CHCl_3$ at 297 K, the four previously observed complex derived transients (T_c) and the four solvent derived transients (T_s) are clearly shown. The appearance of the complex derived transient resonances showed a small but definite induction time (ca. 2 s for the first chlorination stage, and 17 s for the second chlorination stage) which indicates that they may be derived from a free-radical side reaction. The detection of the solvent derived transient resonances in emission (Figure 3.13) strongly suggests a free-radical reaction with the resonances of the species involved enhanced by Chemically Induced Dynamic Nuclear Polarization (CIDNP);[79] this was confirmed by a 'zero-field' experiment (see Appendix 3) where the reactants were mixed in an NMR tube outside the highfield of the Bruker WH 90 spectrometer, ca. 15 s after mixing the sample was introduced into the spectrometer probe and a spectrum was recorded before any nuclear spin-polarization could occur in the magnetic field. This experiment gave a spectrum identical to that of Figure 3.13 except the transient resonances T_c and T_s were absent, thus confirming their free radical derivation and CIDNP enhancement. However, the free radicals were not present in sufficient concentrations to be detectable by electron spin resonance spectroscopy.

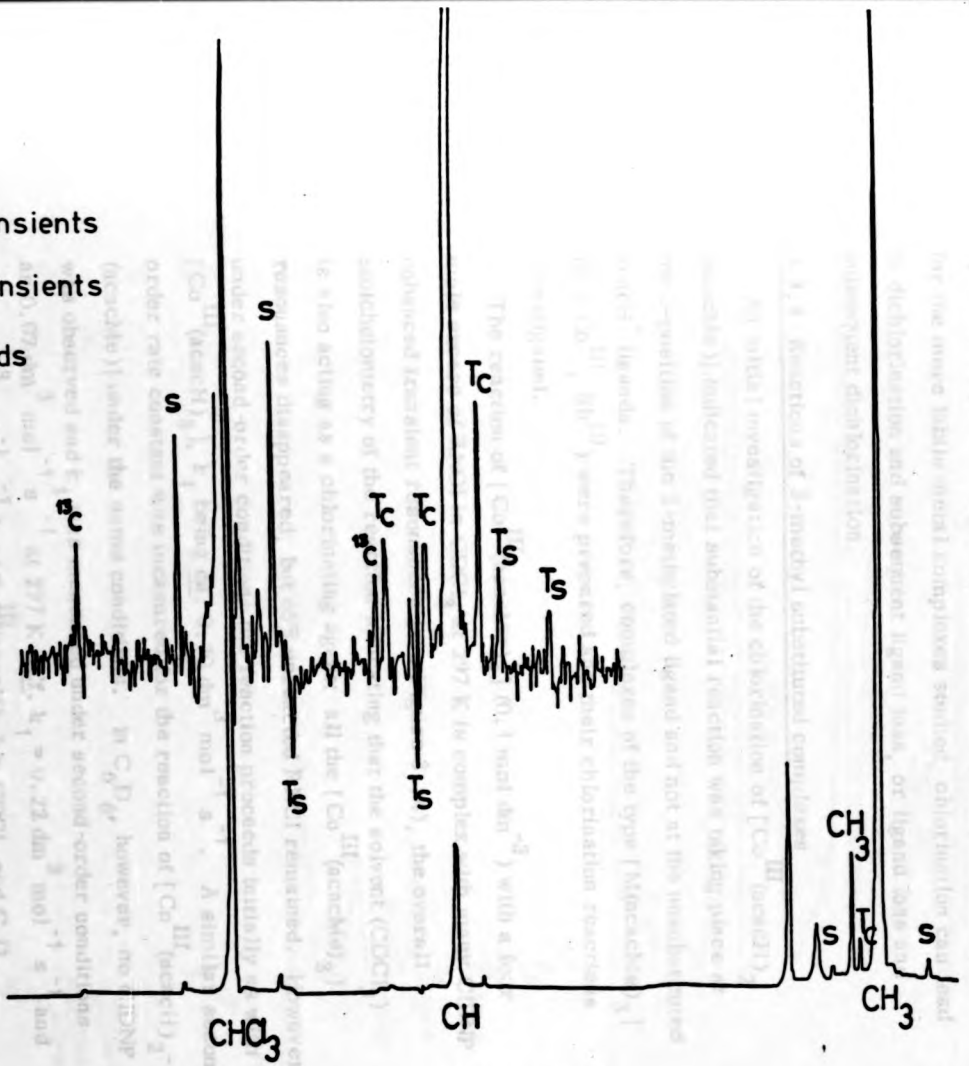

Figure 3.13

^1H NMR spectrum 9s after mixing $[Co^{III}(acacH)_2]$ with RNCl (1:1) in 10% $CHCl_3$ / 90 % $CDCl_3$ at 297 K.

A different secondary reaction was observed for the acetylacetonato complexes of Al^{III}, Ga^{III} and Be^{II} when the mole ratio of RNCl to complex exceeded 1:1. A new resonance appeared at δ 2.46 ppm in the later stages of these reactions, which has been assigned on the basis of its chemical shift to unco-ordinated 3,3-dichloropentante-2,4-dione. It would appear, therefore, that for the more labile metal complexes studied, chlorination can lead to dichlorination and subsequent ligand loss, or ligand loss and subsequent dichlorination.

3.3.4 Reactions of 3-methyl substituted complexes

An initial investigation of the chlorination of $[Co^{III}(acacH)_2(acacMe)]$ indicated that substantial reaction was taking place at the 3-position of the 3-methylated ligand and not at the unsubstituted $acacH^-$ ligands. Therefore, complexes of the type $[M(acacMe)_3]$ ($M = Co^{III}$, Rh^{III}) were prepared and their chlorination reactions investigated.

The reaction of $[Co^{III}(acacMe)_3]$ (0.1 mol dm^{-3}) with a four mole excess of RNCl in $CDCl_3$ at 297 K is complex with many CIDNP enhanced transient resonances (see Figure 3.14), the overall stoichelometry of the reaction indicating that the solvent ($CDCl_3$) is also acting as a chlorinating agent; all the $[Co^{III}(acacMe)_3]$ resonances disappeared, but 66% unreacted RNCl remained. However, under second-order conditions the reaction proceeds initially as with $[Co^{III}(acacH)_3]$, k_1 being ca. 0.70 dm^3 mol^{-1} s^{-1}. A similar second-order rate constant was measured for the reaction of $[Co^{III}(acacH)_2(acacMe)]$ under the same conditions. In C_6D_6, however, no CIDNP was observed and k_1 was measured under second-order conditions as 0.07 dm^3 mol^{-1} s^{-1} at 297 K (Cf. k_1 = 0.22 dm^3 mol^{-1} s^{-1} and 0.062 dm^3 mol^{-1} s^{-1} for $[Co^{III}(acacH)_3]$ in $CDCl_3$ and C_6D_6 respectively). The subsequent reactions were always complex, with the production of CIDNP enhanced resonances, and always resulted in the loss of the ligand 3-methyl-3-chloropentane-2,4-dione (acacMe.Cl) and the precipitation of polymeric paramagnetic cobalt(II) species from the reaction mixture.

Figure 3.14

^{1}H NMR spectrum 6s after mixing [Co^{III}(acacMe)$_3$] with RNCl (1:4) at 297K in $CDCl_3$.

x = [Co^{III}(acacMe)$_3$]

y = (acacMe.Cl)

● = CIDNP species

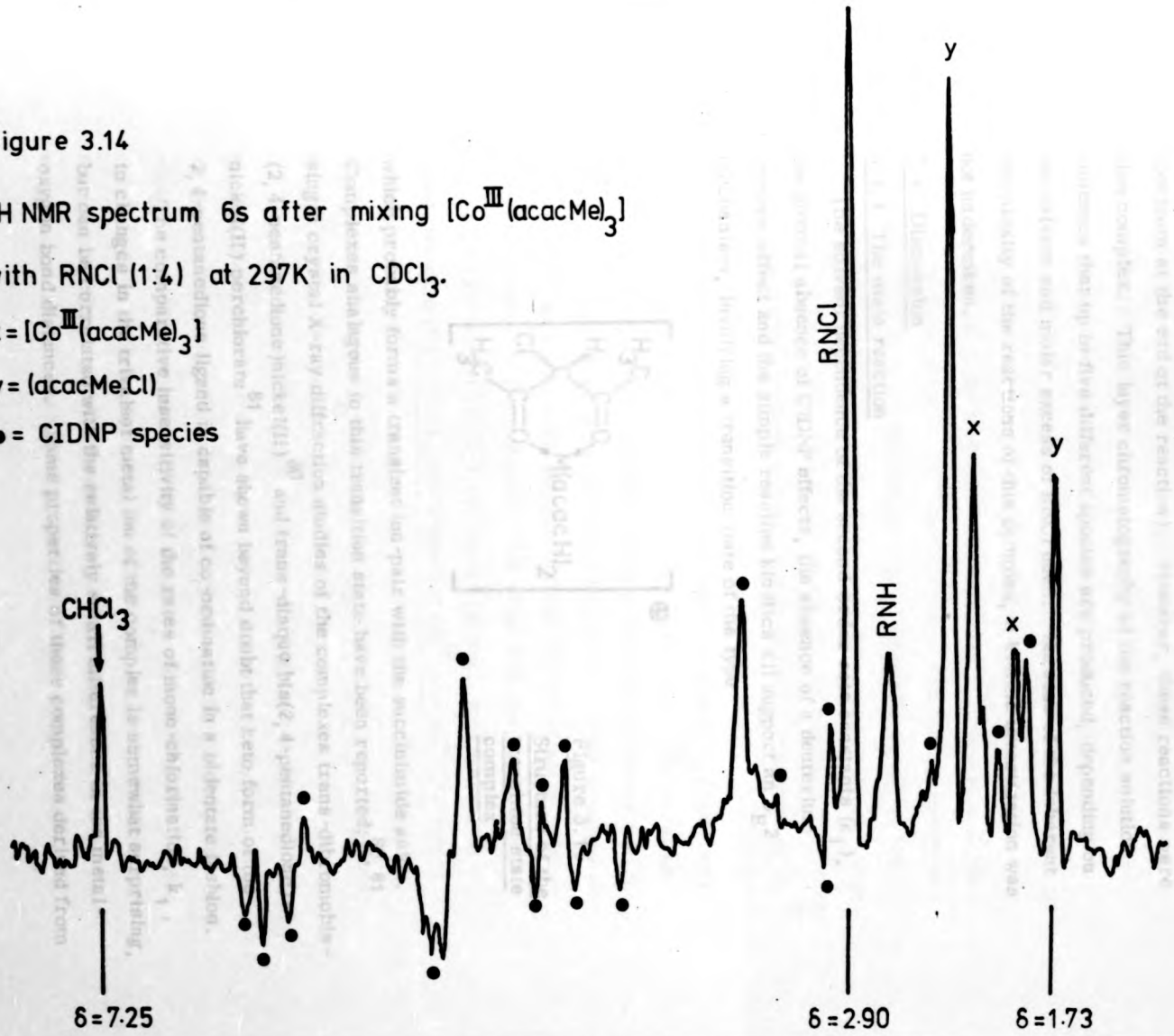

The reactions of the more stable [$Rh^{III}(acacMe)_3$] complex with N-chlorosuccinimide in $CDCl_3$ and CD_3OD gave no indication of ligand loss (unco-ordinated (acacMe.Cl) could not be detected in the ^1H NMR spectrum at the end of the reaction). However, these reactions were also complex. Thin layer chromatography of the reaction solution indicates that up to five different species are produced, depending on the solvent and molar excess of RNCl used. Because of the inherent complexity of the reactions of this complex, a kinetic investigation was not undertaken.

3.4 Discussion

3.4.1 The main reaction

The solvent dependence of the second-order rate constants (k_1), the normal absence of CIDNP effects, the absence of a deuterium isotope effect and the simple reaction kinetics all support an S_E2 mechanism, involving a transition state of the type

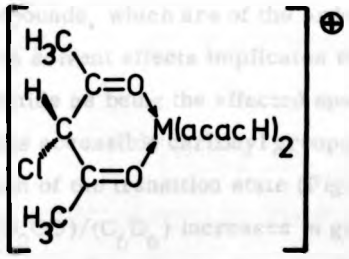

Figure 3.15
Structure of the transition state complex

which probably forms a transient ion-pair with the succinimide anion. Complexes analagous to this transition state have been reported;[80,81] single crystal X-ray diffraction studies of the complexes trans-dibromobis-(2,4-pentanedione)nickel(II)[80] and trans-diaquo bis(2,4-pentanedione)-nickel(II) perchlorate[81] have shown beyond doubt that keto form of the 2,4-pentanedione ligand is capable of co-ordination in a bidentate fashion.

The comparative insensitivity of the rates of mono-chlorination, k_1, to changes in the trivalent metal ion of the complex is somewhat surprising, but can be correlated with the relatively small differences in the metal-oxygen bond distances. Some properties of these complexes derived from

X-ray crystallographic studies are given in Table 3.9, together with selected data derived from Table 3.5. In general, k_1 is increased somewhat by an increase in metal-oxygen bond distances r_{M-O}. A simple interpretation of this is that in the transition state (Figure 3.15) the ligand to metal bond is weakened by the loss of negative ligand charge. Thus the transition state is less accessible when the ligand is tightly bound, and particularly with Be^{II}, which evidently prefers to bind two acacH ligands very tightly instead of three less tightly. This is confirmed by the very rapid chlorination of the free enolate anion of acetylacetone (see Table 3.5). In the case of Co^{III}, Rh^{III} and Ir^{III} the ligand binding energy is affected not only by r_{M-O} but also by crystal field effects, which are larger for Rh^{III} and Ir^{III}. It should be noted that although the values of k_1 for Co^{III} and Al^{III} are similar, the values are not strictly comparable for these two metals because of the influence of the t_{2g}^6 electrons in Co^{III}.

The differences in solvent effect are more substantial, although only that for the Be^{II} complex compares with known effects in S_E2 reactions of aromatic compounds, which are of the order of 10^6. The metal ion dependence of the solvent effects implicates the complex rather than the N-chlorosuccinimide as being the affected species. Polar solvation at the relatively less accessible carbonyl groups would certainly increase k_1 by stabilization of the transition state (Figure 3.15), and would explain why $k(CD_3OD)/(C_6D_6)$ increases in general with increasing molecular size (Table 3.9), but is less for Co^{III} and Rh^{III} because of the more compact structure (greater "bite" angle) and the steric repulsion of the filled t_{2g} orbitals. $k(CD_3OD)/k(C_6D_6)$ is also greater for Be^{II} because of its more accessible structure.

These solvation effects are substantiated by the recent work of Vigee and Watkins[82] who have shown by paramagnetic solvent line-broadening studies in the presence of $[Cr^{III}(acacH)_3]$ that specific solvation in the second co-ordination sphere of $[Cr^{III}(acacH)_3]$ does take place. They conclude from their experimental data that in the case of methanol as the solvent, there is preferential hydrogen bonding of the methanol-OH to the oxygens of the chelated 2,4-pentanedione, with the methanol-OH

Complex	r_{M-O}/pm [a]	<OMO ("bite" angle)	$k_1(C_6D_6)$/ $dm^3 mol^{-1} s^{-1}$ [b]	$k_1(CD_3OD)/k_1(C_6D_6)$ [c]
$[Co^{III}(acacH)_3]$	190	97°	0.062	32
$[Al^{III}(acacH)_3]$	189	91°	0.0063	2100
$[Ga^{III}(acacH)_3]$	195	92°	0.016	4900
$[Rh^{III}(acacH)_3]$	199	95°	0.0093	79
$[Be^{II}(acacH)_2]$	170	105°	–	[d]

[a] Metal-oxygen bond distances from references 92-95.

[b] Second-order rate constants for mono-chlorination in deuteriobenzene.

[c] Relative rates for mono-chlorination in CD_3OD and C_6D_6.

[d] $k_1(CD_3OD)/k_1(CDCl_3) > 450$, *cf.* 370 for Ga^{III}.

TABLE 3.9

Some properties of metal acetylacetonates

3.85 Å and the methanol-CH_3 4.80 Å from the Cr^{III} atom; these values fit very well with the calculated distances of 3.7 Å and 4.7 Å respectively for this type of specific solvation.[82] However, in the case of benzene, Vigee and Watkins conclude that solvation is random.[82]

Kuroda et al. have recently reported a second-order rate constant of 1.68 $dm^3\ mol^{-1}\ s^{-1}$ at 308 K for the reaction of N-chlorosuccinimide with the $[Co^{III}(en)_2(acacH)]^{2+}$ (en = 1,2 diaminoethane) ion in water.[83] This rate is comparable to the observed rate for $[Co^{III}(acacH)_3]$ in methanol (k_1 = 2.1 $dm^3\ mol^{-1}\ s^{-1}$ at 297 K, see Table 3.7). It would appear, therefore, that the expected reduction in k_1 due to the formal 2+ charge on the metal is offset by the effect of the very polar solvent in this case.

3.4.2 The activation parameters and their solvent dependence

The measured values of the enthalpy ($\Delta H^{\ddagger}$) and entropy ($\Delta S^{\ddagger}$) of activation for the mono-chlorination of $[M(acacH)_3]$ (M = Co^{III}, Rh^{III}) and their solvent dependence (see Table 3.8) show quite clearly the effect of polar solvation in this reaction. $\Delta H^{\ddagger}$ for Co^{III} and Rh^{III} in benzene are the same within the experimental error, (ca. 55 kJ mol^{-1}), the $\Delta S^{\ddagger}$ values are also similar within experimental error (-78 ± 9 J K^{-1} mol^{-1} and -106 ± 17 J K^{-1} mol^{-1} for Co^{III} and Rh^{III} respectively). However, in methanol $\Delta H^{\ddagger}$ for Co^{III} is markedly reduced (33 kJ mol^{-1}) and more than compensates for the less favourable $\Delta S^{\ddagger}$ in this solvent (-128 ± 2 J K^{-1} mol^{-1}). Thus strong polar solvation produces a stabilization of the transition state (Figure 3.15), and consequently a reduction in the enthalpy of activation for the reaction. This further substantiates the postulation of a S_E2 mechanism for these reactions, and is consistent with the solvation effects expected for S_E2 reactions.[98]

3.4.3 Substituent effects

The reduction in the rates of chlorination of an unsubstituted acacH ligand caused by -Cl and $-NO_2$ substitution at the 3-position of another ligand in the complex are attributed to ordinary inductive effects, and

further support the S_E2 mechanism. That they are slightly greater for Rh^{III} than for Co^{III} shows that the inductive effect is primarily through bond rather than through space, because the inter-ligand distances are all greater for the Rh^{III} complexes. The quantitative similarity of Al^{III} and Co^{III} in this respect implicates σ- rather than π -bonds as the charge transmitters. All this is consistent with simple electrostatics, which predicts that if one ligand is made to bind less strongly (due to chlorination, say), then the others will bind correspondingly more strongly, and will thus (using the arguments of section 3.4.1) be less reactive. This observed dependence of reaction rate upon the extent of substitution appears to vitiate earlier measurements of chlorination rates based on the "overall chlorination rate" of an $[M(acacH)_3]$ complex.[84]

The increased reactivity of $[Co^{III}(acacMe)_3]$ over $[Co^{III}(acacH)_3]$ could have two causes. Apart from the obvious electron donating properties of the 3-methyl substituent, the relief of steric strain between the three methyl groups upon formation of a tetrahedral intermediate could well enhance the reactivity of the complex. This second cause may also contribute to the surprising reactivity of the chlorinated ligand in the Al^{III}, Ga^{III} and Be^{III} complexes, shown in the secondary reaction which leads to ligand loss. That this secondary reaction does not occur with the Co^{III}, Rh^{III} and Ir^{III} complexes is no doubt due to their greatly reduced lability.

The straight line and large negative slopes (ρ) of plots of log k/dm^3 mol^{-1} s^{-1} for various 3-substituted Co^{III} and Rh^{III} complexes versus σp, the Hammett substituent constant for para substitution in aromatic systems[86] (see Figure 3.16), confirms the pseudo-aromatic character of these complexes and further substantiates an S_E2 mechanism. The σp values have been treated additively for successive Cl- substitutions whereas that of the $[Co^{III}(acacH)_2(acacMe)]$ complex is quoted as $\sigma p(-CH_3)$. The fact that the Rh^{III} complexes fall on a different straight line to that of the Co^{III} complexes is not surprising, and supports

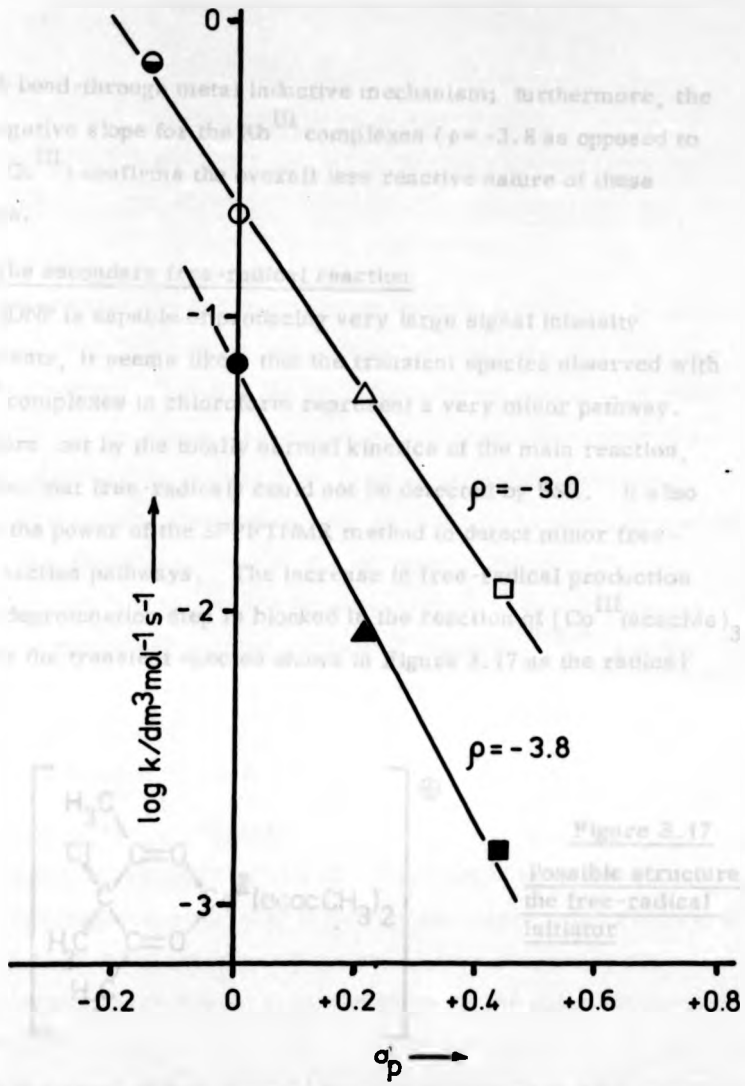

[M(acacH)$_3$] (M=Co^{III} ○, Rh^{III} ●)

[M(acacH)$_2$(acacCl)] (M=Co^{III} △, Rh^{III} ▲)

[M(acacH)(acacCl)$_2$] (M=Co^{III} □, Rh^{III} ■)

⊖ [Co^{III}(acacH)$_2$(acacMe)]

Figure 3.16

Plot of Hammett σ_p values versus log k / dm^3 mol^{-1} s^{-1} for various 3-substituted tris-acetylacetonato metal complexes.

a through bond-through metal inductive mechanism; furthermore, the larger negative slope for the Rh^{III} complexes (ρ= -3.8 as opposed to -3.0 for Co^{III}) confirms the overall less reactive nature of these complexes.

3.4.4 The secondary free-radical reaction

As CIDNP is capable of producing very large signal intensity enhancements, it seems likely that the transient species observed with the Co^{III} complexes in chloroform represent a very minor pathway. This is born out by the totally normal kinetics of the main reaction, and the fact that free-radicals could not be detected by ESR. It also indicates the power of the SFPFTNMR method to detect minor free-radical reaction pathways. The increase in free-radical production when the deprotonation step is blocked in the reaction of $[Co^{III}(acacMe)_3]$ implicates the transient species shown in Figure 3.17 as the radical initiator.

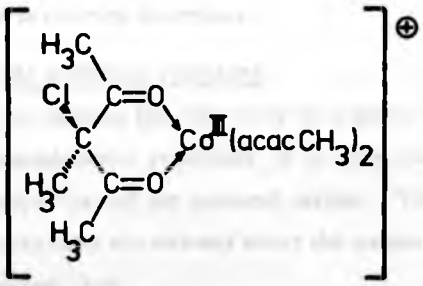

Figure 3.17
Possible structure of the free-radical initiator

Its unique reactivity in this respect may well be related to the presence of an accessible divalent metal oxidation state; an oxidative fission of chloroform involving a $Co^{III} \rightarrow Co^{II}$ change could generate several $Cl^{\cdot}$ radicals which would eventually reoxidise the transient species shown in Figures 3.15 and 3.17 to their original form. This would explain the three transient complex-derived CH resonances observed in the chlorination of $[Co^{III}(acacH)_3]$, the increase in free-radical production in the reaction of $[Co^{III}(acacMe)_3]$ and N-chlorosuccinimide, and the total absence of any CIDNP species in the reaction between $[Rh^{III}(acacMe)_3]$ and RNCl in chloroform.

CHAPTER 4

LIGAND SUBSTITUTION REACTIONS.
A SFPFTNMR INVESTIGATION OF THE SUBSTITUTION REACTIONS OF THE HEXAKIS-(DIMETHYL SULPHOXIDE)ALUMINIUM(III) ION.

4.1 Introduction

The replacement of a solvent molecule bound to a metal ion by another ligand, which may be the same molecule(solvent exchange) or different (complex formation), is one of the most fundamental reactions of metal ions in solution. Such reactions are important elementary steps in a wide range of processes ranging from inner-sphere redox reactions which involve an initial substitution step, to catalysis by metal ions which often involve a substitution reaction of a solvated metal ion. The mechanism of octahedral complex formation reactions by labile metal ions has been extensively studied and is well reviewed,[99-101] and for the purpose of this study will be divided into two sections:-

(i) solvent exchange reactions, and

(ii) complex formation reactions.

4.1.1 Solvent exchange reactions

In order to discuss the reactivity of a metal ion in solution with respect to complexation reactions, it is often necessary to have knowledge of certain properties of the solvated cation. These properties are:-

(i) the structure of the solvent about the cation or the solvation number of the cation, and

(ii) the rate constant for the exchange of the solvent associated with the metal ion with bulk solvent.

Solvation numbers and solvent exchange rates have been measured for a large number of metal ions in different solvents by a variety of techniques including adsorption, diffusion and compressibility measurements.[100] NMR spectroscopic techniques (line-broadening studies) are most commonly used to determine these quantities,[102,128] as the interaction of a solvent molecule with an ion in solution results in a perturbation of the electronic environment and the relaxation times of

magnetically active nuclei (usually ^{1}H or ^{17}O). Thus the chemical shifts and linewidths of NMR resonances arising from these nuclei differ from those of noninteracting, bulk solvent molecules. However, line -broadening measurements of solvent exchange rates can be prone to errors[103] that are not inherent in the SFPFTNMR method of measuring reaction rates.

In this study the DMSO solvent exchange rate at 297 K[38] and activation parameters of dimethyl sulphoxide (DMSO) exchange on the labile aluminium(III) ion were measured in deuterionitromethane-d_3 (CD_3NO_2) solution by the SFPFTNMR method. As the rate of exchange of DMSO on Al^{III} is slow on the NMR timescale ($k = 0.33 \pm 0.44\ s^{-1}$ at 297 K in CD_3NO_2) and separate free and bound DMSO resonances (δ 2.50 and 2.82 ppm respectively) are observed in the ^{1}H NMR spectrum, the solvent exchange rate between the $[Al^{III}(DMSO)_6]^{3+}$ ion and free DMSO can be readily measured by the SFPFTNMR technique by mixing an excess of deuteriodimethyl sulphoxide (DMSO-d_6) with a solution of the $[Al^{III}(DMSO)_6]^{3+}$ ion in CD_3NO_2 and observing the disappearance of the bound DMSO ^{1}H NMR resonance with time.[38] The activation parameters for this process were measured and agree well with those previously reported from line-broadening studies,[56] thus confirming the reliability of $\Delta H^{\ddagger}$ and $\Delta S^{\ddagger}$ measurements made by the SFPFTNMR method described in Chapter 2.

4.1.2 Complex formation reactions

The rates of ligand substitution reactions of the type shown in equations (4.1) to (4.2) are normally governed by the solvent exchange rate (k_{ex}) of the metal solvate $[MS_6]^{n+}$. ($k_{ex} = 6k_1$)

$$[MS_6]^{n+} + L \overset{K_o}{\rightleftharpoons} [MS_6]^{n+}, L \qquad (4.1)$$

$$[MS_6]^{n+}, L \underset{k_{-1}}{\overset{k_1}{\rightleftharpoons}} [MS_5L]^{n+} + S \qquad (4.2)$$

Here K_o is the outer sphere formation constant, M^{n+} = metal ion, S = solvent and L = a neutral ligand. k_f is the rate constant for the formation of the $[MS_5L]^{n+}$ complex and is equal to $K_o k_1$ where K_o is typically < 1.0

for an uncharged ligand (L).[101] The reaction between the $[Al^{III}(DMSO)_6]^{3+}$ ion and aromatic ligands in nitromethane solution can not be followed by UV-visible stopped-flow measurements as the solvent obscures the UV bands of the ligand, and there are no changes in the visible region of the spectrum. However, it is possible to follow the kinetics of these and other ligand substitution reactions of the $[Al^{III}(DMSO)_6]^{3+}$ ion, in nitromethane-d_3 (CD_3NO_2) by detecting the expulsion of DMSO molecules from the inner co-ordination sphere of the Al^{III} by the SFPFTNMR method. One other advantage of the SFPFTNMR method of following reactions of the type (4.3) to 4.6) where L-L-L represents a neutral multidentate ligand such as 2,2':6',2''-terpyridine (terpy) is that each stage of the overall reaction is accompanied by an equal change in the height of the ^1H NMR resonances associated with free and bound solvent molecules. Thus when $k_1 >> k_2 >> k_3$ as was found in the following work, it is easy to determine the point at which the successive ring closure reactions are complete.

$$[MS_6]^{3+} + L\text{-}L\text{-}L \underset{}{\overset{K_o}{\rightleftharpoons}} [MS_6]^{3+},\ L\text{-}L\text{-}L \qquad (4.3)$$

$$[MS_6]^{3+},\ L\text{-}L\text{-}L \underset{}{\overset{k_1}{\rightleftharpoons}} [MS_5\text{-}L\text{-}L\text{-}L]^{3+} + S \qquad (4.4)$$

$$[MS_3\text{-}L\text{-}L\text{-}L]^{3+} \xrightarrow{k_2} [MS_4\overset{L}{\underset{L\text{-}L}{\diagup\diagdown}}]^{3+} + S \qquad (4.5)$$

$$[MS_4\overset{L}{\underset{L\text{-}L}{\diagup\diagdown}}]^{3+} \xrightarrow{k_3} [MS_3\overset{L}{\underset{L}{\diagup\diagdown}}]^{3+} + S \qquad (4.6)$$

The rate of complex formation of the neutral ligands pyridine, 2,2'-bipyridine (bipy), 1,10-phenthroline (phen) and 2,2':6',2''-terpyridine (terpy) with the $[Al^{III}(DMSO)_6]^{3+}$ ion were investigated under second-order conditions by mixing solutions of the ligand in CD_3NO_2 with solutions of the metal solvate in CD_3NO_2 and following the rate of expulsion of DMSO molecules from the inner sphere of the Al^{III} by the SFPFTNMR method. In the case of all these ligands, it was found that k_f, the rate of first bond formation (reaction (4.3) to (4.4)), was greater than the solvent exchange rate (k_1) for DMSO on Al^{III} under the same conditions, thus implying an unusually large value of K_o for these reactions. This effect was further investigated and will be discussed later.

for an uncharged ligand (L).[101] The reaction between the $[Al^{III}(DMSO)_6]^{3+}$ ion and aromatic ligands in nitromethane solution can not be followed by UV-visible stopped-flow measurements as the solvent obscures the UV bands of the ligand, and there are no changes in the visible region of the spectrum. However, it is possible to follow the kinetics of these and other ligand substitution reactions of the $[Al^{III}(DMSO)_6]^{3+}$ ion, in nitromethane-d_3 (CD_3NO_2) by detecting the expulsion of DMSO molecules from the inner co-ordination sphere of the Al^{III} by the SFPFTNMR method. One other advantage of the SFPFTNMR method of following reactions of the type (4.3) to 4.6) where L-L-L represents a neutral multidentate ligand such as 2, 2':6', 2''-terpyridine (terpy) is that each stage of the overall reaction is accompanied by an equal change in the height of the ^1H NMR resonances associated with free and bound solvent molecules. Thus when $k_1 >> k_2 >> k_3$ as was found in the following work, it is easy to determine the point at which the successive ring closure reactions are complete.

$$[MS_6]^{3+} + L\text{-}L\text{-}L \overset{K_o}{\rightleftharpoons} [MS_6]^{3+},\ L\text{-}L\text{-}L \qquad (4.3)$$

$$[MS_6]^{3+},\ L\text{-}L\text{-}L \overset{k_1}{\rightleftharpoons} [MS_5\text{-}L\text{-}L\text{-}L]^{3+} + S \qquad (4.4)$$

$$[MS_3\text{-}L\text{-}L\text{-}L]^{3+} \xrightarrow{k_2} [MS_4(L)(L\text{-}L)]^{3+} + S \qquad (4.5)$$

$$[MS_4(L)(L\text{-}L)]^{3+} \xrightarrow{k_3} [MS_3(L)(L)(L)]^{3+} + S \qquad (4.6)$$

The rate of complex formation of the neutral ligands pyridine, 2, 2'-bipyridine (bipy), 1, 10-phenthroline (phen) and 2, 2':6', 2''-terpyridine (terpy) with the $[Al^{III}(DMSO)_6]^{3+}$ ion were investigated under second-order conditions by mixing solutions of the ligand in CD_3NO_2 with solutions of the metal solvate in CD_3NO_2 and following the rate of expulsion of DMSO molecules from the inner sphere of the Al^{III} by the SFPFTNMR method. In the case of all these ligands, it was found that k_f, the rate of first bond formation (reaction (4.3) to (4.4)), was greater than the solvent exchange rate (k_1) for DMSO on Al^{III} under the same conditions, thus implying an unusually large value of K_o for these reactions. This effect was further investigated and will be discussed later.

With the ligands pyridine and phen, complex formation took place in one step with the expulsion of 1 and 2 DMSO molecules respectively from the inner-co-ordination sphere of the Al^{III}. However, with the non-rigid multidentate ligands bipy[104] and terpy, direct evidence for rate determining ring closure was found [i.e. for terpy $k_1 \gg k_2 \gg k_3$, reactions (4.3) to (4.6)] Activation parameters ($\Delta H^{\ddagger}$ and $\Delta S^{\ddagger}$ for all of the first bond-formation reactions were measured by the method described in chapter 2, and in the case of the reactions of bipy and terpy $\Delta H^{\ddagger}$ and $\Delta S^{\ddagger}$ were also measured for each of the subsequent ring closure reactions.

4.2 Solvent exchange studies

4.2.1 Experimental

4.2.1a Materials and methods

$[Al^{III}(DMSO)_6](ClO_4)_3$ was prepared by the method of Cotton and Francis,[105] recrystallised from anhydrous DMSO, washed with dry diethylether to remove any unco-ordinated DMSO, dried by vacuum desiccation and stored under nitrogen. Its purity was checked by ^1H NMR, showing only one resonance at δ 2.82 ppm in CD_3NO_2 corresponding to Al^{III} bound DMSO. Deuterionitromethane-d_3 (CD_3NO_2) was purchased from Merck, Sharp and Dohme, Ltd., and was reclaimed by successive vacuum distillations from aluminium chloride (to remove any DMSO) and then sodium bicarbonate (to remove any HCl produced during the first distillation). Because of the hygroscopic nature of $[Al^{III}(DMSO)_6](ClO_4)_3$, the CD_3NO_2 was stored over molecular sieves (type 3A) under nitrogen. The purity of the reclaimed CD_3NO_2 was checked by ^1H NMR before the solvent was reused.

4.2.1b Kinetic measurements

Variable temperature kinetic measurements were carried out with the attachment described in chapter 2, the temperatures being quoted to ± 0.5 K.

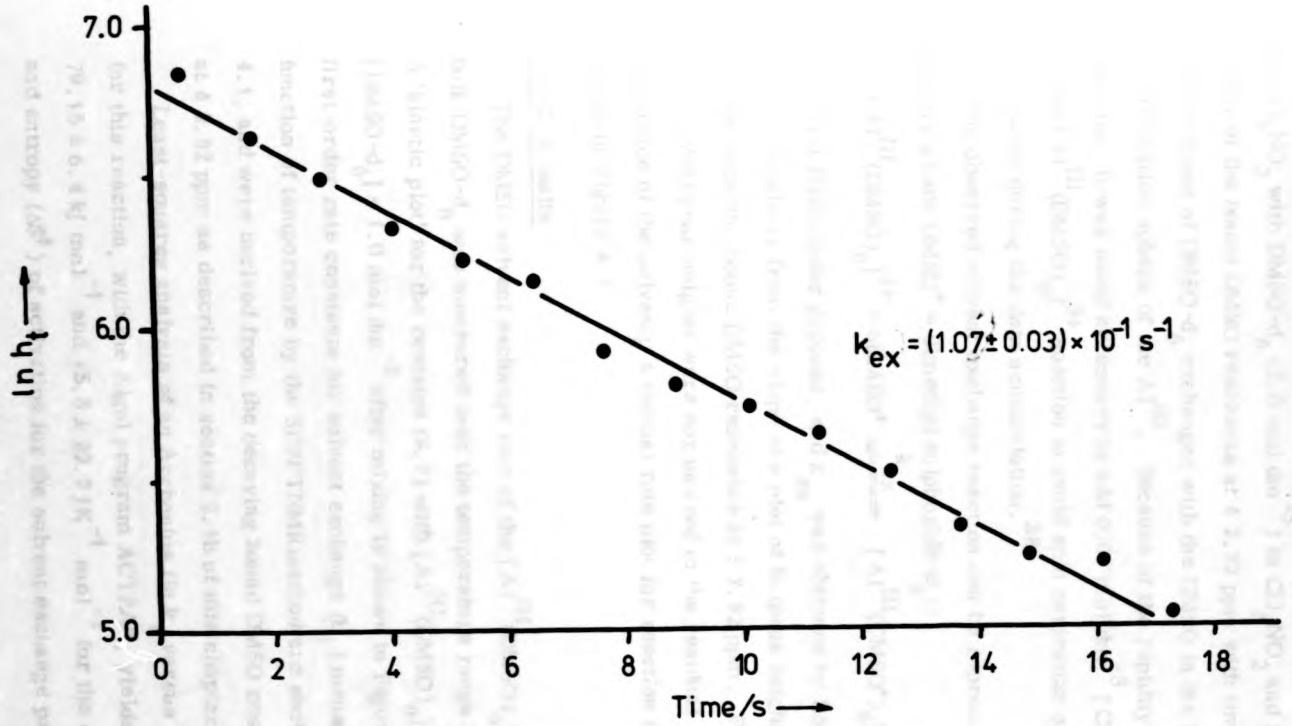

Figure 4.1

A first-order rate plot for the reaction between DMSO-d_6 (1.0 mol dm^{-3}) and the $[Al^{III}(DMSO)_6]^{3+}$ ion (10^{-2} mol dm^{-3}) in CD_3NO_2 at 293K.

The solvent exchange rate of the $[Al^{III}(DMSO)_6]^{3+}$ ion with bulk DMSO was measured by mixing $[Al^{III}(DMSO)_6](ClO_4)_3$ (0.02 mol dm^{-3}) in CD_3NO_2 with DMSO-d_6 (2.0 mol dm^{-3}) in CD_3NO_2 and following the decay of the bound DMSO resonance at δ 2.82 ppm with time as the large excess of DMSO-d_6 exchanges with the DMSO in the inner co-ordination sphere of the Al^{III}. Because of the rapidity of this reaction, it was found necessary to add 0.01 mol dm^{-3} $[Cr^{III}(acacH)_3]$ to the $[Al^{III}(DMSO)_6]^{3+}$ solution to avoid spin saturation of the DMSO resonance during the data accumulation.[38]

The observed solvent exchange reaction can be represented as follows where DMSO* = dimethyl sulphoxide-d_6:-

$$[Al^{III}(DMSO)_6]^{3+} + 6DMSO^* \rightleftharpoons^{k_{ex}} [Al^{III}(DMSO^*)_6]^{3+} + 6DMSO \quad (4.7)$$

This is a first-order process, and k_{ex} was obtained by linear least squares analysis from the slope of a plot of ln (peak height) versus time for the decaying bound DMSO resonance at δ 2.82 ppm. For all of these plots DMSO peak heights were normalized to the residual ^1H NMR resonance of the solvent; a typical rate plot for reaction (4.7) is shown in Figure 4.1.

4.2.2 Results

The DMSO solvent exchange rate of the $[Al^{III}(DMSO)_6]^{3+}$ ion with bulk DMSO-d_6 was measured over the temperature range 297 to 262 K. A 'kinetic plot' for the reaction (4.7) with $[Al^{III}(DMSO)_6]^{3+}$ = 0.01 [DMSO-d_6] = 1.0 mol dm^{-3} after mixing is shown in Figure 4.2. The first-order rate constants for solvent exchange (k_1) measured as a function of temperature by the SFPFTNMR method are shown in Table 4.1, and were derived from the decaying bound DMSO resonance observed at δ 2.82 ppm as described in section 2.1b of this chapter.

Least-squares analysis of an Arrhenius (ln k_1 versus 1/T(K)) plot for this reaction, with the Algol program ACTPAR, yielded values of 79.15 ± 6.4 kJ mol^{-1} and -5.5 ± 22.7 JK^{-1} mol^{-1} for the enthalpy ($\Delta H^{\ddagger}$) and entropy ($\Delta S^{\ddagger}$) of activation for the solvent exchange process.

$$[Al^{III}(DMSO)_6]^{(a)} + 6\,DMSO^{*} \underset{}{\overset{k_{ex}}{\rightleftharpoons}} [Al^{III}(DMSO^{*})_6] + 6\,DMSO^{(b)}$$

($DMSO^{*}$ = DMSO-d_6)

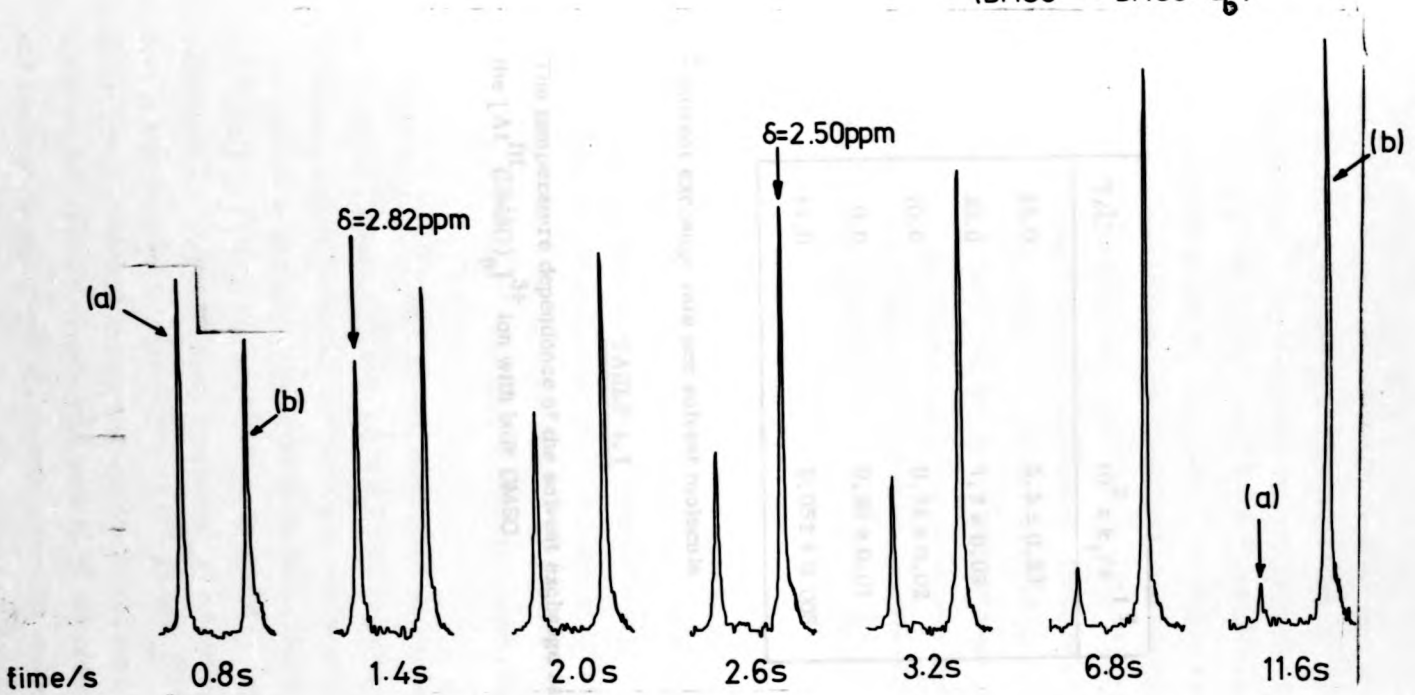

Figure 4.2

A 'kinetic plot' of the high field region of the observed ^{1}HNMR spectra during the reaction of DMSO-d_6 (1.0 mol dm^{-3}) with the $[Al^{III}(DMSO)_6]^{3+}$ ion (10^{-2} mol dm^{-3}) in CD_3NO_2 at 298K.

T/°C	$10^2 \times k_1/s^{-1}$ [a]
24.0	5.5 ± 0.33
20.0	1.7 ± 0.03
10.0	0.74 ± 0.02
0.0	0.20 ± 0.01
-11.0	0.052 ± 0.003

[a] Solvent exchange rate per solvent molecule

TABLE 4.1

The temperature dependence of the solvent exchange rate of the $[Al^{III}(DMSO)_6]^{3+}$ ion with bulk DMSO.

These values are in good agreement with those for single solvent exchange determined by Thomas and Reynolds from ^{1}H NMR line-broadening studies,[56] their experimental values being 84.1 ± 3.3 kJ mol^{-1} and 13.3 ± 10.25 J K^{-1} mol^{-1} for $\Delta H^{\ddagger}$ and $\Delta S^{\ddagger}$ respectively. A combined Arrhenius plot for these two sets of data is shown in Figure 4.3. The agreement between the SFPFTNMR data and that of Thomas and Reynolds is gratifying, and shows the accuracy of the SFPFTNMR method of measuring activation parameters. Combination of the two sets of data shown in Figure 4.3 yielded values of 85.2 ± 1.8 kJ mol^{-1} and 16.4 ± 6.0 J K^{-1} mol^{-1} for $\Delta H^{\ddagger}$ and $\Delta S^{\ddagger}$ for the single solvent exchange process, the SFNMR method having extended the observable range of reaction (4.7) and resulted in more accurate activation parameters for this reaction.

4.2.3 Discussion

Thomas and Reynolds[56] concluded from their determination of $\Delta H^{\ddagger}$ and $\Delta S^{\ddagger}$ for reaction (4.7) that if the rate determining step in the solvent exchange process involves the exchange of a highly orientated solvent molecules between the first and second co-ordination shells of the $[Al^{III}(DMSO)_6]^{3+}$ ion, then the small magnitude of $\Delta S^{\ddagger}$ could be understood. The more accurate value of $\Delta S^{\ddagger}$ determined in this work (16.4 ± 6.0 J K^{-1} mol^{-1}) confirms this small positive magnitude of $\Delta S^{\ddagger}$.

Vigee *et al.*[82, 106] have investigated the solvent exchange rate of the inert $[Cr^{III}(DMSO)_6]^{3+}$ ion with bulk DMSO by paramagnetic line-broadening studies, and concluded that there is substantial second co-ordination sphere alignment of the DMSO molecules to the $[Cr^{III}(DMSO)_6]^{3+}$ ion, with a $\Delta H^{\ddagger}$ of *ca.* 30 kJ mol^{-1}. Hence, it is reasonable to assume that there is preferential second co-ordination sphere alignment taking place with the $[Al^{III}(DMSO)_6]^{3+}$ ion, as a direct result of the high charge and small radius of the Al^{III}. This would indeed explain the small magnitude of $\Delta S^{\ddagger}$ for reaction (4.7) and result in the postulation of an outer-sphere ion-dipole mechanism for the solvent exchange reaction between the $[Al^{III}(DMSO)_6]^{3+}$ ion and free DMSO.

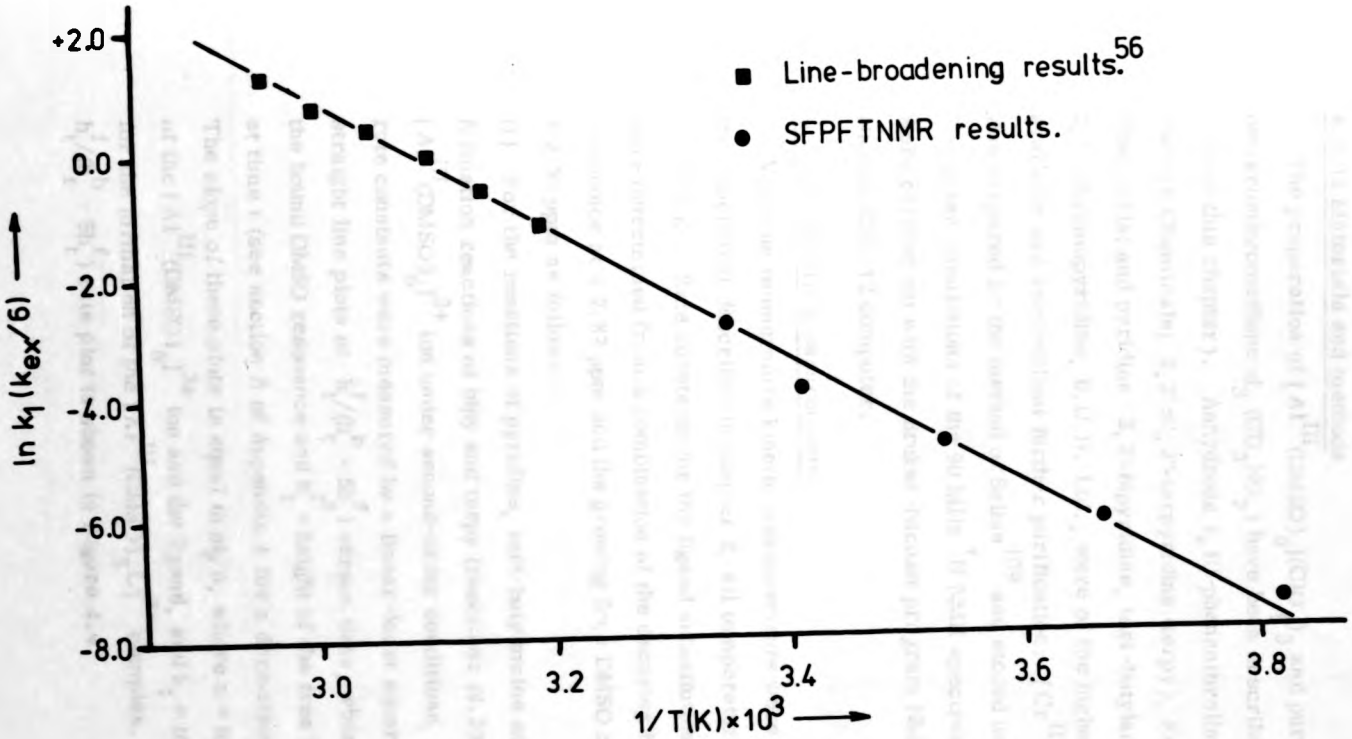

Figure 4.3

Arrhenius plot for the solvent exchange reaction of the $[Al^{III}(DMSO)_6]^{3+}$ ion with bulk DMSO in CD_3NO_2.

4.3 Ligand substitution studies

4.3.1 Experimental

4.3.1a Materials and methods

The preparation of $[Al^{III}(DMSO)_6](ClO_4)_3$ and purification of deuterionitromethane-d_3 (CD_3NO_2) have been described (see section 2.1a of this chapter). Anhydrous 1,10-phenanthroline (phen), Aldrich Chemicals; 2,2':6',2''-terpyridine (terpy), Koch-Light Chemicals; and pyridine, 2,2'-bipyridine, tert-butylamine and 2,6-dibromopyridine, B.D.H. Ltd., were of the highest purity available and used without further purification. $[Cr^{III}(DMSO)_6](ClO_4)_3$ was prepared by the method of Selbin[109] and stored under nitrogen. Computer simulations of the 90 MHz ^1H NMR spectrum of pyridine were carried out with the Bruker-Nicolet program NMRCAL on a Nicolet BNC-12 computer.

4.3.1b Kinetic measurements

Variable temperature kinetic measurements were carried out with the attachment described in chapter 2, all temperatures being quoted to ± 0.5 K. Rate constants for the ligand substitution reactions studied were determined from a combination of the decaying bound DMSO resonance at δ 2.82 ppm and the growing free DMSO resonance at δ 2.50 ppm as follows:-

(i) For the reactions of pyridine, tert-butylamine and the first bond formation reactions of bipy and terpy (reactions (4.3) to (4.4)) with the $[Al^{III}(DMSO)_6]^{3+}$ ion under second-order conditions, second-order rate constants were measured by a linear-least squares analysis of straight line plots of $h_t^f/(h_t^b - 5h_t^f)$ versus time, where h_t^b = height of the bound DMSO resonance and h_t^f = height of the free DMSO resonance at time t (see section A of Appendix 4 for a derivation of this plot). The slope of these plots is equal to $ak_f/6$, where a = initial concentration of the $[Al^{III}(DMSO)_6]^{3+}$ ion and the ligand, and k_f = the rate constant for the formation of the $[Al^{III}(DMSO)_5L]^{3+}$ complex. A typical $h_t^f/(h_t^b - 5h_t^f)$ rate plot is shown in Figure 4.4.

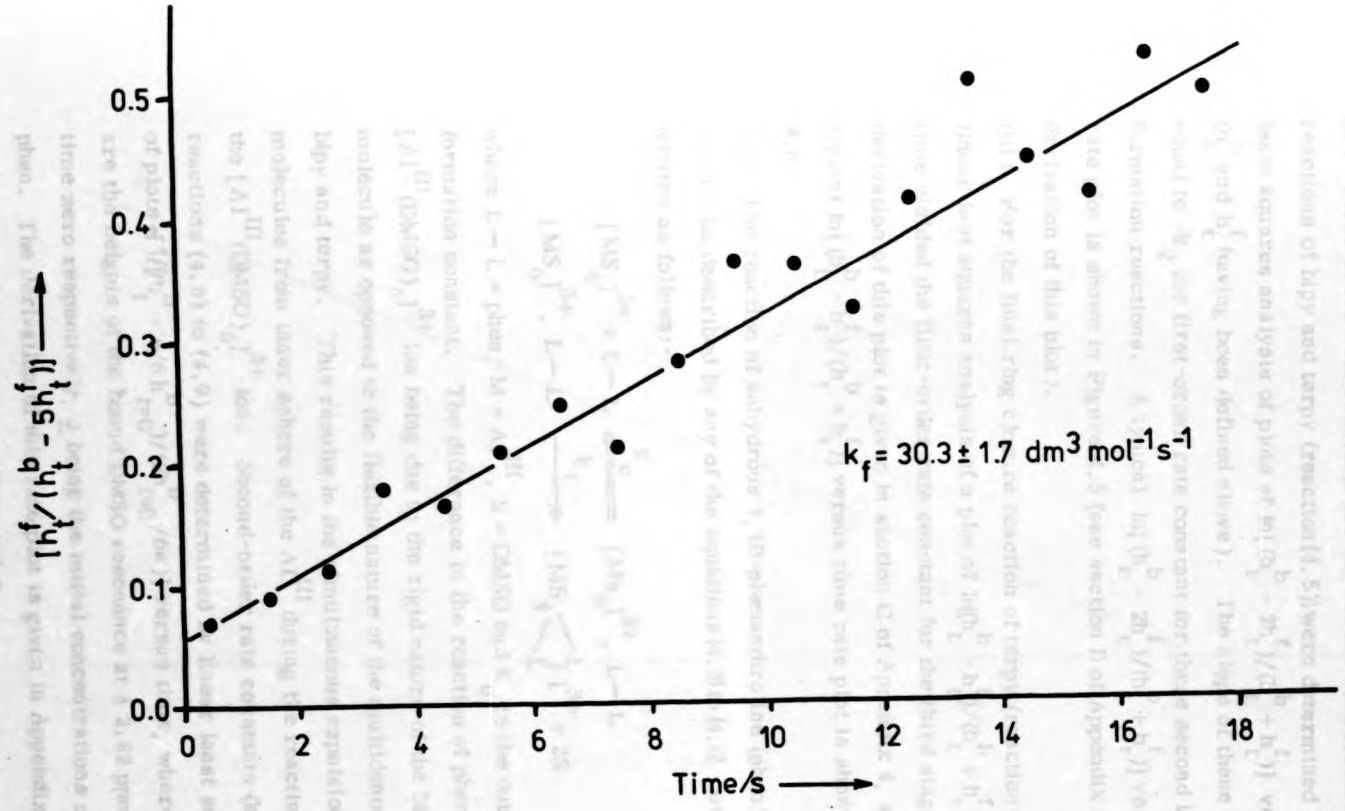

Figure 4.4

A second-order rate plot for the first bond formation reaction (k_f) between bipy (5×10^{-3} mol dm^{-3}) and the $[Al^{III}(DMSO)_6]^{3+}$ ion (5×10^{-3} mol dm^{-3}) in CD_3NO_2 at -10.0°C.

(ii) First-order rate constants for the second bond formation reactions of bipy and terpy (reaction (4.5)) were determined by linear least squares analysis of plots of $\ln[(h_t^b - 2h_t^f)/(h_t^b + h_t^f)]$ versus time (h_t^b and h_t^f having been defined above). The slope of these plots is equal to $-k_2$ the first-order rate constant for these second bond formation reactions. A typical $\ln[(h_t^b - 2h_t^f)/(h_t^b + h_t^f)]$ versus time rate plot is shown in Figure 4.5 (see section B of Appendix 4 for a derivation of this plot).

(iii) For the final ring closure reaction of terpy (reaction (4.6)), linear last squares analysis of a plot of $\ln[(h_t^b - h_t^f)/(h_t^b + h_t^f)]$ versus time yielded the first-order rate constant for the third stage. The derivation of this plot is given in section C of Appendix 4, and a typical $\ln[(h_t^b - h_t^f)/(h_t^b + h_t^f)]$ versus time rate plot is shown in Figure 4.6.

(iv) The reaction of anhydrous 1,10-phenanthroline (phen), however, can not be described by any of the equations (4.3) to (4.6), but must be written as follows:-

$$[MS_6]^{3+} + L{-}L \xrightleftharpoons{K_o} [Ms_6]^{3+},\ L{-}L \qquad (4.8)$$

$$[MS_6]^{3+},\ L{-}L \xrightarrow{k_1} [MS_4\langle{}^{L}_{L}\rangle]^{3+} + 2S \qquad (4.9)$$

where L — L = phen, M = Al^{III}, S = DMSO and K_o is the outer sphere formation constant. The difference in the reaction of phen with the $[Al^{III}(DMSO)_6]^{3+}$ ion being due to the rigid nature of the bidentate phen molecule as opposed to the flexible nature of the multidentate ligands bipy and terpy. This results in the simultaneous expulsion of two DMSO molecules from inner sphere of the Al^{III} during the reaction of phen with the $[Al^{III}(DMSO)_6]^{3+}$ ion. Second-order rate constants (k_f) for reactions (4.8) to (4.9) were determined by linear least squares analysis of plots of $1/[(h_t^b - 4/6\, h_{t=0}^b)/(2h_{t=0}^b/6a)]$ versus time, where h_t^b and $h_{t=0}^b$ are the heights of the bound DMSO resonance at δ 2.82 ppm at time t and time zero respectively, $\underline{a}$ being the initial concentrations of $[MS_6]^{3+}$ and phen. The derivation of this rate plot is given in Appendix 5, and a typical rate plot is shown in Figure 4.7.

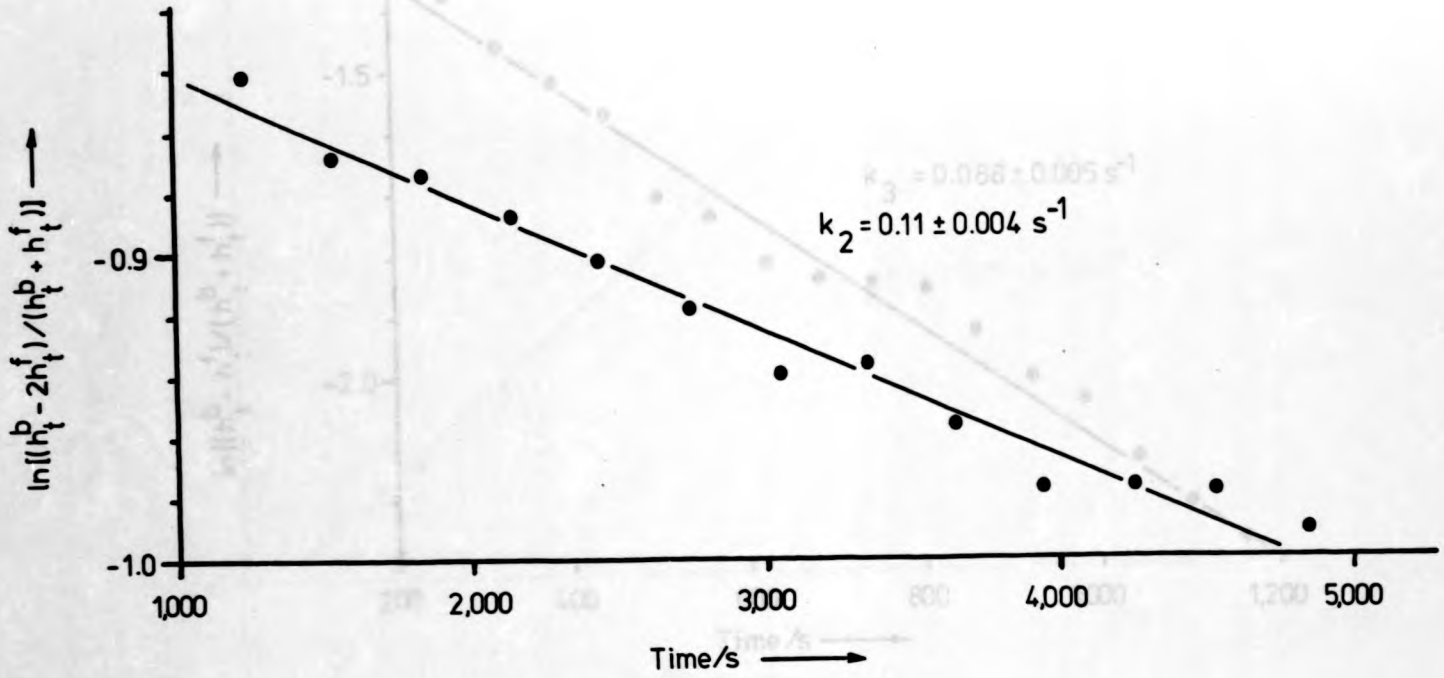

Figure 4.5

A first-order rate plot for the first ring closure reaction (k_2) between terpy (5×10^{-3} mol dm^{-3}) and the $[Al^{III}(DMSO)_6]^{3+}$ ion (5×10^{-3} mol dm^{-3}) in CD_3NO_2 at -0.5°C.

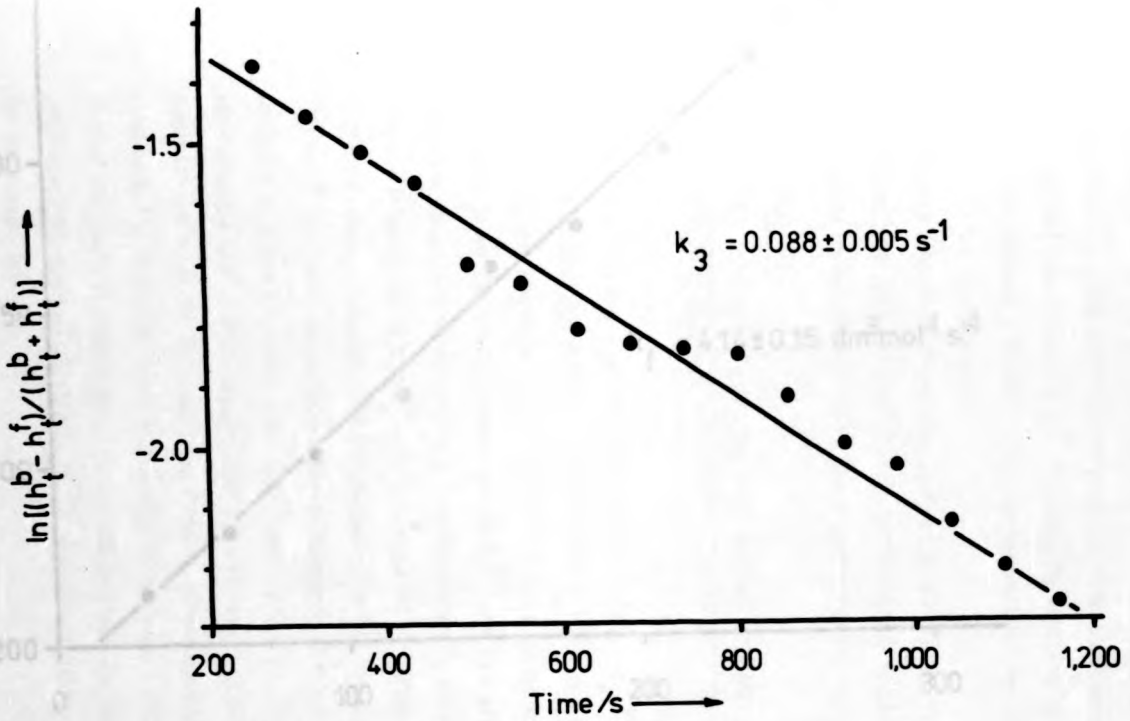

Figure 4.6

A first-order rate plot for the final ring closure reaction (k_3) between terpy (5×10^{-3} mol dm^{-3}) and the $[Al^{III}(DMSO)_6]^{3+}$ ion (5×10^{-3} mol dm^{-3}) in CD_3NO_2 at +40.0°C.

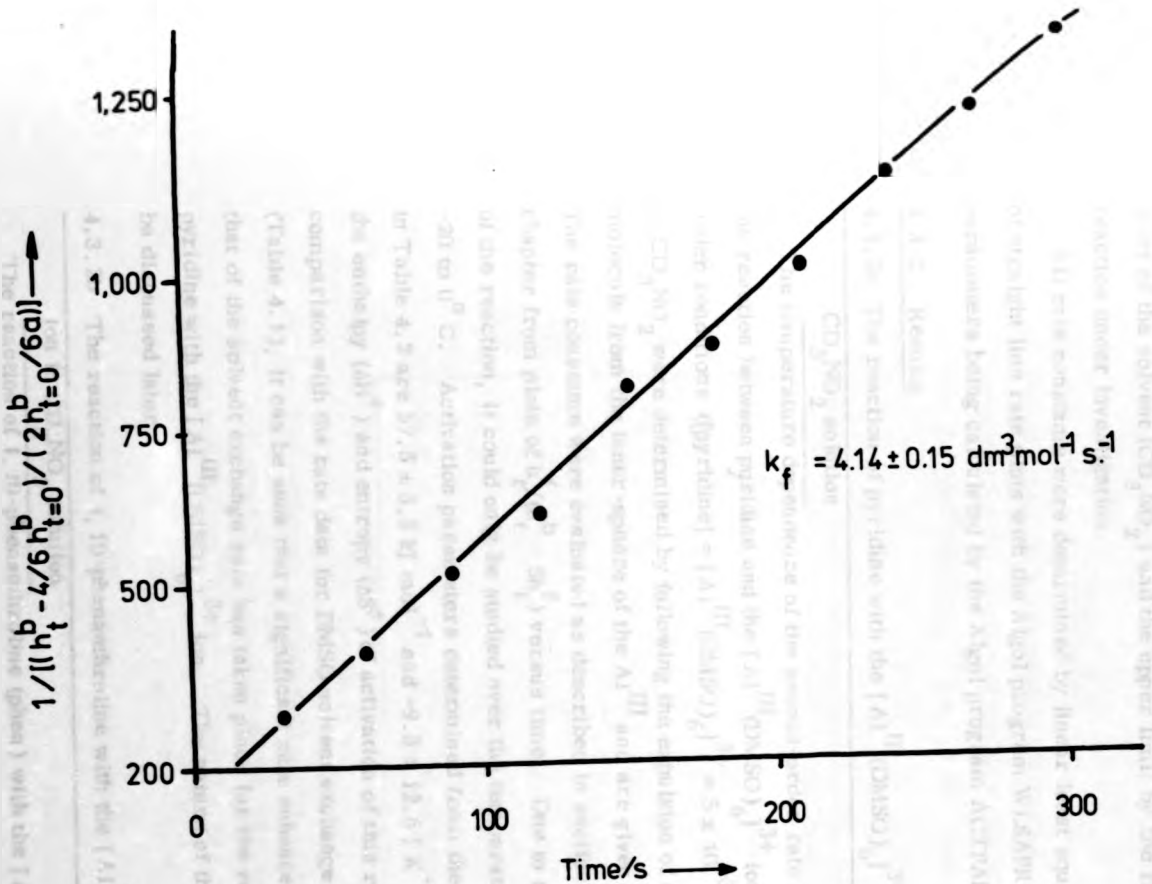

Figure 4.7

A second-order rate plot for the reaction between phen (5×10^{-3} mol dm^{-3}) and the $[Al^{III}(DMSO)_6]^{3+}$ ion (5×10^{-3} mol dm^{-3}) in CD_3NO_2 at -22.7°C.

Due to the rapidity of the ligand substitution reactions studied, it was necessary to add 0.01 mol dm^{-3} $[Cr^{III}(acacH)_3]$ to the $[Al^{III}(DMSO)_6](ClO_4)_3$ solution to avoid spin-saturation of the DMSO molecules during the data accumulation. All variable temperature measurements were carried out over as wide a temperature range as possible, the lower limit (-20° C) being determined by the freezing point of the solvent (CD_3NO_2) and the upper limit by the rate of the reaction under investigation.

All rate constants were determined by linear least squares analysis of straight line rate plots with the Algol program WLSAPROG, activation parameters being calculated by the Algol program ACTPAR.

4.3.2 Results

4.3.2a The reaction of pyridine with the $[Al^{III}(DMSO)_6]^{3+}$ ion in CD_3NO_2 solution

The temperature dependence of the second-order rate constants for the reaction between pyridine and the $[Al^{III}(DMSO)_6]^{3+}$ ion under second-order conditions ([pyridine] = $[Al^{III}(DMSO)_6]^{3+}$ = 5 x 10^{-3} mol dm^{-3}) in CD_3NO_2 were determined by following the expulsion of one DMSO molecule from the inner-sphere of the Al^{III} and are given in Table 4.2. The rate constants were evaluated as described in section 3.1b of this chapter from plots of $h_t^f/(h_t^b - 5h_t^f)$ versus time. Due to the rapidity of the reaction, it could only be studied over the temperature range -20 to 0° C. Activation parameters determined from the rate constants in Table 4.2 are 57.5 ± 3.3 kJ mol^{-1} and -9.3 ± 12.6 J K^{-1} mol^{-1} for the enthalpy ($\Delta H^{\ddagger}$) and entropy ($\Delta S^{\ddagger}$) of activation of this reaction. By comparison with the rate data for DMSO solvent exchange on Al^{III} (Table 4.1), it can be seen that a significant rate enhancement over that of the solvent exchange rate has taken place for the reaction of pyridine with the $[Al^{III}(DMSO)_6]^{3+}$ ion. The nature of this effect will be discussed later.

4.3.2b The reaction of 1,10-phenanthroline with the $[Al^{III}(DMSO)_6]^{3+}$ ion in CD_3NO_2 solution

The reaction of 1,10-phenanthroline (phen) with the $[Al^{III}(DMSO)_6]^{3+}$

T/°C	$k_f/dm^3\ mol^{-1}\ s^{-1}$
+0.3	18.1 ± 0.9
-9.7	7.4 ± 0.5
-19.9	2.2 ± 0.1

TABLE 4.2

The temperature dependence of the second-order rate constants for the reaction of pyridine (5×10^{-3} mol dm^{-3}) with the $[Al^{III}(DMSO)_6]^{3+}$ ion (5×10^{-3} mol dm^{-3}) in CD_3NO_2

T/°C	$k_f/dm^3\ mol^{-1}\ s^{-1}$
-2.1	85.0 ± 7.0
-5.3	57.3 ± 5.1
-7.8	32.8 ± 4.0
-10.0	33.4 ± 4.5
-15.5	11.3 ± 1.0
-22.7	4.14 ± 0.15

TABLE 4.3

The temperature dependence of the second-order rate constants for the reaction of phen (5×10^{-3} mol dm^{-3}) with the $[Al^{III}(DMSO)_6]^{3+}$ ion (5×10^{-3} mol dm^{-3}) in CD_3NO_2

ion in CD_3NO_2 under second-order conditions ([phen] = $[Al^{III}(DMSO)_6]^{3+}$ = 5 x 10^{-3} mol dm^{-3}) results in the simultaneous expulsion of two DMSO molecules from the inner-sphere of the Al^{III} as shown by the 'kinetic plot' for this reaction (see Figure 4.8). As with the pyridine ligand substitution reaction, the rapidity of the phen substitution reaction only permitted rate measurements over the temperature range -22 to -2° C. The temperature dependence of the second-order rate constants determined from plots of $[(h^b_t - 4/6\, h^b_{t=0})/(2h^b_{t=0}/6a)]$ versus time (see section 3.1b of this chapter) for the reaction of phen with the $[Al^{III}(DMSO)_6]^{3+}$ ion are shown in Table 4.3; activation parameters determined from these rate constants are as follows: $\Delta H^{\ddagger}$ 81.5 ± 4.4 kJ mol^{-1} and $\Delta S^{\ddagger}$ 99.3 ± 16.7 J K^{-1} mol^{-1}. As with pyridine, it is seen that there is appreciable rate enhancement in the ligand substitution reaction of phen with the $[Al^{III}(DMSO)_6]^{3+}$ ion over that of the solvent exchange rate. The mechanism of this rate enhancement is to be discussed later.

4.3.2c The reaction of 2,2'-bipyridine (bipy) with the $[Al^{III}(DMSO)_6]^{3+}$ ion in CD_3NO_2

Unlike the reaction of phen, the reaction of bipy with the $[Al^{III}(DMSO)_6]^{3+}$ ion under second-order conditions ([bipy] = $[Al^{III}(DMSO)_6]^{3+}$ = 5 x 10^{-3} mol dm^{-3}) in CD_3NO_2 showed two distinct stages.[104] These can be interpreted in terms of equations (4.3) to (4.5) (i.e. first bond formation followed by rate determining ring closure). This can be clearly seen in the observed ^1H NMR spectra as the rapid expulsion of one DMSO followed by the slow expulsion of a second DMSO molecule from the inner-sphere of the Al^{III} (see Figure 4.9). Due to rate enhancement of the first bond formation reaction (to be discussed later) kinetic measurements were only possible over the temperature range -20 to -5° C. The ring closure, however, is much slower, and was followed over the temperature range -10 to +20°C. The temperature dependence of the second-order rate constants for first bond formation (k_f) and subsequent first-order rate constants for ring closure (k_2) determined from the rate plots described in section 3.1b of this chapter are shown in

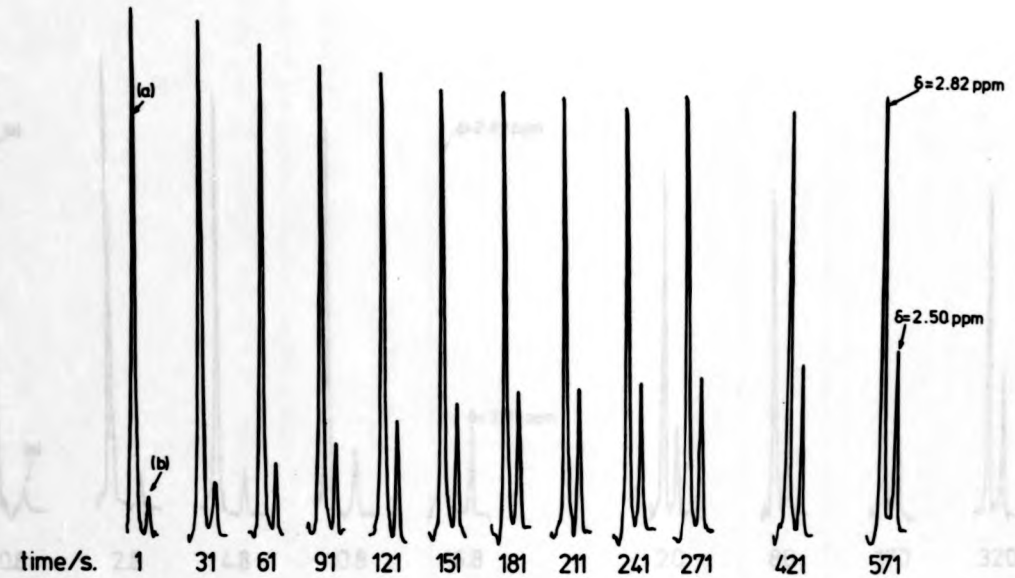

Figure 4.8

A 'kinetic plot' of the high field region of the observed ^1H NMR spectra during the reaction of 1,10-phenanthroline (5×10^{-3} mol dm^{-3}) with the $[Al(DMSO)_6]^{3+}$ ion (5×10^{-3} mol dm^{-3}) in CD_3NO_2 at -22.7°C.

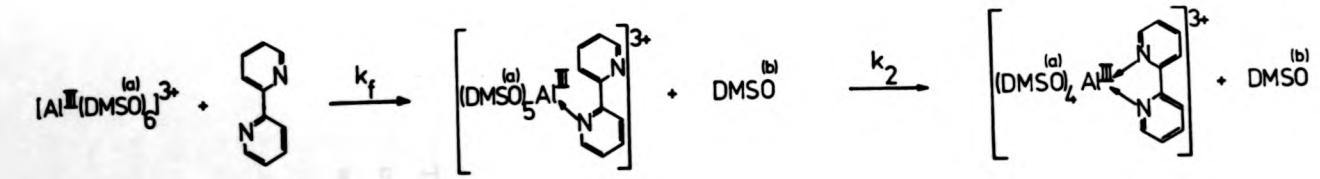

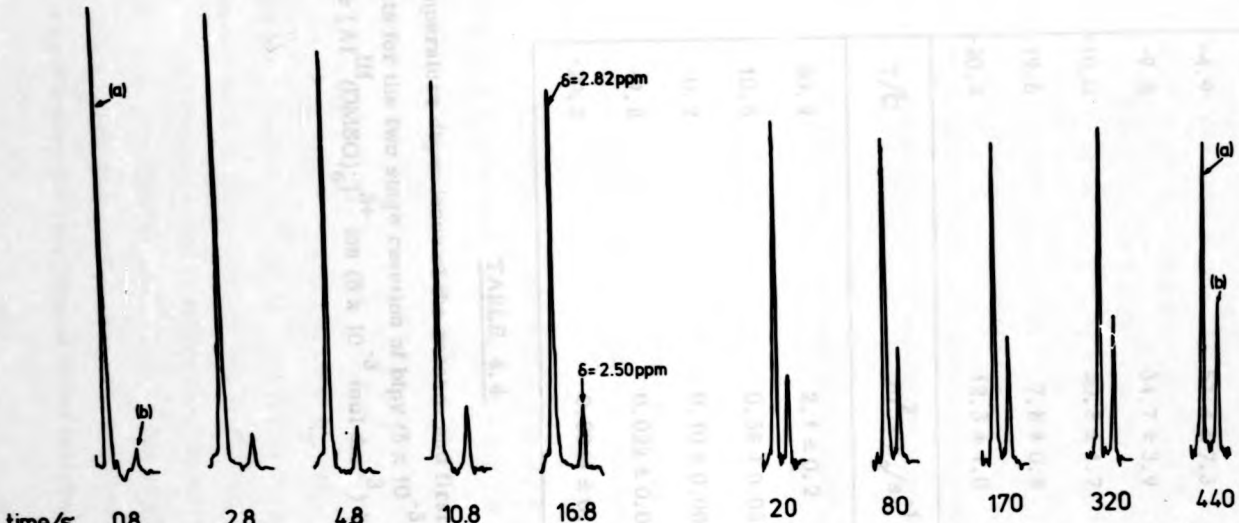

A 'kinetic plot' of the high field region of the observed ^{1}H NMR spectra during the reaction of 2,2'-bipyridine (5×10^{-3} mol dm^{-3}) with the $[Al(DMSO)_6]^{3+}$ ion (5×10^{-3} mol dm^{-3}) in CD_3NO_2.

Figure 4.9

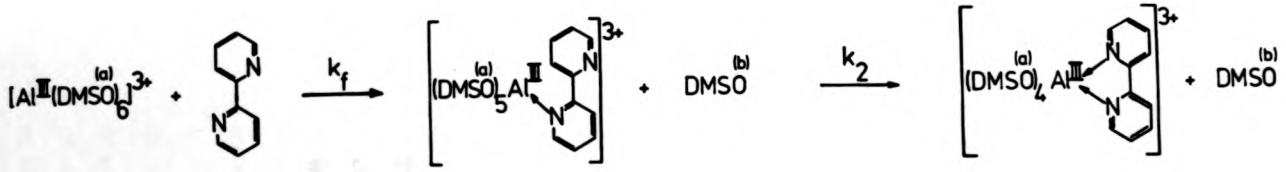

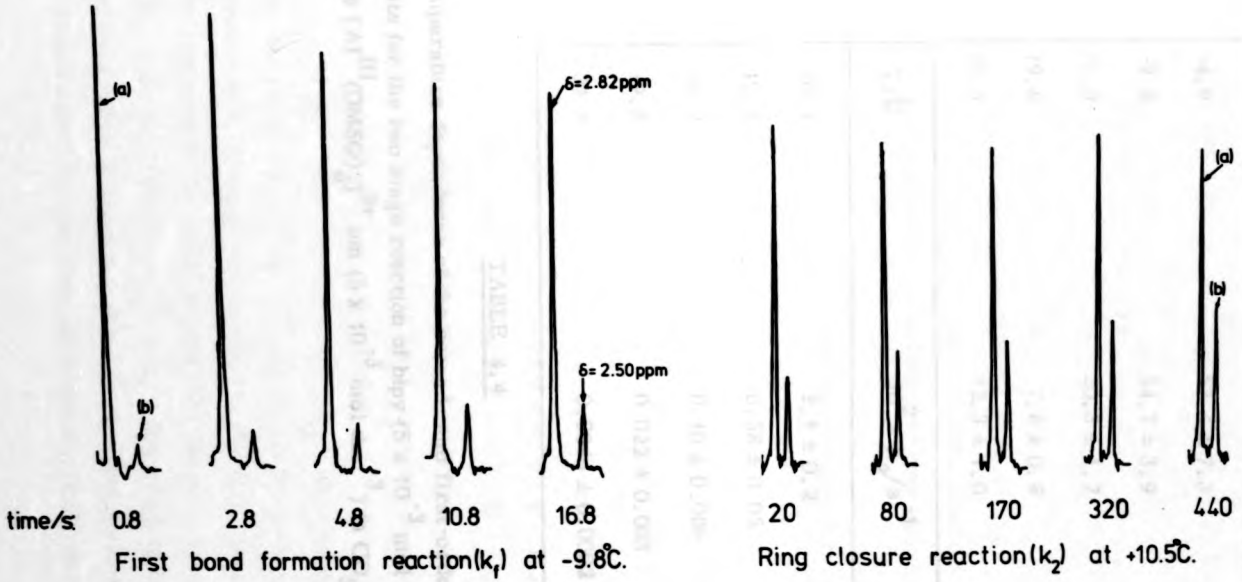

A 'kinetic plot' of the high field region of the observed ^{1}H NMR spectra during the reaction of 2,2'-bipyridine (5×10^{-3} mol dm^{-3}) with the $[Al(DMSO)_6]^{3+}$ ion (5×10^{-3} mol dm^{-3}) in CD_3NO_2.

Figure 4.9

T/°C	k_f/dm^3 mol^{-1} s^{-1}
-4.9	57.4 ± 7.3
-9.8	34.7 ± 3.9
-10.0	30.3 ± 1.7
-19.6	7.8 ± 0.8
-20.3	12.3 ± 1.0
T/°C	**$10^2 \times k_2$/s^{-1}**
20.2	2.1 ± 0.2
10.5	0.58 ± 0.05
-0.2	0.10 ± 0.006
-9.8	0.022 ± 0.003
-20.3	0.0044 ± 0.0002

TABLE 4.4

The temperature dependence of the second- and first-order rate constants for the two stage reaction of bipy (5 x 10^{-3} mol dm^{-3}) with the $[Al^{III}(DMSO)_6]^{3+}$ ion (5 x 10^{-3} mol dm^{-3}) in CD_3NO_2.

Table 4.4. The first bond formation reaction (k_f) is expected to be second-order overall whereas that of the ring closure reaction (k_2) is expected to be first-order (see Appendix 4). This was verified by carrying out the above reaction with both the reactant concentrations doubled. With both reactants at 10^{-2} mol dm^{-3}, $k_f = 22.5 \pm 1.1$ dm^3 mol^{-1} s^{-1} at -20.3° C (cf. $k_f = 12.3 \pm 1.0$ dm^3 mol^{-1} s^{-1} at -20.3° C when [bipy] = $[Al^{III}(DMSO)_6]^{3+}$ = 5×10^{-3} mol dm^{-3}) and $k_2 = (3.5 \pm 0.4) \times 10^{-4}$ s^{-1} at -10.0° C (cf. $k_2 = (2.2 \pm 0.3) \times 10^{-4}$ s^{-1} at -9.8° C when [bipy] = $[Al^{III}(DMSO)_6]^{3+}$ = 5×10^{-3} mol dm^{-3}). The doubling of k_f and the relative insensitivity (within the errors) of k_2 confirms the second-order nature of the first bond formation reaction (k_f) of bipy and the first-order nature of the subsequent ring closure reaction (k_2).

As with pyridine and phen, k_f for bipy shows significant rate enhancement over k_1, the solvent exchange rate for the $[Al^{III}(DMSO)_6]^{3+}$ ion, whereas k_2 is comparable to k_1 ($k_1 = (1.7 \pm 0.03) \times 10^{-2}$ s^{-1} at 20° C and $k_2 = (2.1 \pm 0.2) \times 10^{-2}$ s^{-1} at 20.2° C). Activation parameters determined for the two separate stages of the reaction between bipy and the $[Al^{III}(DMSO)_6]^{3+}$ ion from the data shown in Table 4.4 are as follows:-

k_f $\Delta H^{\ddagger} = 75.8 \pm 4.2$ kJ mol^{-1}, $\Delta S^{\ddagger} = 72.9 \pm 16.2$ J K^{-1} mol^{-1}.

k_2 $\Delta H^{\ddagger} = 91.9 \pm 1.71$ kJ mol^{-1}, $\Delta S^{\ddagger} = 36.5 \pm 6.3$ J K^{-1} mol^{-1}.

$\Delta H^{\ddagger}$ and $\Delta S^{\ddagger}$ for k_2 are similar to the values obtained for the solvent exchange rate for the $[Al^{III}(DMSO)_6](ClO_4)_3$ complex in section 2 of this chapter ($\Delta H^{\ddagger} = 85.2 \pm 1.8$ kJ mol^{-1} and $\Delta S^{\ddagger} = 16.4 \pm 6.0$ J K^{-1} mol^{-1}). However, as k_2 = ca. $1.2 k_1$, and a value of $k_2 = 4k_1$ would be expected for the $[(DMSO)_5Al^{III}\text{-L-L}]^{3+}$ ion if only the solvent molecules in a cis-position to L-L (bipy) are involved in the ring closure, it can be seen that ring closure is rather slower than the total solvent exchange process ($5k_1$) for the $[(DMSO)_5Al^{III}\text{-L-L}]^{3+}$ ion which is in line with previous studies which indicate that there is significant steric hindrance to chelate-ring-closure for reactions of metal ion-DMSO solvates.[107, 108]

4.3.2d The reaction of 2,2':6',2"-terpyridine with the $[Al^{III}(DMSO)_6]^{3+}$ ion in CD_3NO_2

The reaction of 2,2':6',2"-terpyridine (terpy) with the $[Al^{III}(DMSO)_6]^{3+}$ ion in CD_3NO_2 under second-order conditions ([terpy] = $[Al^{III}(DMSO)_6]^{3+}$ = 5×10^{-3} mol dm^{-3}) investigated by the SFPFTNMR method showed three distinct stages, each of which is accompanied by the expulsion of one DMSO molecule from the inner sphere of the Al^{III} as shown in Figure 4.10. These three stages can be rationalized (as with two stages of the bipy reaction) to a second-order first bond formation reaction (k_f) and two subsequent first-order ring closure reactions (k_2 and k_3) as depicted by equations (4.3) to (4.6). The temperature dependence of the rate constants for these three reactions, determined from the rate plots derived in Appendix 4, is given in Table 4.5.

As with all the other ligands studied, k_f for terpy is enhanced above the solvent exchange rate (k_1); this only permitted rate measurements of the first bond formation reaction over the temperature range -20 to 0° C. However, both the subsequent ring closure reactions are slow, ($k_f >> k_2 >> k_3$), which allowed k_2 and k_3 to be measured independently of each other. Activation parameters derived from the data in Table 4.5 for the three separate stages of the terpy reaction are as follows:-

k_f $\Delta H^{\ddagger} = 78.4 \pm 2.8$ kJ mol^{-1}, $\Delta S^{\ddagger} = 81.8 \pm 11.1$ J K^{-1} mol^{-1}

k_2 $\Delta H^{\ddagger} = 103.3 \pm 3.5$ kJ mol^{-1}, $\Delta S^{\ddagger} = 59.1 \pm 12.2$ J K^{-1} mol^{-1}

k_3 $\Delta H^{\ddagger} = 106.2 \pm 3.5$ kJ mol^{-1}, $\Delta S^{\ddagger} = 35.9 \pm 10.8$ J K^{-1} mol^{-1}

From these values, it can be seen that the rate enhancement of k_f is due to a reduced $\Delta H^{\ddagger}$, and more favourable $\Delta S^{\ddagger}$, compared to those of the solvent exchange process, as is the case with the first bond formation reaction of bipy and the formation reaction of phen and pyridine. The rate enhancement of all these reactions can be explained if the formation of the outer-sphere complex (reaction (4.3)) is slightly exothermic (ca. 9 kJ mol^{-1}) and is associated with a large positive entropy change (ca. 40 J K^{-1} mol^{-1}), possibly arising from desolvation of the $[Al^{III}(DMSO)_6]^{3+}$ ion.

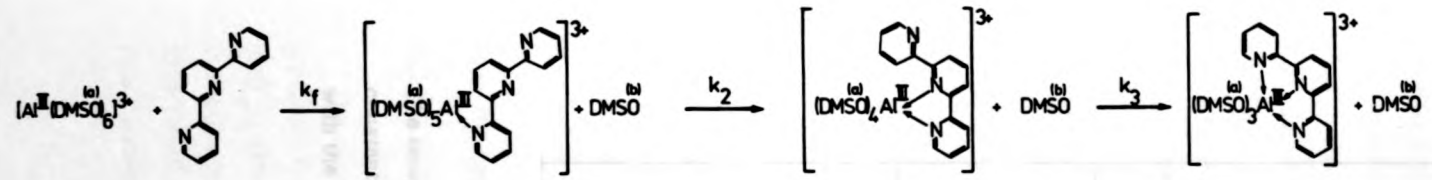

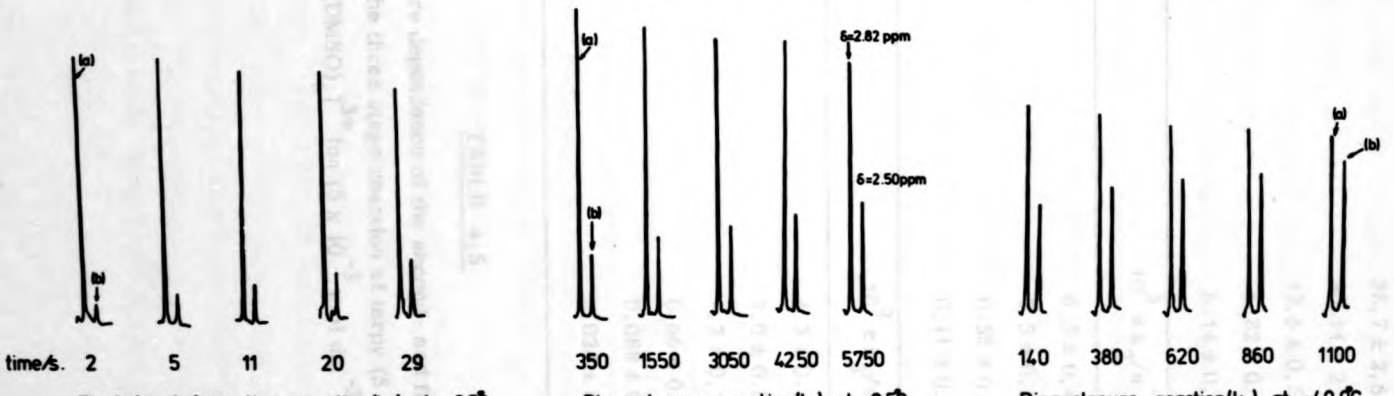

First bond formation reaction (k_1) at -0.5°C. Ring closure reaction (k_2) at -0.5°C. Ring closure reaction (k_3) at +40.0°C.

Figure 4.10

A 'kinetic plot' of the high field region of the observed ^{1}H NMR spectra during the reaction of 2,2':6,2"-terpyridine (5×10^{-3} mol dm^{-3}) with the $[Al^{III}(DMSO)_6]^{3+}$ ion (5×10^{-3} mol dm^{-3}) in CD_3NO_2.

T/°C	k_f/dm^3 mol^{-1} s^{-1}
-0.5	99.9 ± 3.5
-5.1	38.7 ± 2.6
-10.1	30.11 ± 2.5
-14.8	12.6 ± 0.5
-19.9	6.82 ± 0.48
-20.5	6.14 ± 0.79
	$10^3 \times k_2$/s^{-1}
28.2	6.3 ± 0.4
20.0	2.5 ± 0.3
9.6	0.55 ± 0.02
-0.5	0.11 ± 0.004
	$10^2 \times k_3$/s^{-1}
70.6	4.3 ± 0.4
60.8	1.0 ± 0.08
60.2	1.2 ± 0.13
50.5	0.66 ± 0.03
40.0	0.088 ± 0.005
29.8	0.024 ± 0.002

TABLE 4.5

The temperature dependence of the second- and first-order rate constants for the three stage reaction of terpy (5 x 10^{-3} mol dm^{-3}) with the $[Al^{III}(DMSO)_6]^{3+}$ ion (5 x 10^{-3} mol dm^{-3}) in CD_3NO_2.

$\Delta H^{\ddagger}$ for the first ring closure reaction of terpy (k_2) shows a marked increase compared to the $\Delta H^{\ddagger}$ of k_2 for bipy. This is consistent with the increased steric hindrance expected for the ring-closure reactions of terpy, the $\Delta H^{\ddagger}$ of k_3 for terpy being even larger than that of k_2. The $\Delta S^{\ddagger}$ values for both the ring-closure reactions of terpy and the ring-closure reaction of bipy are all comparable, which would be expected for similar steric controlled ring closure reactions.

In section 2.3 of this chapter, it was concluded that there may well be appreciable formation of a strong outer-sphere ion-dipole complex in the solvent exchange reaction of the $[Al^{III}(DMSO)_6]^{3+}$ ion with bulk DMSO. This effect could well be taking place in the formation reactions described here, especially in the reaction of pyridine with the $[Al^{III}(DMSO)_6]^{3+}$ ion which has a small $\Delta H^{\ddagger}$ and $\Delta S^{\ddagger}$ (57.5 ± 3.3 kJ mol^{-1} and -9.3 ± 12.6 J K^{-1} mol^{-1} respectively). It seems from the low value of $\Delta S^{\ddagger}$ that desolvation of the $[Al^{III}(DMSO)_6]^{3+}$ ion during the reaction with pyridine is not as marked as in the first bond formation reactions of bipy, phen and terpy, which would be expected simply from the physical size of a pyridine ligand compared to that of bipy, phen and terpy. The formation reaction of pyridine was repeated in the presence of a large excess of a non-co-ordinating pyridine type ligand (2,6-dibromopyridine) to investigate the effect of saturating the outer sphere of the $[Al^{III}(DMSO)_6]^{3+}$ ion with an aromatic non-co-ordinating molecule.

4.3.2e The reaction of pyridine with the $[Al^{III}(DMSO)_6]^{3+}$ ion in the presence of an excess of 2,6-dibromopyridine in CD_3NO_2

The reaction was carried out by mixing a CD_3NO_2 solution of pyridine (10^{-2} mol dm^{-3}) with a CD_3NO_2 solution of $[Al^{III}(DMSO)_6](ClO_4)_3$ (10^{-2} mol dm^{-3}) and 2,6-dibromopyridine (10^{-1} mol dm^{-3}) and following the resulting ligand substitution reaction by the SFPFTNMR method. The temperature dependence of the second-order rate constant for the formation of the $[Al^{III}(DMSO)_5(pyridine)]^{3+}$ ion

under these conditions is given in Table 4.6. The solubility of 2,6-dibromopyridine and the rapidity of the reaction only permitted rate measurements over the temperature range -10 to +10° C.

Activation parameters derived from Table 4.6 are as follows:- $\Delta H^{\ddagger}$ 83.1 ± 0.2 k J mol^{-1} and $\Delta S^{\ddagger}$ 70.2 ± 0.6 J K^{-1} mol^{-1}. Hence, by comparison with the $\Delta H^{\ddagger}$ and $\Delta S^{\ddagger}$ values for solvent exchange and the reaction of pyridine with the $[Al^{III}(DMSO)_6]^{3+}$ ion, it can be seen that saturation of the outer-sphere of the hexa solvate ion, with an aromatic non-co-ordinating molecule, reduces the rate of k_f for pyridine to that of the solvent exchange rate ($\Delta H^{\ddagger}$ = 83.1 kJ mol^{-1} as opposed to 85.2 kJ mol^{-1} for k_{ex}). The increase in $\Delta S^{\ddagger}$ (to 70.2 J K^{-1} mol^{-1}) would be expected in this reaction as the presence of a large excess of 2,6-dibromopyridine in the reaction mixture will result in a marked desolvation of the $[Al^{III}(DMSO)_6]^{3+}$ ion as a result of the strong outer-sphere ion-dipole association which seems to be taking place.

4.3.2f A study of the interaction between pyridine and the $[Cr^{III}(DMSO)_6]^{3+}$ ion in CD_3NO_2

To further substantiate the postulation of a strong ion-dipole outer-sphere association in the reactions of the heterocyclic ligands pyridine, phen, bipy and terpy with the $[Al^{III}(DMSO)_6]^{3+}$ ion, the nature of the interaction between the inert $[Cr^{III}(DMSO)_6]^{3+}$ ion and pyridine was investigated. The DMSO solvent exchange rate on Cr^{III} is known to be slow;[106] any specific outer-sphere interaction between the $[Cr^{III}(DMSO)_6]^{3+}$ ion and pyridine will then show up as preferential paramagnetic line broadening of the pyridine ^1H NMR resonances, as the rate of formation of the $[Cr^{III}(DMSO)_5(pyridine)]^{3+}$ ion will be very slow at room temperature. Figure 4.11a shows the ^1H NMR spectrum of a solution of 5 x 10^{-3} mol dm^{-3} $[Cr^{III}(DMSO)_6](ClO_4)_3$ and 5 x 10^{-2} mol dm^{-3} pyridine in CD_3NO_2 at 20° C. Comparison with the computer simulated spectra b, c and d of Figure 4.11 reveals that the 2,6 protons of the

T/°C	k_f/dm^3 mol^{-1} s^{-1}
10.0	10.0 ± 1.6
0.0	3.4 ± 0.6
-9.9	0.84 ± 0.03

TABLE 4.6

The temperature dependence of the second-order rate constant for the ligand substitution reaction between pyridine (5 x 10^{-3} mol dm^{-3}) and the $[Al^{III}(DMSO)_6]^{3+}$ ion (5 x 10^{-3} mol dm^{-3}) in the presence of 2,6-dibromopyridine (5 x 10^{-2} mol dm^{-3}) in CD_3NO_2.

T/°C	k_f/dm^3 mol^{-1} s^{-1}
0.0	144.4 ± 28.0
-9.9	50.4 ± 4.3
-19.8	14.4 ± 2.7

TABLE 4.7

The temperature dependence of the second-order rate constant for the ligand substitution reaction between tert-butylamine (5 x 10^{-3} mol dm^{-3}) and the $[Al^{III}(DMSO)_6]^{3+}$ ion (5 x 10^{-3} mol dm^{-3}) in CD_3NO_2.

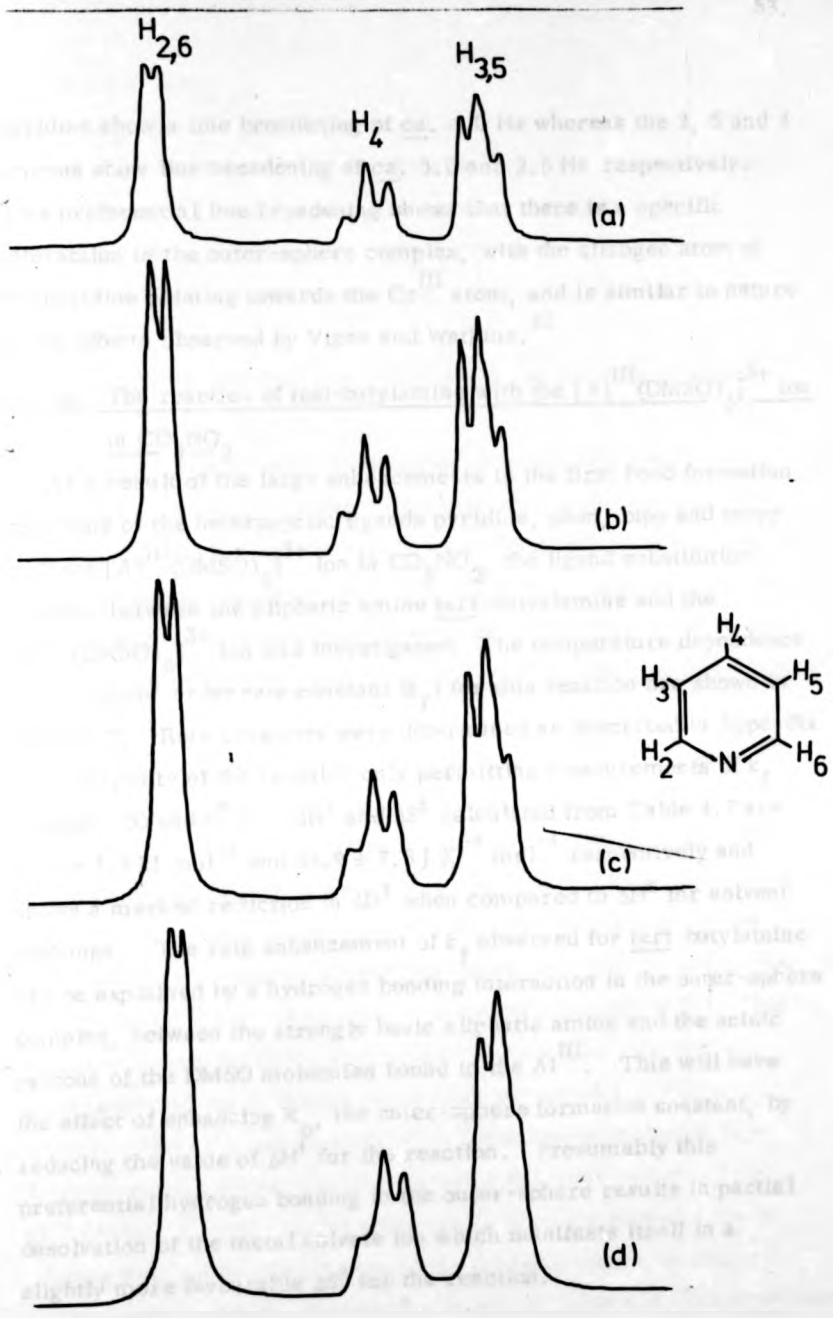

(a) measured (in the presence of 5×10^{-3} mol dm^{-3} $[Cr^{III}(DMSO)_6]^{3+}$).
(b) simulated (2.5Hz line width). (c) simulated (3.0Hz line width).
(d) simulated (4.0 Hz line width).

Figure 4.11

90MHz ^{1}HNMR spectra of pyridine.

pyridine show a line broadening of ca. 4.0 Hz whereas the 3, 5 and 4 protons show line broadening of ca. 3.0 and 2.5 Hz respectively. This preferential line broadening shows that there is a specific interaction in the outer-sphere complex, with the nitrogen atom of the pyridine pointing towards the Cr^{III} atom, and is similar in nature to the effects observed by Vigee and Watkins.[82]

4.3.2g The reaction of tert-butylamine with the $[Al^{III}(DMSO)_6]^{3+}$ ion in CD_3NO_2

As a result of the large enhancements in the first bond formation reactions of the heterocyclic ligands pyridine, phen, bipy and terpy with the $[Al^{III}(DMSO)_6]^{3+}$ ion in CD_3NO_2, the ligand substitution reaction between the aliphatic amine tert-butyalamine and the $[Al^{III}(DMSO)_6]^{3+}$ ion was investigated. The temperature dependence of the second-order rate constant (k_f) for this reaction are shown in Table 4.7. Rate constants were determined as described in Appendix 4, the rapidity of the reaction only permitting measurements of k_f between -20 and 0^{o} C. $\Delta H^{\ddagger}$ and $\Delta S^{\ddagger}$ calculated from Table 4.7 are 64.9 ± 1.9 kJ mol^{-1} and 34.9 ± 7.5 J K^{-1} mol^{-1} respectively and shows a marked reduction in $\Delta H^{\ddagger}$ when compared to $\Delta H^{\ddagger}$ for solvent exchange. The rate enhancement of k_f observed for tert-butylamine can be explained by a hydrogen bonding interaction in the outer-sphere complex, between the strongly basic aliphatic amine and the acidic protons of the DMSO molecules bound to the Al^{III}. This will have the effect of enhancing K_o, the outer-sphere formation constant, by reducing the value of $\Delta H^{\ddagger}$ for the reaction. Presumably this preferential hydrogen bonding in the outer-sphere results in partial desolvation of the metal solvate ion which manifests itself in a slightly more favourable $\Delta S^{\ddagger}$ for the reaction.

4.3.3. Discussion

4.3.3a The first bond formation reactions

The outer-sphere formation constant K_o as defined by equation (4.3) for the interaction between a neutral ligand and a charged complex is normally < 1.0,[101] and can be calculated from the Fuoss

equation as follows:-

$$K_o = (4\pi Na^3/3000)\exp(-U/kT) \qquad (4.10)$$

where N = Avogadro's number (6.022×10^{23}), a = distance of closest approach (in cm) of the ligand to the metal in the outer-sphere complex (ca. 5 Å), U = 0 for an uncharged ligand, k = Boltzmann's constant and T = absolute temperature. Thus, for a value of a = 5 Å, K_o is ca. 0.3.

K_o can also be obtained experimentally from the relationship:-

$$K_o = k_f/k_{ex} \qquad (4.11)$$

where k_f is the rate of aligand formation reaction with a solvated metal and k_{ex} is the total solvent exchange rate of the metal solvate. From equation (4.11) and the results described earlier in this chapter it can be seen that values of ca. 10^2 to 10^3 for K_o exist for some of the ligand substitution reactions investigated. Factors which have been observed previously to enhance K_o, such as stacking interactions[110] and internal conjugate-base formation [111] do not appear to be relevant to the present situation. This, together with the fact that values of 10^2 for K_o when substituted into equation 4.10 gives a value of 70 Å for the distance of closest approach between the metal and ligand in the outer-sphere complex, leads us to conclude that there could be a very strong outer sphere ion-dipole interaction taking place in the ligand formation reactions of pyridine, phen, bipy and terpy with the $[Al^{III}(DMSO)_6]^{3+}$ ion, which results in an enhancement of K_o. This postulation is substantiated by the ligand substitution reaction of pyridine carried out in the presence of an excess of 2,6-dibromo-pyridine. Here the non-co-ordinating heterocyclic molecule (2,6-dibromopyridine) appears to be saturating the outer-sphere of the $[Al^{III}(DMSO)_6]^{3+}$ ion; under these conditions, the rate of solvent exchange then dominates the rate of the pyridine formation reaction, as seen by the activation parameters shown in Table 4.8. Furthermore, the specific line broadening effects on the ^1H NMR spectrum of pyridine in the presence of $[Cr^{III}(DMSO)_6](ClO_4)_3$ in CD_3NO_2 (see Figure 4.11) indicates that there is preferential alignment of the pyridine molecules in the outer-sphere complex, with the dipole of

Ligand	k_f		k_2		k_3	
	$\Delta H^{\ddagger}$/kJ mol^{-1}	$\Delta S^{\ddagger}$/J K^{-1}mol^{-1}	$\Delta H^{\ddagger}$/kJ mol^{-1}	$\Delta S^{\ddagger}$/J K^{-1}mol^{-1}	$\Delta H^{\ddagger}$/kJ mol^{-1}	$\Delta S^{\ddagger}$/J K^{-1}mol^{-1}
DMSO[a]	85.2 ± 1.8	16.4 ± 6.0				
Pyridine	57.5 ± 3.3	-9.3 ± 12.6				
Phen	81.5 ± 4.4	99.3 ± 16.7				
Bipy	75.8 ± 4.2	72.9 ± 16.2	91.9 ± 1.7	36.5 ± 6.3		
Terpy	78.4 ± 2.8	81.8 ± 11.1	103.3 ± 3.5	59.1 ± 12.2	106.2 ± 3.5	35.9 ± 10.8
Pyridine + 2,6-dibromopyridine	83.1 ± 0.2	70.2 ± 0.6				
tert-butylamine	64.9 ± 1.9	34.9 ± 7.5				

[a] Combined line-broadening and SFPFTNMR data for single solvent exchange.

TABLE 4.8

Activation parameters for the reactions of some ligands with the $[Al^{III}(DMSO)_6]^{3+}$ ion in CD_3NO_2.

the pyridine pointing towards the Cr^{III} metal.

Preferential solvation and the role of the solvent in the kinetics of ligand substitution reactions has recently been reviewed by Langford and Tong.[114] They point out that in several solvents there is evidence for stabilization of Ni^{II} outer-sphere complexes with pyridine type ligands, especially 1,10-phenanthroline, by steric effects and by the interaction with polarized ligand molecules bound in the inner sphere of the Ni^{II}. Coetzee et al.,[115,116] from their studies of ligand subsitution reactions of Ni^{II} solvates, conclude that the outer-sphere stabilization of ligands such as phen with the $[Ni^{II}(acetonitrile)_6]^{2+}$ ion in acetonitrile (K_o is ca. 20[116]) can be attributed to two types of electrostatic interaction: a dipole-dipole interaction between the ligand and the polarized solvent molecules of the inner-sphere and also a direct ion-dipole interaction between the incoming ligand and the effective positive charge of the Ni^{II} ion. In the present study this ion-dipole interaction would be expected to be even more pronounced, due to the small ionic radius and high effective charge of the Al^{III} ion, and may well be the reason for the abnormally high values of K_o observed for the ligand substitution reactions investigated in this chapter.

Comparing the activation parameters for the first bond formation reactions (k_f) of the ligands studied (see Table 4.8), it can be seen that the presence of a strong ion-dipole outer-sphere interaction for the ligands pyridine, bipy, phen and terpy results in a reduced value of $\Delta H^{\ddagger}$ for all of these ligands, compared to $\Delta H^{\ddagger}$ for solvent exchange. This strong outer-sphere interaction would result in desolvation of the $[Al^{III}(DMSO)_6]^{3+}$ ion, which explains the large positive values of $\Delta S^{\ddagger}$ observed for these reactions. However, only when the outer-sphere of the $[Al^{III}(DMSO)_6]^{3+}$ ion is presaturated with a non-co-ordinating pyridine-type molecule does the rate of solvent exchange dominate the rate of the ligand substitution reaction.

The reaction of tert-butylamine with the $[Al^{III}(DMSO)_6]^{3+}$ ion in CD_3NO_2 however, has an even higher value of K_o (ca. 5×10^3). As this aliphatic amine is very much more basic than pyridine (pK tert-butylamine = 10.24; pK pyridine = 5.52), it is felt that there could well be a strong hydrogen bonding effect between the very basic aliphatic amine and the acidic protons of the co-ordinated DMSO molecules[117] in the outer-sphere complex. This type of effect would be expected to greatly enhance K_o and result in a greatly reduced $\Delta H^{\ddagger}$ for this reaction (see Table 4.8). Again a high positive value of $\Delta S^{\ddagger}$ is observed ($+35\ J\ K^{-1}\ mol^{-1}$), which is probably due to desolvation of the outer-sphere complex as a result of this strong outer-sphere interaction and the bulkiness of the amine.

4.3.3b The ring closure reactions

In only a few cases has evidence been found for rate determining ring closure in the reactions of multidentate ligands with metal ions,[100-107,118-122] although intermediates in the reactions of 1,2-diaminoethane[123,124] and bipy[125,126] with inert metal ions (Pt^{II}, Co^{III} or Cr^{III}) have been isolated. Usually for metal complex formation reactions involving multidentate ligands, chelate ring closure is much faster than that of the first bond formation reaction. In this study it was found that the rate of the first bond formation reactions of the ligands bipy and terpy were not dependent on the solvent exchange rate of the $[Al^{III}(DMSO)_6]^{3+}$ ion in CD_3NO_2. However, a comparison of the activation parameters for the ring closure reactions of bipy (k_2) and terpy (k_2 and k_3) with the $[Al^{III}(DMSO)_6]^{3+}$ ion with that of the solvent exchange rate of the $[Al^{III}(DMSO)_6]^{3+}$ ion (as shown in Table 4.8) shows clearly that the ring closure reactions are dominated by the solvent exchange rate of the complex [$\Delta H^{\ddagger}(k_2$ and $k_3) > \Delta H^{\ddagger}(k_{ex})$].

The ligands bipy and terpy exist in trans- and trans-trans coplanar forms in solution[127] as shown in Figure 4.12. It is not surprising therefore that $\Delta H^{\ddagger}$ (k_2) terpy > $\Delta H^{\ddagger}$ (k_2) bipy, due to the increased steric hindrance for the second bond formation reaction of terpy

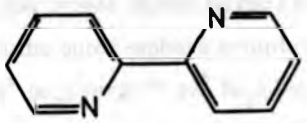

Bipy

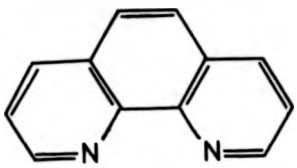

Phen

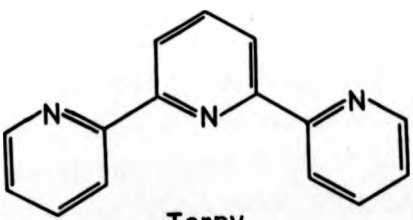

Terpy

Figure 4.12

Structures of the ligands bipy, phen and terpy in solution.

compared to that of bipy. Similarly $\Delta H^{\ddagger}$ (k_2) terpy < $\Delta H^{\ddagger}$ (k_3) terpy due to the increased steric strain in the ligand on forming the third bond to the metal. The values of $\Delta S^{\ddagger}$ for bipy and terpy parallel the $\Delta H^{\ddagger}$ trends, in that the larger ligand (terpy) has a more pronounced desolvation effect in the outer-sphere complex (i.e. $\Delta S^{\ddagger}$ (k_f) terpy > $\Delta S^{\ddagger}$ (k_f) bipy and $\Delta S^{\ddagger}$ (k_2) terpy > $\Delta S^{\ddagger}$ (k_2) bipy). However, the final ring closure reactions for these two ligands result in similar $\Delta S^{\ddagger}$ values, as there should be no marked difference in the desolvation effects for these reactions ($\Delta S^{\ddagger}(k_2)$ bipy = 36 J K^{-1} mol^{-1} = $\Delta S^{\ddagger}$ (k_3) terpy).

CHAPTER 5

NUCLEOPHILIC ATTACK AT CO-ORDINATED LIGANDS. A SFPFTNMR INVESTIGATION OF THE NATURE OF THE TRANSIENT INTERMEDIATES INVOLVED IN THE REACTIONS BETWEEN TRICARBONYL (TROPYLIUM) TUNGSTEN(0) AND MOLYBDENUM(0) FLUOROBORATES AND IODIDE ION

5.1 Introduction

Metal complexes of the type $[\eta\text{-}(C_nH_n)M(CO)_3]^+$, where M is a transition metal and n = 4-7, are known to undergo nucleophilic ligand substitution reactions by a variety of mechanisms. Previous studies have shown that nuclephiles such as HS^-, MeO^- and H^- attack directly at the organic moiety (e.g. M = Cr, n = 7).[129] Phosphines and phosphites are also known to attack at the C_nH_n ring (e.g. when M = Fe, n = 6;[130] M = Cr, n = 7;[130,134] M = Cr, Mo, W, n = 7;[131] M = Mn, n = 6;[132] M = Cr, n = 8;[133] and M = Fe, n = 4[135]). In other cases nucleophilic attack at the carbonyl groups has been established as in the reactions of amines or hydrazines (M = Mo, W, n = 5),[136] or the reactions of dienyl(tricarbonyl) iron(0) with MeO^- where there is infra-red evidence for the formation of an acyl derivative.[137] Nucleophilic attack at the metal centre is also known to occur during the reactions of $[M(C_7H_7)(CO)_3]^+$ (M = Cr, Mo, W) with acetonitrile;[138] here displacement of the tropylium ion ($C_7H_7^+$) takes place with $[M(MeCN)_3(CO)_3]$ as the final product.

The reactions between iodide ion and the complexes tricarbonyl-(tropylium)tungsten(0) fluoroborate $[(C_7H_7)W(CO)_3](BF_4)$ and tricarbonyl-(tropylium)molybdenum(0) fluoroborate $[(C_7H_7)Mo(CO)_3](BF_4)$ are both known to produce brown transient intermediates,[139] the overall reaction being as follows:-

$$[(C_7H_7)M(CO)_3^+]+I^- \overset{K}{\rightleftharpoons} [A] \underset{k_{-1}}{\overset{k_1}{\rightleftharpoons}} [B] \underset{k_{-2}}{\overset{k_2}{\rightleftharpoons}} [(C_7H_7)M(CO)_2I]+CO \quad (5.1)$$

where M = Mo, W; $(C_7H_7^+)$ = tropylium ion, [A] is a rapidly formed transient complex and [B] is the brown intermediate.

A stopped-flow spectrophotometric study of reaction (5.1) where M = W in acetone at 297.2 K has shown that the formation of the brown intermediate, B, follows the rate law:-

CHAPTER 5

NUCLEOPHILIC ATTACK AT CO-ORDINATED LIGANDS. A SFPFTNMR INVESTIGATION OF THE NATURE OF THE TRANSIENT INTERMEDIATES INVOLVED IN THE REACTIONS BETWEEN TRICARBONYL (TROPYLIUM) TUNGSTEN(0) AND MOLYBDENUM(0) FLUOROBORATES AND IODIDE ION

5.1 Introduction

Metal complexes of the type $[\eta\text{-}(C_nH_n)M(CO)_3]^+$, where M is a transition metal and n = 4-7, are known to undergo nucleophilic ligand substitution reactions by a variety of mechanisms. Previous studies have shown that nuclephiles such as HS^-, MeO^- and H^- attack directly at the organic moiety (e.g. M = Cr, n = 7).[129] Phosphines and phosphites are also known to attack at the C_nH_n ring (e.g. when M = Fe, n = 6;[130] M = Cr, n = 7;[130,134] M = Cr, Mo, W, n = 7;[131] M = Mn, n = 6;[132] M = Cr, n = 8;[133] and M = Fe, n = 4[135]). In other cases nucleophilic attack at the carbonyl groups has been established as in the reactions of amines or hydrazines (M = Mo, W, n = 5),[136] or the reactions of dienyl(tricarbonyl) iron(0) with MeO^- where there is infra-red evidence for the formation of an acyl derivative.[137] Nucleophilic attack at the metal centre is also known to occur during the reactions of $[M(C_7H_7)(CO)_3]^+$ (M = Cr, Mo, W) with acetonitrile;[138] here displacement of the tropylium ion ($C_7H_7^+$) takes place with $[M(MeCN)_3(CO)_3]$ as the final product.

The reactions between iodide ion and the complexes tricarbonyl-(tropylium)tungsten(0) fluoroborate $[(C_7H_7)W(CO)_3](BF_4)$ and tricarbonyl-(tropylium)molybdenum(0) fluoroborate $[(C_7H_7)Mo(CO)_3](BF_4)$ are both known to produce brown transient intermediates,[139] the overall reaction being as follows:-

$$[(C_7H_7)M(CO)_3^+] + I^- \overset{K}{\rightleftharpoons} [A] \underset{k_{-1}}{\overset{k_1}{\rightleftharpoons}} [B] \underset{k_{-2}}{\overset{k_2}{\rightleftharpoons}} [(C_7H_7)M(CO)_2I] + CO \quad (5.1)$$

where M = Mo, W; $(C_7H_7^+)$ = tropylium ion, [A] is a rapidly formed transient complex and [B] is the brown intermediate.

A stopped-flow spectrophotometric study of reaction (5.1) where M = W in acetone at 297.2 K has shown that the formation of the brown intermediate, B, follows the rate law:-

$$d[B]/dt = \{a/(1 + K[I^-])\}[I^-][(C_7H_7)W(CO)_3^+] \quad (5.2)$$

where $a = k_1K$, and the rate limiting value of k_1 at high $[I^-]$ (0.1 mol dm^{-3}) is 12.0 s^{-1} ($[(C_7H_7)W(CO)_3^+] = 10^{-3}$ mol dm^{-3}). The rate of decay of B was shown to be independent of the concentration of I^- ($k_2 = 1.2 \times 10^{-2}$ s^{-1}), and the rapidly formed transient complex, A, was thought to be an ion pair where $K = K_o$ the outer sphere formation constant for reaction (5.1).[140] However, this study could not yield any information as to the nature of the intermediates A and B or the mechanism of the reaction due to the lack of structural information obtainable from UV-visible stopped-flow measurements. Thus, a SFPFTNMR study of reaction (5.1) was undertaken (with M = Mo, W) in acetone d_{-6}. The nature of the transient intermediates A and B were investigated by variable temperature SFPFTNMR kinetic measurements, variable temperature ^1H NMR and longitudinal spin-lattice relaxation (T_1) measurements. The enthalpy ($\Delta H^{\ddagger}$) and entropy ($\Delta S^{\ddagger}$) of formation of the intermediate, B, were measured for M = Mo and W, and the rate of decay of the brown intermediate B (M = W) was measured at a higher complex concentration ($[(C_7H_7)W(CO)_3^+] = 10^{-2}$ mol dm^{-3}) and found to agree with the previously determined value of k_2.

5.2 Experimental

5.2.1 Materials and Methods

The complexes $[(C_7H_7)M(CO)_3](BF_4)$ (M = Mo, W) were a gift from Dr. P. Powell, Department of Chemistry, Royal Holloway College, Egham, Surrey, and were used without further purification. Acetone-d_6 was purchased from Merck, Sharp and Dohme, Ltd., and reclaimed by vacuum distillation after use, the purity of the reclaimed solvent being checked by ^1H NMR before re-use. Fluorotrichloromethane ($FCCl_3$), B.D.H. Ltd., was vacuum distilled before use. Proton longitudinal spin-lattice relaxation times (T_1's) were measured by the inversion-recovery pulse sequence method $[(180^o - \tau - 90^o - 5T_1)_n]$ using the Bruker-Nicolet program T1PRGM.[141] The ^1H NMR spectrum of the $[(C_7H_7P(^nBu)_3)W(CO)_3](BF_4)$ complex was simulated with the Fortran program LAME8.

$$d[B]/dt = \{\underline{a}/(1 + K[I^-])\}[I^-][(C_7H_7)W(CO)_3^+] \qquad (5.2)$$

where $\underline{a} = k_1K$, and the rate limiting value of k_1 at high $[I^-]$ (0.1 mol dm^{-3}) is 12.0 s^{-1} ($[(C_7H_7)W(CO)_3^+] = 10^{-3}$ mol dm^{-3}). The rate of decay of B was shown to be independent of the concentration of I^- ($k_2 = 1.2 \times 10^{-2}$ s^{-1}), and the rapidly formed transient complex, A, was thought to be an ion pair where $K = K_o$ the outer sphere formation constant for reaction (5.1).[140] However, this study could not yield any information as to the nature of the intermediates A and B or the mechanism of the reaction due to the lack of structural information obtainable from UV-visible stopped-flow measurements. Thus, a SFPFTNMR study of reaction (5.1) was undertaken (with M = Mo, W) in acetone d_{-6}. The nature of the transient intermediates A and B were investigated by variable temperature SFPFTNMR kinetic measurements, variable temperature ^1H NMR and longitudinal spin-lattice relaxation (T_1) measurements. The enthalpy ($\Delta H^{\ddagger}$) and entropy ($\Delta S^{\ddagger}$) of formation of the intermediate, B, were measured for M = Mo and W, and the rate of decay of the brown intermediate B (M = W) was measured at a higher complex concentration ($[(C_7H_7)W(CO)_3^+] = 10^{-2}$ mol dm^{-3}) and found to agree with the previously determined value of k_2.

5.2 Experimental

5.2.1 Materials and Methods

The complexes $[(C_7H_7)M(CO)_3](BF_4)$ (M = Mo, W) were a gift from Dr. P. Powell, Department of Chemistry, Royal Holloway College, Egham, Surrey, and were used without further purification. Acetone-d_6 was purchased from Merck, Sharp and Dohme, Ltd., and reclaimed by vacuum distillation after use, the purity of the reclaimed solvent being checked by ^1H NMR before re-use. Fluorotrichloromethane ($FCCl_3$), B.D.H. Ltd., was vacuum distilled before use. Proton longitudinal spin-lattice relaxation times (T_1's) were measured by the inversion-recovery pulse sequence method $[(180^o - \tau - 90^o - 5T_1)_n]$ using the Bruker-Nicolet program T1PRGM.[141] The ^1H NMR spectrum of the $[(C_7H_7P(^nBu)_3)W(CO)_3](BF_4)$ complex was simulated with the Fortran program LAME8.

5.2.2 Kinetic measurements

All variable temperature kinetic measurements were carried out with the attachment described in Chapter 2, temperatures being quoted to ± 0.5 K.

Rate constants for the production of the brown intermediate (B in equation (5.1)) were determined under psuedo-first-order conditions with $[I^-]$ = 10 x [complex] in acetone-d_6. Pseudo-first-order rate constants were obtained from a linear least squares analysis of plots of the logarithm of the height of the decaying $[(C_7H_7)M(CO)_3](BF_4)$ ^1H NMR resonance at δ = 6.56 (M = W) and 6.62 ppm (M = Mo) versus time with the Algol program WLSAPROG. A typical ln (peak height, h_t) versus time plot for this reaction is shown in Figure 5.1. Activation parameters ($\Delta H^{\ddagger}$ and $\Delta S^{\ddagger}$) were determined with the Algol program ACTPAR.

5.3 Results

5.3.1 Formation of the brown intermediate, B

The rate of production of the transient intermediate B in reaction (5.1) (M = W) at 297.2 K is known to be rate limiting (k_1 = 12.0 s^{-1}) when $[I^-]$ = 0.1 mol dm^{-3}.[140] The dependence of k_1 for M = Mo on the concentration of I^- was investigated under pseudo-first-order conditions by the SFPFTNMR method with [complex] = 5 x 10^{-3} mol dm^{-3} as shown in Figure 5.2. This investigation suggests that the more reactive $[(C_7H_7)Mo(CO)_3](BF_4)$ complex obeys the same rate law (equation (5.2)) as the tungsten complex, the rate limiting value of k_1 being 5.25 x 10^{-2} s^{-1} (M = Mo) when $[I^-]$ = 0.1 mol dm^{-3} at 250.5 K.

Pseudo-first-order rate constants (k_1) for the rate of production of the brown intermediate B in reaction (5.1) (M = Mo, W) were measured as a function of temperature under rate limiting conditions $[I^-]$ = 10[complex] = 10^{-2} mol dm^{-3} in acetone-d_6. The temperature dependence of k_1 for M = Mo and W is given in Table 5.1, and activation parameters derived from these results are as follows:-

5.2.2 Kinetic measurements

All variable temperature kinetic measurements were carried out with the attachment described in Chapter 2, temperatures being quoted to ± 0.5 K.

Rate constants for the production of the brown intermediate (B in equation (5.1)) were determined under psuedo-first-order conditions with $[I^-]$ = 10 x [complex] in acetone-d_6. Pseudo-first-order rate constants were obtained from a linear least squares analysis of plots of the logarithm of the height of the decaying $[(C_7H_7)M(CO)_3](BF_4)$ ^{1}H NMR resonance at δ = 6.56 (M = W) and 6.62 ppm (M = Mo) versus time with the Algol program WLSAPROG. A typical ln (peak height, h_t) versus time plot for this reaction is shown in Figure 5.1. Activation parameters ($\Delta H^{\ddagger}$ and $\Delta S^{\ddagger}$) were determined with the Algol program ACTPAR.

5.3 Results

5.3.1 Formation of the brown intermediate, B

The rate of production of the transient intermediate B in reaction (5.1) (M = W) at 297.2 K is known to be rate limiting ($k_1 = 12.0\ s^{-1}$) when $[I^-] = 0.1$ mol dm^{-3}.[140] The dependence of k_1 for M = Mo on the concentration of I^- was investigated under pseudo-first-order conditions by the SFPFTNMR method with [complex] = 5 x 10^{-3} mol dm^{-3} as shown in Figure 5.2. This investigation suggests that the more reactive $[(C_7H_7)Mo(CO)_3](BF_4)$ complex obeys the same rate law (equation (5.2)) as the tungsten complex, the rate limiting value of k_1 being 5.25 x 10^{-2} s^{-1} (M = Mo) when $[I^-] = 0.1$ mol dm^{-3} at 250.5 K.

Pseudo-first-order rate constants (k_1) for the rate of production of the brown intermediate B in reaction (5.1) (M = Mo, W) were measured as a function of temperature under rate limiting conditions $[I^-]$ = 10[complex] = 10^{-2} mol dm^{-3} in acetone-d_6. The temperature dependence of k_1 for M = Mo and W is given in Table 5.1, and activation parameters derived from these results are as follows:-

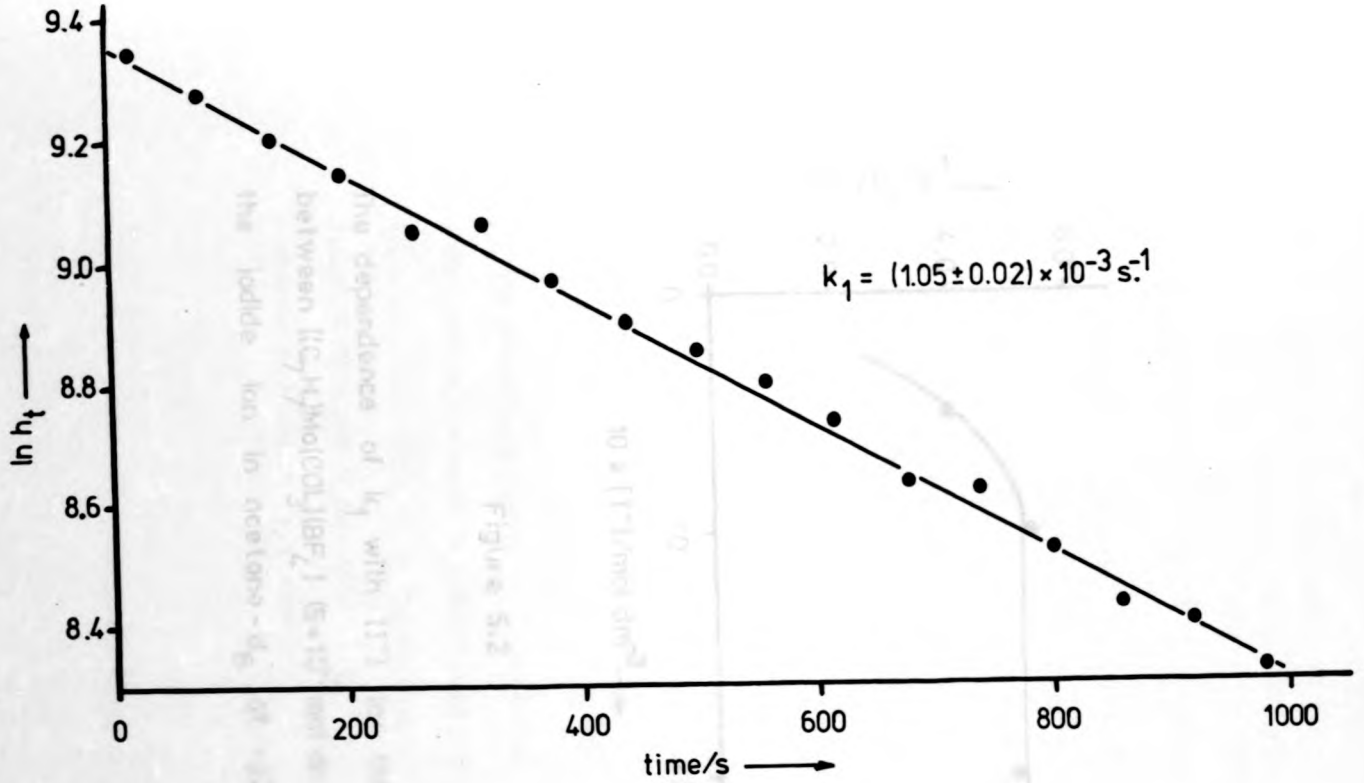

Figure 5.1

Pseudo-first-order rate plot for the reaction between the $[(C_7H_7)W(CO)_3]^+$ ion (10^{-2} mol dm^{-3}) and iodide ion (0.1 mol dm^{-3}) in acetone-d_6 at -36°C.

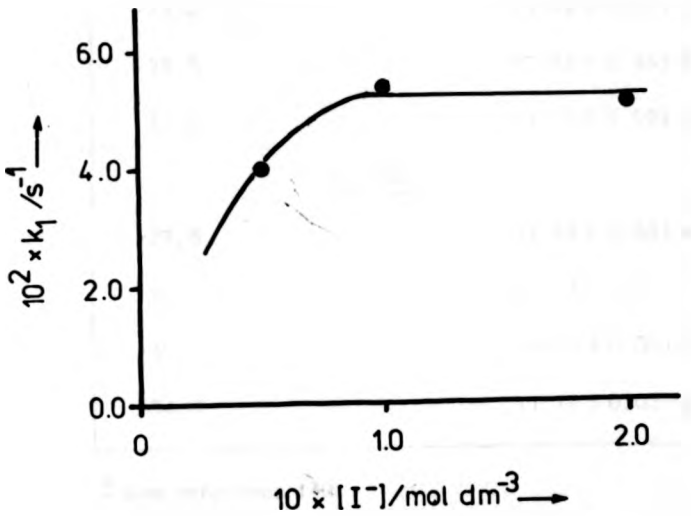

Figure 5.2

The dependence of k_1 with $[I^-]$ for the reaction between $[(C_7H_7)Mo(CO)_3](BF_4)$ (5×10^{-3} mol dm^{-3}) and the iodide ion in acetone-d_6 at -22.7°C.

T/°C	k_1/s^{-1}
M = W	
+24.0	12.7[a]
-15.0	$(1.62 \pm 0.07) \times 10^{-2}$
-25.5	$(7.38 \pm 0.38) \times 10^{-3}$
-36.0	$(1.05 \pm 0.02) \times 10^{-3}$
M = Mo	
-27.5	$(4.99 \pm 0.32) \times 10^{-2}$
-36.0	$(1.52 \pm 0.07) \times 10^{-2}$
-45.7	$(4.80 \pm 0.06) \times 10^{-3}$
-54.0	$(1.17 \pm 0.03) \times 10^{-3}$

[a] see reference 140.

TABLE 5.1

The temperature dependence of the rate limiting pseudo-first-order rate constants (k_1) for the rate of production of the brown intermediate, B, during the reaction of the complexes $[(C_7H_7)M(CO)_3](BF_4)$ (M = Mo, W) (10^{-2} mol dm^{-3}) with iodide ion (0.1 mol dm^{-3}) in acetone-d_6.

M = Mo; $\Delta H^{\ddagger} = 60.3 \pm 2.4$ kJ mol^{-1}, $\Delta S^{\ddagger} = -22.9 \pm 10.2$ J K^{-1} mol^{-1}

M = W; $\Delta H^{\ddagger} = 89.0 \pm 8.2$ kJ mol^{-1}, $\Delta S^{\ddagger} = 73.3 \pm 31.8$ J K^{-1} mol^{-1}

'Kinetic plots' of the methine (C-H) region of the observed ^{1}H NMR spectra during these reactions are shown in Figures 5.3 (M = Mo) and 5.4 (M = W). From these 'kinetic plots', it can be seen that a second intermediate (B') is formed in ca. 7% abundance at δ = 5.44 (M = Mo) and 5.19 (M = W) ppm throughout the reaction. In the case of both of these reactions, the intermediate B' is to low frequency of the intermediate B (δ B = 5.79, B' = 5.44 ppm (M = Mo); δ B = 5.47, B' = 5.19 ppm (M = W)), and both intermediates decay to zero on formation of the final green product of reaction (5.1) $[(C_7H_7)M(CO)_2I]$. Furthermore, during the reaction where M = W, broadening (but no chemical shift change) of the ^{1}H NMR resonance of the $[(C_7H_7)W(CO)_3](BF_4)$ complex is observed upon mixing with excess iodide ion and before any of the brown intermediate B has formed (see Figure 5.4); $\Delta\nu_{\frac{1}{2}}$ = 1.36 Hz for $[(C_7H_7)W(CO)_3](BF_4)$ in the absence of iodide ion, 2.85 Hz for $[(C_7H_7)W(CO)_3](BF_4)$ in the presence of iodide ion and 1.86 Hz for the brown intermediate B, where $\Delta\nu_{\frac{1}{2}}$ = width at half-height of the observed ^{1}H NMR resonances at -36° C in acetone-d_6. This initial broadening of the reactant's ^{1}H NMR resonance could be due to either a longitudinal (T_1) or transverse (T_2) spin-lattice relaxation effect. Therefore, the T_1's of the reactant $[(C_7H_7)W(CO)_3](BF_4)$ in the absence and presence of iodide ion and the brown intermediate (B) at δ = 5.47 ppm were measured by means of the Bruker-Nicolet program TIPRGM at -36° C in acetone-d_6. The observed T_1's being as follows:-

species	T_1/s
$\{[(C_7H_7)W(CO)_3](BF_4)\}$	4.5 ± 0.9
$\{[(C_7H_7)W(CO)_3](BF_4) + I^-\}$	3.9 ± 0.8
{brown intermediate B}	1.4 ± 0.2

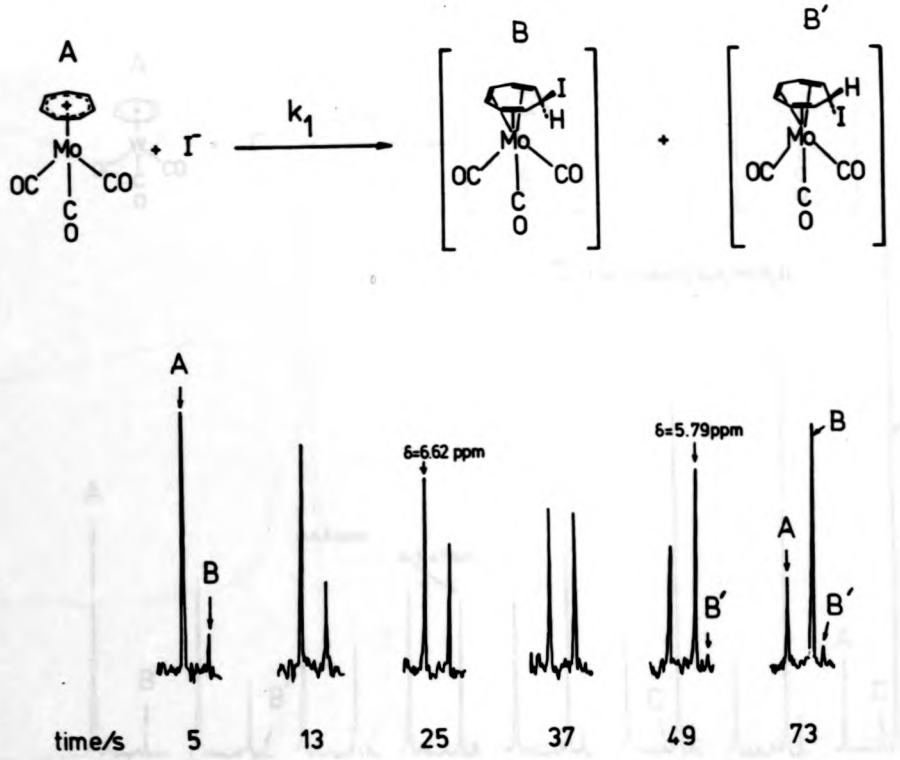

Figure 5.3

A 'kinetic plot' of the methine(C-H) region of the observed ^{1}H NMR spectra during the reaction of sodium iodide(0.1 mol dm^{-3}) with the $[\eta^7(C_7H_7)Mo(CO)_3]^+$ ion (10^{-2} mol dm^{-3}) in acetone-d_6 at -36.0°C.

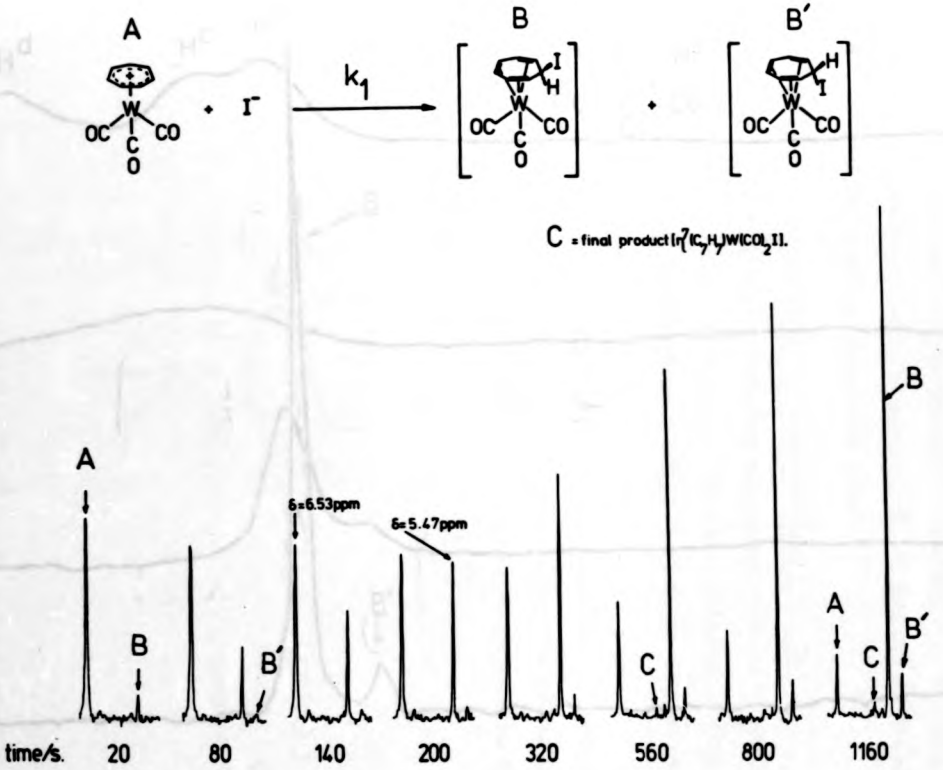

Figure 5.4

A 'kinetic plot' of the methine (C-H) region of the observed ^{1}HNMR spectra during the reaction of sodium iodide(0.1 mol dm^{-3}) with the [$\eta^7(C_7H_7)W(CO)_3$]$^+$ ion(10^{-2} mol dm^{-3}) in acetone-d_6 at -36.0°C.

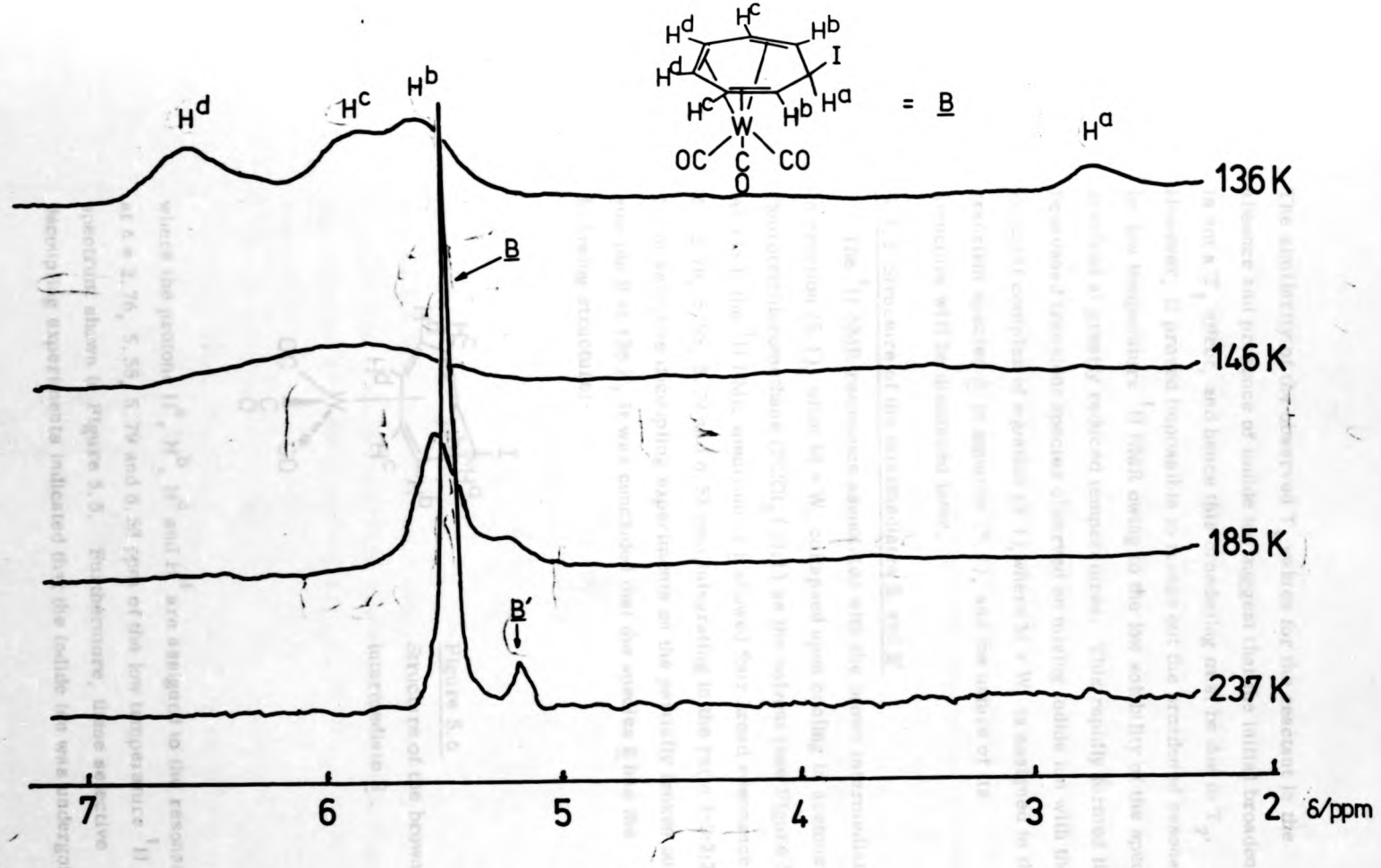

Figure 5.5

Variable temperature 90 MHz ^{1}H NMR spectra of the brown transient species B (M=W) in acetone-d_6/$FCCl_3$ (1:1).

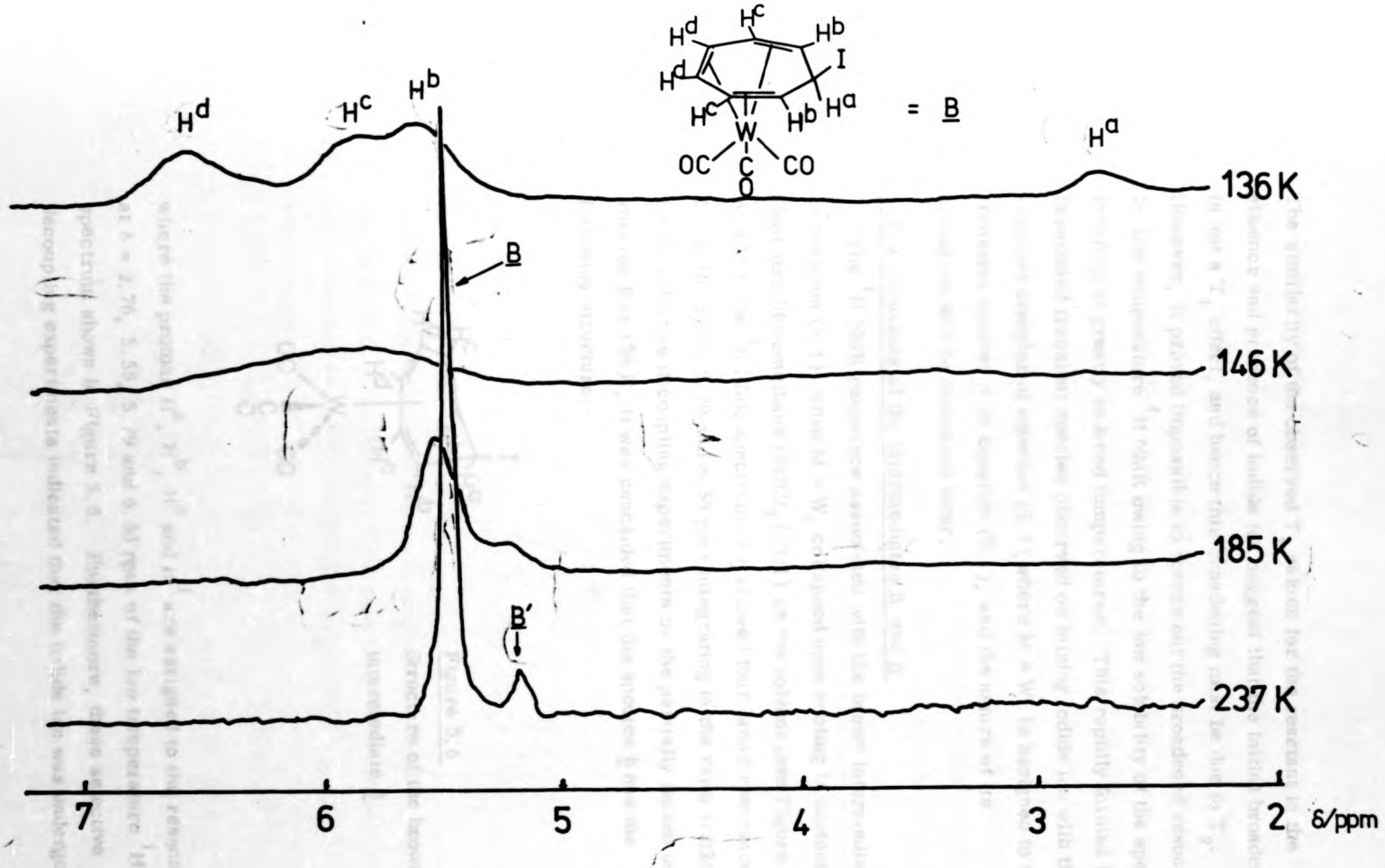

Figure 5.5

Variable temperature 90 MHz ^{1}H NMR spectra of the brown transient species B (M=W) in acetone-d_6/$FCCl_3$ (1:1).

The similarity of the observed T_1 values for the reactant in the absence and presence of iodide ion suggest that the initial broadening is not a T_1 effect, and hence this broadening must be due to T_2. However, it proved impossible to freeze out the broadened resonance by low temperature ^{1}H NMR owing to the low solubility of the species involved at greatly reduced temperatures. This rapidly formed line-broadened transient species observed on mixing iodide ion with the reactant complex of equation (5.1), where M = W, is assigned to the transient species A in equation (5.1), and the nature of its structure will be discussed later.

5.3.2 Structure of the intermediates B and B'

The ^{1}H NMR resonance associated with the brown intermediate B in reaction (5.1), when M = W, collapsed upon cooling in acetone-d_6/fluorotrichloromethane ($FCCl_3$) (1:1) as the solvent (see Figure 5.5). At 136 K the ^{1}H NMR spectrum of B showed four broad resonances at δ = 2.76, 5.55, 5.79 and 6.53 ppm, integrating in the ratio 1:2:2:2. From selective decoupling experiments on the partially frozen out species B at 136 K, it was concluded that the species B has the following structure:-

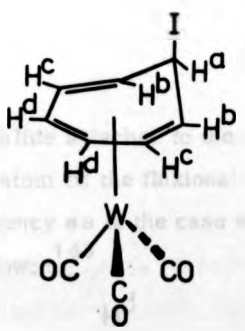

Figure 5.6
Structure of the brown intermediate B.

where the protons H^a, H^b, H^c and H^d are assigned to the resonances at δ = 2.76, 5.55, 5.79 and 6.53 ppm of the low temperature ^{1}H NMR spectrum shown in Figure 5.5. Furthermore, these selective decoupling experiments indicated that the iodide ion was undergoing

1,3 sigmatropic shifts round the C_7H_7 ring as decoupling of H^a at 136 K resulted in the transfer of the homonuclear decoupling frequency to H^c and H^d (spin saturation of H^a resulted in a large reduction of the signal intensity associated with H^c and a partial reduction of the signal intensity associated with H^d). The spectral assignments for this fluxional structure (Figure 5.6) with the iodide exocyclic (exo) on the cycloheptatriene ring are consistent with some closely related structures as shown in Table 5.2, the unique hydrogen atom (H^a) in these structures always having a resonance at low frequency. The room temperature spectrum and computer simulated spectrum for the exocyclic adduct between the $[(C_7H_7)W(CO)_3]^+$ ion and tri-n-butylphosphine ($(^nBu)_3P$) in acetone-d_6 is shown in Figure 5.7 for comparison. If the structure of the transient species B were as follows:-

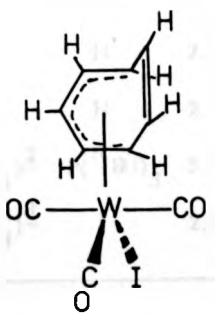

with the halide attached to the metal centre of the complex, the unique hydrogen atom of the fluxional C_7H_7 ring would be expected to be at high frequency as is the case with the $[(C_5H_7)Fe(CO)_3]^+$ ion as shown below:-[143]

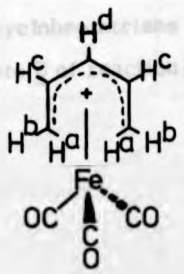

δ H^a = 2.17, H^b = 3.75, H^c = 6.26 and H^d = 7.22 ppm

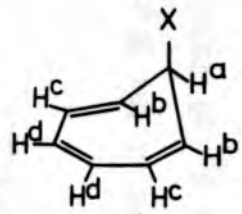

Species	X	δ/ppm H^a	H^b	H^c	H^d	X
(C_7H_7X)[1]	H	2.12	5.27	6.09	6.51	2.12
$[(C_7H_7X)W(CO)_3]$[1]	H	2.8	3.9	4.82	6.04	2.8
$[(C_7H_7X)W(CO)_3](BF_4)$[2]	$P(^nBu)_3$	3.21	5.51	6.57	6.74	–
$[(C_7H_7X)W(CO)_3](BF_4)$[3]	I	2.76	5.55	5.79	6.53	–

1. Reference 142.
2. Reference 131.
3. This work.

TABLE 5.2

Comparison of the ^1H NMR chemical shifts of some known exocyclic cycloheptatriene adducts with those of the brown intermediate B of reaction (5.1).

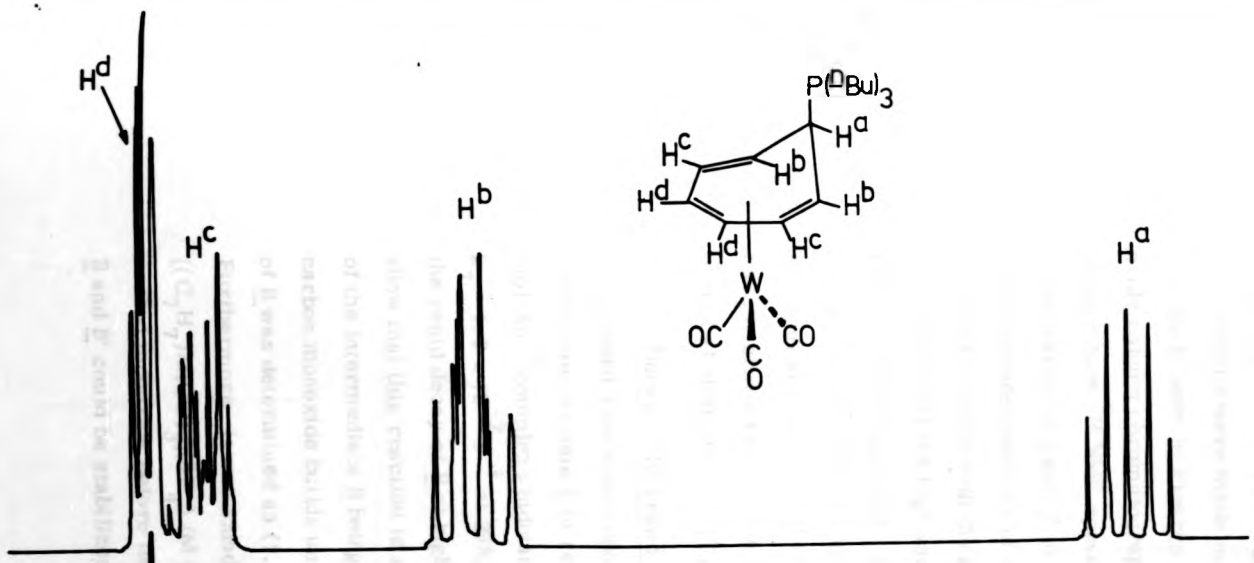

Figure 5.7

90MHz ^{1}HNMR spectra of the $[(C_7H_7P(^nBu)_3)W(CO)_3](BF_4$ complex in acetone-d_6 at 297K.

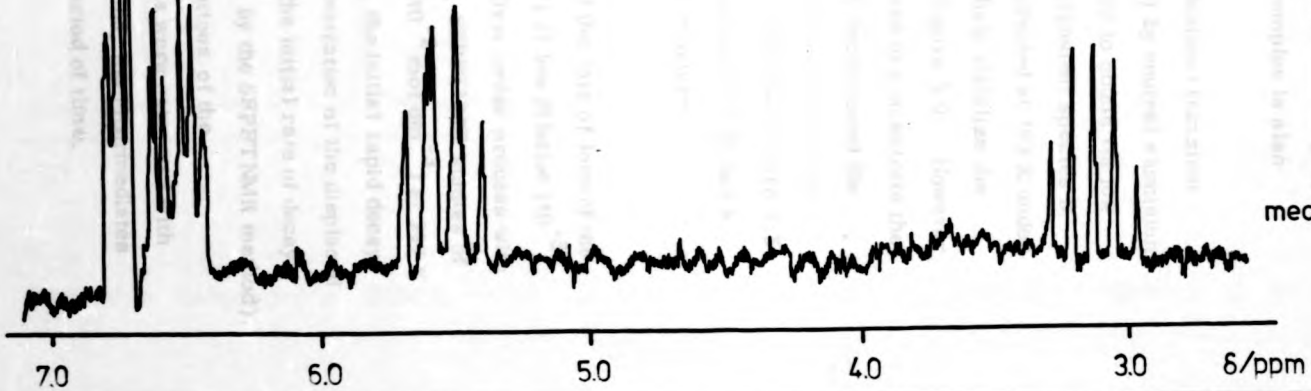

The ^{1}H NMR reaonance associated with the brown intermediate B of reaction (5.1) when M = Mo could not be frozen out even at 136 K. However, significant line-broadening did occur at greatly reduced temperatures, which shows that this complex is also fluxional in nature (see Figure 5.8).

Attempts were made to isolate the minor fluxional transient species B' seen in Figures 5.4 and 5.5 (M = W) by neutral aluminium oxide column chromatography at 193 K, in order to obtain its low temperature ^{1}H NMR spectrum free from the transient species B. A separation of B and B' in acetone could be effected at 193 K under 1 atmosphere pressure of carbon monoxide to help stabilize the transient species with the apparatus shown in Figure 5.9. However, it is likely that the high vacuum process,required to concentrate the resulting eluted acetone solution of B' at 193 K,decomposed the species, as its low temperature ^{1}H NMR spectrum showed a non-fluxional singlet at δ = 7.66 ppm even at 136 K, whereas Figure 5.5 clearly shows that the freshly produced transient species B' has a chemical shift of δ = 5.19 ppm and is fluxional in nature.

5.3.3 Decay of the brown intermediate, B

Stopped-flow spectrophotometric studies of the rate of loss of the brown intermediate B in reaction (5.1) (M = W) at low dilution (10^{-3} mol dm^{-3} complex) indicated an irreversible first-order process with $k_2 = 1.2 \times 10^{-2}$ s^{-1} at 298.2 K.[140] However, SFPFTNMR studies of the rapid decay of B at higher concentrations (10^{-2} mol dm^{-3}) at 297 K show that this reaction is reversible reaction, the initial rapid decay of the intermediate B being slowed as the concentration of the displaced carbon monoxide builds up in solution (k_2 for the initial rate of decay of B was determined as $(1.1 \pm 0.1) \times 10^{-2}$ s^{-1} by the SFPFTNMR method). Furthermore, it was found that if acetone solutions of the $[(C_7H_7)M(CO)_3](BF_4)$ (M = Mo, W) complexes were saturated with carbon monoxide before the addition of iodide ion, the intermediates B and B' could be stabilized for quite a long period of time.

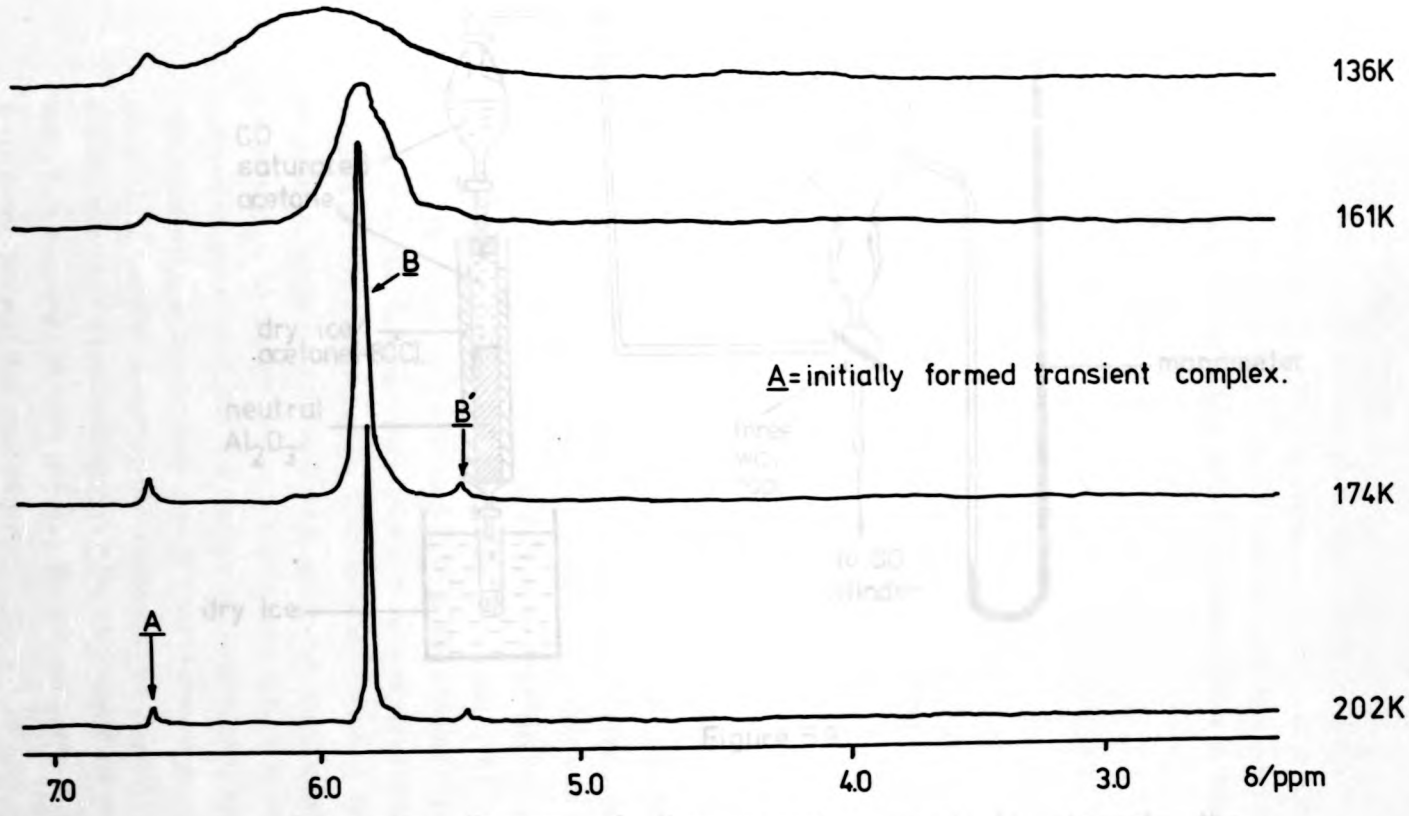

Figure 5.8

Variable temperature 90MHz ^{1}HNMR spectra of the brown transient species B (M=Mo) in acetone-d_6 /$FCCl_3$ (1:1).

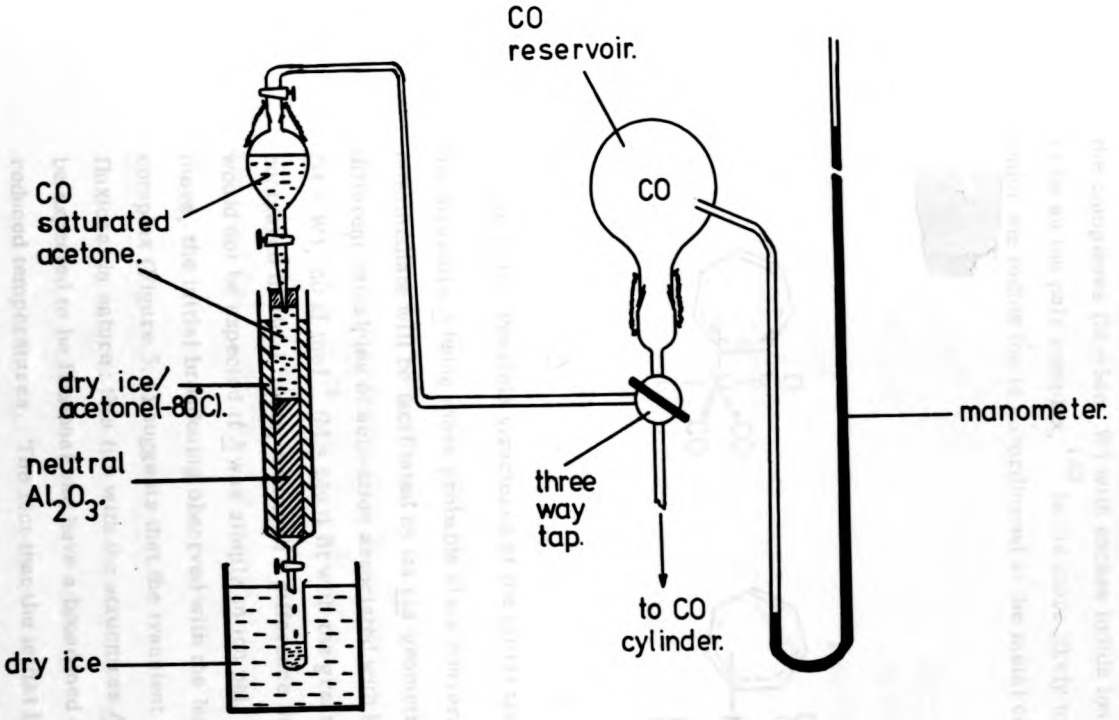

Figure 5.9

Schematic diagram of the apparatus used to separate the brown transient intermediates B and B'

5.4 Discussion

5.4.1 The transient species A

Intermediate A of reaction (5.1), which forms rapidly upon mixing the complexes (M = Mo, W) with excess iodide ion, was thought not to be an ion pair complex,[140] but is more likely to be a complex in which the iodide ion is co-ordinated at the metal centre as follows,

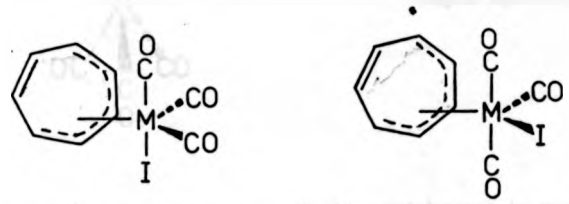

A A'

Figure 5.10 Possible structures of the initial transient complex A.

the structure A being more probable since conversion to the brown intermediate will be facilitated by its cis-geometry. The significantly different enthalpies of activation associated with k_1 ($\Delta H^{\ddagger}$ = 89 kJ mol^{-1} (M = W), 60 kJ mol^{-1} (M = Mo)) fit with the greater strength of W-I compared to Mo-I bonds, and such a difference in $\Delta H^{\ddagger}$ (29 kJ mol^{-1}) would not be expected if A was simply an ion pair complex. Furthermore, the initial broadening observed with the less reactive tungsten complex (Figure 5.4) suggests that the transient species A is fluxional in nature; this fits with the structures A and A' which would be expected to be fluxional and have a broadened C_7H_7 resonance at reduced temperatures. The fact that the initial broadening associated with transient A is not observed when M = Mo is consistent with the known $C_7H_7^+$-M bond strengths which decease in the order W > Mo,[138] and the fact that the transient species B (M = Mo) could not be frozen out. This suggests that when M = Mo, the transient species A and B are more fluxional than when M = W.

5.4.2 The transient species B and B'

The major transient species B of reaction (5.1) is unambiguously assigned the following structure with the iodide ion undergoing 1,3 sigmatropic shifts round the C_7H_7 ring:-

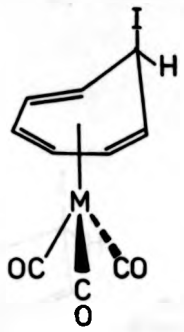

Figure 5.11
The structure of the major transient species B

where the iodide ion is exocyclic on the cycloheptatriene ring of the complex. The minor species B' (see Figures 5.3 and 5.4) is postulated as being the endocyclic (endo) isomer of B; interconversion between B' and B presumably occurring via SN_2 attack of excess iodide ion at the sp^3 carbon atom in the fluxional rings of these complexes. The chemical shift of B' is always to low frequency of that of B which is consistent with the observations of Foreman and Haque[144] who have analysed the endo and exo structures of the complexes $[(C_7H_8R)Mn(CO)_3]$ (R = H, Me, MeO) by ^1H NMR and concluded that for the CH_2 ring protons in these systems $\delta H_{exo} < \delta H_{endo}$.

5.4.3 The overall reaction scheme

In reaction (5.1) decomposition of the rapidly formed transient A (see Figure 5.10) will produce B' where the iodide ion is in an endo-position to the $C_7H_7^+$ ring, interconversion of B' to B (the more stable structure) and vice versa occurring by means of the excess iodide ion in solution: B' finally decomposes to give the final product

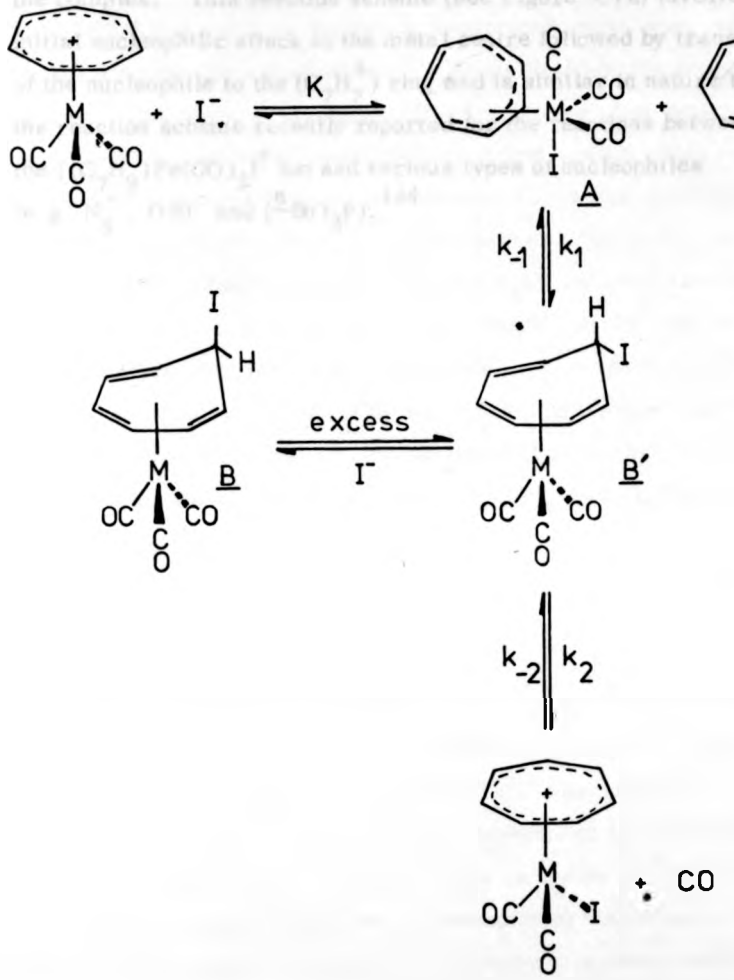

Figure 5.12

Overall reaction scheme for the reaction between $[(C_7H_7)M(CO)_3](BF_4)$ (M = Mo, W) and excess iodide ion in acetone solution.

via the displacement of a carbonyl group from the metal centre of the complex. This reaction scheme (see Figure 5.12) involves initial nucleophilic attack at the metal centre followed by transfer of the nucleophile to the ($C_7H_7^+$) ring and is similar in nature to the reaction scheme recently reported for the reactions between the $[(C_7H_9)Fe(CO)_3]^+$ ion and various types of nucleophiles (e.g. N_3^-, OEt^- and $(^nBu)_3P$).[144]

CHAPTER 6

CONCLUSIONS

The SFPFTNMR method of monitoring moderately rapid reactions in solution has proved to be a powerful technique for determining reaction mechanisms. For example, the minor free-radical reaction between some tris-(pentane-2,4-dionato)cobalt(III) complexes and N-chloro-succinimide in deuteriochloroform, discussed in Chapter 3, probably could not have been detected by any other technique. Similarly, the ligand substitution reactions of the $[Al^{III}(DMSO)_6]^{3+}$ ion discussed in Chapter 4 could not have been monitored by conventional UV-visible stopped-flow spectrophotometric methods because of the nature of the solvent used, as nitromethane absorbs strongly in the UV spectral region where the complexes absorb. The investigation of the transient intermediates produced during the reaction of the $[(C_7H_7)M(CO)_3](BF_4)$ (M = Mo, W) complexes with excess iodide ion, discussed in Chapter 5, shows the extent of structural information obtainable for some reaction systems by the SFPFTNMR method. Furthermore, in general only NMR can detect deuteriation reactions readily in solution.[5']

Although the SFPFTNMR method can only be used to monitor reactions with a half life longer than ca. 3 s at room temperature (297 K), the development of a variable temperature SFPFTNMR attachment has permitted reactions with second-order rate constants of ca. 10^4 dm^3 mol^{-1} s^{-1} (at 297 K) to be measured at temperatures as low as -60° C. Furthermore, reasonably reliable enthalpies and entropies of activation can be measured with this variable temperature attachment, a temperature range of more than 100° C being possible, depending on the reaction under investigation and the solvent system used (200 to 343 K have been used so far).

An obvious extension of the SFPFTNMR technique described in Chapter 2 which has still to be developed is to use the full multinuclear capability of the Bruker WH90 Fourier-transform NMR spectrometer. Use of the instrument's interchangeable probe systems would easily permit kinetic

CHAPTER 6

CONCLUSIONS

The SFPFTNMR method of monitoring moderately rapid reactions in solution has proved to be a powerful technique for determining reaction mechanisms. For example, the minor free-radical reaction between some tris-(pentane-2, 4-dionato)cobalt(III) complexes and N-chloro-succinimide in deuteriochloroform, discussed in Chapter 3, probably could not have been detected by any other technique. Similarly, the ligand substitution reactions of the $[Al^{III}(DMSO)_6]^{3+}$ ion discussed in Chapter 4 could not have been monitored by conventional UV-visible stopped-flow spectrophotometric methods because of the nature of the solvent used, as nitromethane absorbs strongly in the UV spectral region where the complexes absorb. The investigation of the transient intermediates produced during the reaction of the $[(C_7H_7)M(CO)_3](BF_4)$ (M = Mo, W) complexes with excess iodide ion, discussed in Chapter 5, shows the extent of structural information obtainable for some reaction systems by the SFPFTNMR method. Furthermore, in general only NMR can detect deuteriation reactions readily in solution.[57]

Although the SFPFTNMR method can only be used to monitor reactions with a half life longer than ca. 3 s at room temperature (297 K), the development of a variable temperature SFPFTNMR attachment has permitted reactions with second-order rate constants of ca. 10^4 dm^3 mol^{-1} s^{-1} (at 297 K) to be measured at temperatures as low as -60° C. Furthermore, reasonably reliable enthalpies and entropies of activation can be measured with this variable temperature attachment, a temperature range of more than 100° C being possible, depending on the reaction under investigation and the solvent system used (200 to 343 K have been used so far).

An obvious extension of the SFPFTNMR technique described in Chapter 2 which has still to be developed is to use the full multinuclear capability of the Bruker WH90 Fourier-transform NMR spectrometer. Use of the instrument's interchangeable probe systems would easily permit kinetic

measurement to be carried out by some other magnetically active nuclei (e.g. ^{31}P, ^{19}F and ^{27}Al) without any modification to the existing SF attachment. For example, ligand substitution reactions similar to those described in Chapter 4 could be carried out with some of the more sterically crowded organophosphorus tetrahedral and octahedral solvates of the Al(III) ion[145,146] by ^{31}P and ^{27}Al SFPFTNMR, thus enabling a correlation of the effect of changing solvation number and inner-sphere steric crowding on the rate determining ring closure reactions of the ligands 2,2'-bipyridine and 2,2':6'2''-terpyridine with the Al(III) ion. Similarly, an investigation of the electrophilic substitution reactions of tris-(pentane-2,4-dionato) metal complexes of the type $[M^{III}(acacH)_n\text{-}(F_6\text{-}acacH)_m]$ $(n + m = 3)$ where $(F_6\text{-}acacH)$ = the ligand 1,5-hexafluoro-2,4-pentanedione and M = Co^{III}, Rh^{III}, could be carried out by ^{19}F SFPFTNMR measurements.

This development of variable temperature multinuclear SFPFTNMR kinetic measurements alongside the already successful SFPFT ^{1}H NMR experiment will go a long way to making stopped-flow NMR a versatile and indispensable technique for the elucidation of reaction mechanisms in solution.

measurement to be carried out by some other magnetically active nuclei (e.g. ^{31}P, ^{19}F and ^{27}Al) without any modification to the existing SF attachment. For example, ligand substitution reactions similar to those described in Chapter 4 could be carried out with some of the more sterically crowded organophosphorus tetrahedral and octahedral solvates of the Al(III) ion[145,146] by ^{31}P and ^{27}Al SFPFTNMR, thus enabling a correlation of the effect of changing solvation number and inner-sphere steric crowding on the rate determining ring closure reactions of the ligands 2,2'-bipyridine and 2,2':6'2''-terpyridine with the Al(III) ion. Similarly, an investigation of the electrophilic substitution reactions of tris-(pentane-2,4-dionato) metal complexes of the type $[M^{III}(acacH)_n(F_6\text{-}acacH)_m]$ $(n + m = 3)$ where $(F_6\text{-}acacH)$ = the ligand 1,5-hexafluoro-2,4-pentanedione and M = Co^{III}, Rh^{III}, could be carried out by ^{19}F SFPFTNMR measurements.

This development of variable temperature multinuclear SFPFTNMR kinetic measurements alongside the already successful SFPFT ^1H NMR experiment will go a long way to making stopped-flow NMR a versatile and indispensable technique for the elucidation of reaction mechanisms in solution.

APPENDIX 1

DISKFT PROGRAM COMMANDS

MODE SETTINGS

VI	VIEW INPUT
VM	VIEW MEMORY
CD	CONTINUOUS DISPLAY
AR	AUTO RECUR
PT	POSITIVE TRIGGER
NT	NEGATIVE TRIGGER
AD	ADD DATA
SB	SUBTRACT DATA
IA	INTERNAL ADDRESS ADVANCE
XA	EXTERNAL ADDRESS ADVANCE

DATA ACCUMULATION

ZE	ZERO DISPLAYED MEMORY
GO	START SPECTRUM ACCUMULATION
CO	CONTINUE INTERRUPTED ACCUMULATION (NOTE 1)
	DURING ACCUMULATION:
	M: VIEW MEMORY
	I: VIEW INPUT
	C: CONTINUOUS DISPLAY
	OTHER:STOP ACCUMULATION
NS	SET NUMBER OF SWEEPS (0 FOR UNLIMITED NUMBER)(NOTE 1)
DR	SET OR EXAMINE DIGITISER RESOLUTION (NOTE 2)
MR	SET MINIMUM DIGITISER RESOLUTION (NOTE 2)
SW	SET SWEEP WIDTH IN HZ
DW	SET DWELL TIME IN MICROSECONDS
DE	SET DELAY TIME IN MICROSECONDS
NU	NUCLEUS SELECTION (NOTE 3)
SC	PRINT NUMBER OF SWEEPS COMPLETED SINCE LAST GO COMMAND
TG	START TWO-PULSE SEQUENCE ACCUMULATION (NOTE 5)

DATA PROCESSING

T1	FIRST LIMIT FOR TRAPEZOIDAL MULTIPLICATION
T2	SECOND LIMIT FOR TRAPEZOIDAL MULTIPLICATION
TR	TRAPEZOIDAL MULTIPLICATION
TC	TIME CONSTANT FOR EXPONENTIAL MULTIPLICATION
EM	EXPONENTIAL MULTIPLICATION
BC	BASELINE CORRECTION (TO FID)
FT	FOURIER TRANSFORM

PHASE CORRECTION

PA	SET ZERO ORDER PHASE PARAMETER FOR PC
PB	SET FIRST ORDER PHASE PARAMETER FOR PC
PC	"TELETYPE" PHASE CORRECTION

PH PHASE CORRECTION USING KNOBS (NOTE 4)
F: MAKE ADJUSTMENT FINER
C: RETURN TO COARSE ADJUSTMENT
RETURN:EXIT
PS PHASE CORRECTION USING SAME TOTAL (KNOB) CORRECTION AS FOR PREVIOUS SPECTRUM
TP PRINT TOTAL PHASE CORRECTION SINCE LAST FT (NOTE 21)
IS INVERT SPECTRUM (NOTE 22)

DATA TRANSFERS

DF SELECT "DATA FROM" BLOCK AND TYPE RETURN
DT SELECT "DATA TO" BLOCK AND TYPE RETURN
DC SET DATA CONSTANT FOR AT
MV MOVE DATA FROM DF BLOCK TO DT BLOCK
AT ADDITIVE TRANSFER. DF BLOCK MULTIPLIED BY DC AND ADDED TO DT BLOCK

DISPLAY

PL PLOT DISPLAYED SPECTRUM
F: FASTER (NOTE 6)
S: SLOWER
Q: ABORT PLOT
RETURN:START PLOT, AND RETURN PEN AT END OF PLOT
PP PRINT LIST OF PEAKS IN DISPLAYED REGION (NOTE 7)
Q: ABORT LISTING
SF ENTER SPECTROMETER FREQUENCY IN MHZ
MH SET MINIMUM HEIGHT THRESHOLD FOR PP
K: SET WITH KNOB A (THEN TYPE RETURN)
CU "TELETYPE" CURSOR (NOTES 8, 9)
L: MOVE ONE POINT LEFT
R: MOVE ONE POINT RIGHT
ML: START MOVING LEFT
MR: START MOVING RIGHT
OTHER:STOP MOVING

OTHER SUBCOMMANDS FOR CU AND SK:
RETURN: EXIT
A: ENTER ASSIGNMENT (NOTE 8)
C1:) TAKE CURRENT POINT AS ONE LIMIT FOR LATER
C2: ∫ EXPANSION ETC WITH IR OR KP COMMAND
F: PRINT FREQUENCY, DELTA VALUE AND CURSOR NUMBER OF CURRENT POINT
CTRL/Z: ZERO CURRENT POINT (NOTE 10)
CTRL/O: OFFSET SPECTRUM SO THAT CURRENT POINT MOVES TO RIGHT-HAND END OF DISPLAY (NOTE 11)
CTRL/A: OFFSET CURRENT POINT TO TMS POSITION AND ASSIGN AS 0 DELTA (NOTE 11)

SK SINGLE KNOB CURSOR. KNOB A GIVES COARSE CONTROL, KNOB B FINE CONTROL OF CURSOR POSITION. SWEEP COUNTER SHOWS CURSOR NUMBER.
SUBCOMMANDS AS ABOVE. ALSO:
X: EXPAND. KNOB A CONTROLS CENTRE, KNOB B WIDTH OF EXPANSION
B: BINARY EXPANSION. SAME AS X EXCEPT NUMBER OF

POINTS DISPLAYED IS $2^{\dagger}$ N+1. SWEEP COUNTER SHOWS NUMBER OF POINTS

SUBCOMMANDS FOR SK-X, SK-B, DK(-X) AND IR
C: CONTRACT TO NORMAL SPECTRUM
RETURN:EXIT FROM MAIN COMMAND
I: INTEGRATE AXPANDED REGION. KNOBS CONTROL SLOPE AS FOR ID
P: PLOT EXPANDED REGION (OR INTEGRAL). F,S,Q,RETURN AS FOR PL
D: "DUMP" SELECTED REGION (NOTE 12). Q: ABORT
A: } PRINT INTEGRAL
R: } OF EXPANDED
L: } REGION (NOTE 19)

DK DOUBLE KNOB CURSOR. EACH KNOB CONTROLS ONE CURSOR. SUBCOMMANDS AS ABOVE. ALSO:
X: EXPAND. EACH KNOB CONTROLS ONE END OF EXPANSION

ID INTEGRATE DISPLAY. KNOBS CONTROL FIRST AND SECOND ORDER CORRECTIONS TO SLOPE. FINENESS OF CORRECTIONS IS CONTROLLED BY VERTICAL DISPLAY SCALE SWITCH.
RETURN: EXIT
F: FIX CORRECTIONS IN MEMORY AND EXIT (NOTE 13)
P: PLOT INTEGRAL. F,S,Q,RETURN AS FOR PL
R: RESET INTEGRAL TO ZERO (DURING PLOTTING)

IR INTENSITY REGION SELECTED BY C1 AND C2 (CU, SK), BY LAST EXPANSION (SK-X OR SK-B) OR BY DK.
SUBCOMMANDS AS ABOVE. ALSO:
X: EXPAND

AC ADD CONSTANT. HEIGHT AND SLOPE OF SPECTRUM BASELINE ARE CONTROLLED BY KNOBS A AND B RESPECTIVELY. FINENESS OF CORRECTIONS IS CONTROLLED BY VERTICAL DISPLAY SCALE SWITCH.
RETURN: PERFORM CORRECTIONS TO MEMORY AND EXIT
Q: EXIT WITHOUT ALTERING MEMORY (NOTE 23)

OTHER COMMANDS

MO CALL IN THE DISC MONITOR

LI LINK UP TO 16 COMMANDS. END THE LIST WITH TWO RETURNS (NOTE 14)

LL PRINT THE CURRENT LINK LIST

AU EXECUTE THE LINKED COMMANDS AUTOMATICALLY

ST ≠ (WHERE ≠ IS A DIGIT) STORE THE DISPLAYED SPECTRUM ON DISC WITH THE FILE NAME TEMP≠. ANY EXISTING FILE OF THAT NAME IS DELETED.

LT ≠ LOAD THE SPECTRUM TEMP≠

CB CHANGE BLOCK. THE DISPLAYED BLOCK IS DEFINED AS THE REAL PART OF THE "LAST FOURIER TRANSFORMED SPECTRUM". THE FREQUENCY SCALE IS RECALCULATED FROM THE CURRENT VALUE OF SW.

NC PRINT THE NORMALISATION CONSTANT USED IN THE LAST FOURIER TRANSFORM

POINTS DISPLAYED IS $2^{\uparrow}$ N+1. SWEEP COUNTER SHOWS NUMBER OF POINTS

SUBCOMMANDS FOR SK-X, SK-B, DK(-X) AND IR
C: CONTRACT TO NORMAL SPECTRUM
RETURN:EXIT FROM MAIN COMMAND
I: INTEGRATE AXPANDED REGION. KNOBS CONTROL SLOPE AS FOR ID
P: PLOT EXPANDED REGION (OR INTEGRAL). F,S,Q,RETURN AS FOR PL
D: "DUMP" SELECTED REGION (NOTE 12). Q: ABORT
A: } PRINT INTEGRAL
R: } OF EXPANDED
L: } REGION (NOTE 19)

DK DOUBLE KNOB CURSOR. EACH KNOB CONTROLS ONE CURSOR. SUBCOMMANDS AS ABOVE. ALSO:
X: EXPAND. EACH KNOB CONTROLS ONE END OF EXPANSION

ID INTEGRATE DISPLAY. KNOBS CONTROL FIRST AND SECOND ORDER CORRECTIONS TO SLOPE. FINENESS OF CORRECTIONS IS CONTROLLED BY VERTICAL DISPLAY SCALE SWITCH.
RETURN: EXIT
F: FIX CORRECTIONS IN MEMORY AND EXIT (NOTE 13)
P: PLOT INTEGRAL. F,S,Q,RETURN AS FOR PL
R: RESET INTEGRAL TO ZERO (DURING PLOTTING)

IR INTENSITY REGION SELECTED BY C1 AND C2 (CU, SK), BY LAST EXPANSION (SK-X OR SK-B) OR BY DK.
SUBCOMMANDS AS ABOVE. ALSO:
X: EXPAND

AC ADD CONSTANT. HEIGHT AND SLOPE OF SPECTRUM BASELINE ARE CONTROLLED BY KNOBS A AND B RESPECTIVELY. FINENESS OF CORRECTIONS IS CONTROLLED BY VERTICAL DISPLAY SCALE SWITCH.
RETURN: PERFORM CORRECTIONS TO MEMORY AND EXIT
Q: EXIT WITHOUT ALTERING MEMORY (NOTE 23)

OTHER COMMANDS

MO CALL IN THE DISC MONITOR

LI LINK UP TO 16 COMMANDS. END THE LIST WITH TWO RETURNS (NOTE 14)

LL PRINT THE CURRENT LINK LIST

AU EXECUTE THE LINKED COMMANDS AUTOMATICALLY

ST ≠ (WHERE ≠ IS A DIGIT) STORE THE DISPLAYED SPECTRUM ON DISC WITH THE FILE NAME TEMP≠. ANY EXISTING FILE OF THAT NAME IS DELETED.

LT ≠ LOAD THE SPECTRUM TEMP≠

CB CHANGE BLOCK. THE DISPLAYED BLOCK IS DEFINED AS THE REAL PART OF THE "LAST FOURIER TRANSFORMED SPECTRUM". THE FREQUENCY SCALE IS RECALCULATED FROM THE CURRENT VALUE OF SW.

NC PRINT THE NORMALISATION CONSTANT USED IN THE LAST FOURIER TRANSFORM

SP SAVE CURRENT STATE OF PROGRAMME ON DISC
RS REVERSE SPECTRUM
D1 } DELAYS FOR TG, KG
D2 } (NOTES 5, 16)

KINETICS COMMANDS (NOTE 15)

NE SET NUMBER OF EXPERIMENTS (SPECTRA) FOR KG
KN SET NUMBER OF SWEEPS PER SPECTRUM
KG START KINETICS SPECTRUM ACCUMULATION (NOTE 16)
RETURN:STOP ACCUMULATION, BUT SAVE SPECTRA ALREADY COMPLETED
Q: ABORT RUN COMPLETELY
IT USE INTERNAL TIMING (NOTE 5)
XT USE EXTERNAL TIMING (FROM GATED DECOUPLER)
VW VIEW KINETICS DATA
N: VIEW NEXT SPECTRUM
R: VIEW PREVIOUS SPECTRUM
RETURN:EXIT
PW PROCESS KINETIC DATA AND WRITE ON DISC. FIDS ARE READ IN, ZERO-FILLED TO CURRENTLY SELECTED MEMORY SIZE, PROCESSED ACCORDING TO PREVIOUSLY SET LI LIST AND WRITTEN BACK ON DISC. (NOTES 17, 18)
PR SAME AS PW, EXCEPT SPECTRA ARE NOT WRITTEN BACK ON DISC (NOTE 18)
LS LIST TITLE AND PARAMETERS FOR KINETICS DATA
KP AUTOMATIC PLOT OF REGION WHICH HAS PREVIOUSLY BEEN SELECTED BY SK-X, SK-B, CU, SK-C1, C2 OR DK. MEMORY SIZE ALLOCATION CONTROLS HORIZONTAL EXPANSION
OF SET OFFSET (SPACING BETWEEN SPECTRA) FOR KP
LH LIST HEIGHTS AND CALCULATE RATE CONSTANT FOR SELECTED PEAK (NOTE 20)
FD ENTER FIELD DRIFT COMPENSATION FOR LH

NOTES

1 THE VALUE OF NS MAY BE CHANGED DURING AN ACCUMULATION. CONTINUE AVERAGING WITH CO.

2 NORMALLY ADC RESOLUTION IS CONTROLLED COMPLETELY AUTOMATICALLY, AND THERE IS NO NEED TO USE THE DR AND MR COMMANDS. RESOLUTION IS INITIALLY SET TO 12 BITS ON EACH GO COMMAND. IF OVERFLOW IS IMMINENT THE RESOLUTIONS IS REDUCED BY TWO BITS AND THE MEMORY CONTENTS ARE DIVIDED BY 4. TO PREVENT THE RESOLUTION FROM GOING TOO LOW, THE VALUE OF MR (MINIMUM RESOLUTION) MAY BE SET TO 8, 10 OR 12 BITS INSTEAD OF 6. WHEN OVERFLOW IS IMMINENT AT THIS RESOLUTION, ACCUMULATION STOPS AND THE MESSAGE "OVERFLOW" IS PRINTED. THE DR COMMAND MAY BE USED TO EXAMINE THE VALUE OF THE RESOLUTION AT THE END OF A RUN. IF A VALUE IS ENTERED IT ISUSED AS THE INITIAL SETTING FOR THE NEXT GO COMMAND. OTHERWISE 12 BITS IS ASSUMED. "ADC RESOLUTION" SHOULD ALWAYS BE SET AT "PROGRAM CONTROL."

SP SAVE CURRENT STATE OF PROGRAMME ON DISC
RS REVERSE SPECTRUM
D1 } DELAYS FOR TG, KG
D2 } (NOTES 5, 16)

KINETICS COMMANDS (NOTE 15)

NE SET NUMBER OF EXPERIMENTS (SPECTRA) FOR KG
KN SET NUMBER OF SWEEPS PER SPECTRUM
KG START KINETICS SPECTRUM ACCUMULATION (NOTE 16)
RETURN:STOP ACCUMULATION, BUT SAVE SPECTRA ALREADY COMPLETED
Q: ABORT RUN COMPLETELY
IT USE INTERNAL TIMING (NOTE 5)
XT USE EXTERNAL TIMING (FROM GATED DECOUPLER)
VW VIEW KINETICS DATA
N: VIEW NEXT SPECTRUM
R: VIEW PREVIOUS SPECTRUM
RETURN:EXIT
PW PROCESS KINETIC DATA AND WRITE ON DISC. FIDS ARE READ IN, ZERO-FILLED TO CURRENTLY SELECTED MEMORY SIZE, PROCESSED ACCORDING TO PREVIOUSLY SET LI LIST AND WRITTEN BACK ON DISC. (NOTES 17, 18)
PR SAME AS PW, EXCEPT SPECTRA ARE NOT WRITTEN BACK ON DISC (NOTE 18)
LS LIST TITLE AND PARAMETERS FOR KINETICS DATA
KP AUTOMATIC PLOT OF REGION WHICH HAS PREVIOUSLY BEEN SELECTED BY SK-X, SK-B, CU, SK-C1, C2 OR DK. MEMORY SIZE ALLOCATION CONTROLS HORIZONTAL EXPANSION
OF SET OFFSET (SPACING BETWEEN SPECTRA) FOR KP
LH LIST HEIGHTS AND CALCULATE RATE CONSTANT FOR SELECTED PEAK (NOTE 20)
FD ENTER FIELD DRIFT COMPENSATION FOR LH

NOTES

1 THE VALUE OF NS MAY BE CHANGED DURING AN ACCUMULATION. CONTINUE AVERAGING WITH CO.

2 NORMALLY ADC RESOLUTION IS CONTROLLED COMPLETELY AUTOMATICALLY, AND THERE IS NO NEED TO USE THE DR AND MR COMMANDS. RESOLUTION IS INITIALLY SET TO 12 BITS ON EACH GO COMMAND. IF OVERFLOW IS IMMINENT THE RESOLUTIONS IS REDUCED BY TWO BITS AND THE MEMORY CONTENTS ARE DIVIDED BY 4. TO PREVENT THE RESOLUTION FROM GOING TOO LOW, THE VALUE OF MR (MINIMUM RESOLUTION) MAY BE SET TO 8, 10 OR 12 BITS INSTEAD OF 6. WHEN OVERFLOW IS IMMINENT AT THIS RESOLUTION, ACCUMULATION STOPS AND THE MESSAGE "OVERFLOW" IS PRINTED. THE DR COMMAND MAY BE USED TO EXAMINE THE VALUE OF THE RESOLUTION AT THE END OF A RUN. IF A VALUE IS ENTERED IT ISUSED AS THE INITIAL SETTING FOR THE NEXT GO COMMAND. OTHERWISE 12 BITS IS ASSUMED. "ADC RESOLUTION" SHOULD ALWAYS BE SET AT "PROGRAM CONTROL."

3 THIS SINGLE COMMAND SELECTS FOUR PARAMETERS FOR EACH OF THE NUCLEI PROTON, C-13, P-31 AND B-11. TYPE H, C, P OR B. THE SELECTED VALUES ARE:

	H	C	P	B
SW	1200	6000	6000	5000
DW	416	83	83	100
DE	200	200	200	100
SF	90.02	22.628	36.43	28.87

4 THE INITIAL CORRECTION PERFORMED AFTER A FOURIER TRANSFORM IS THE SAME AS THE TOTAL CORRECTION FOR THE PREVIOUS SPECTRUM.

5 FOR TG, D1 = DELAY BETWEEN PULSES (TAU); D2 = TOTAL RECOVERY TIME (INCLUDING ACQUISITION TIME), BOTH IN MILLISECONDS.
FOR KG, D1 = INITIAL DELAY (FROM MIXING TO FIRST SPECTRUM); D2 = TOTAL REPETITION TIME (INCLUDING ACQUISITION TIME), BOTH IN SECONDS.

6 F OR S MAY BE TYPED BEFORE A RETURN AT THE END OF A PLOT TO SET THE SPEED FOR THE NEXT PLOT.

7 DURING THE PEAK LISTING THE SPECTRUM IS DISPLAYED WITH A CURSOR DOT ON THE PEAK CURRENTLY BEING LISTED. THE MEMORY ALLOCATION MAY BE CHANGED AFTER THE HEADING HAS BEEN PRINTED WITHOUT AFFECTING THE LISTING.

8 THE CURSOR POSITION MAY BE SPECIFIED IN HZ, DELTA OR TAU UNITS BY TERMINATING THE ENTRY WITH H, D OR T RESPECTIVELY INSTEAD OF A RETURN. AN ENTRY TERMINATED BY ANY OTHER CHARACTER (E.G. RETURN) IS REGARDED AS A CURSOR NUMBER. SIMILARLY, AN ASSIGNMENT MAY BE ENTERED IN DELTA OR TAU UNITS WITH A D OR T TERMINATION, WHILE ANY OTHER TERMINATION IS TAKEN TO MEAN HZ UNITS.

9 THE RANGE OF THE CURSOR IS ALWAYS THE WHOLE OF THE REAL PART OF THE LAST FOURIER TRANSFORMED BLOCK, AND THE CURSOR NUMBER IS RELATIVE TO THE START OF THAT BLOCK. THE BLOCK MAY BE REDEFINED BY THE CB COMMAND.

10 THIS COMMAND IS INTENDED FOR REMOVING "SPIKES" ON THE FID.

11 THESE COMMANDS ARE INTENDED FOR POSITIONING THE TMS PEAK ON NORMAL CHART PAPER AND ON CHART PAPER WHICH HAS THE ZERO POSITION 2 CM FROM THE RIGHT-HAND END. CTRL/A ALSO ASSIGNS THE SELECTED PEAK TO ZERO OFFSET.

12 THIS COMMAND IS INTENDED FOR OUTPUTTING THE CONTENTS OF A SELECTED REGION OF MEMORY ON PUNCHED TAPE IN A FORMAT WHICH IS MOST EASILY READ BY A COMPUTER PROGRAMMED IN FORTRAN, ALGOL ETC, E.G. FOR LINE SHAPE ANALYSIS. IT PRODUCES SIGNED SIX-DIGIT DECIMAL NUMBERS WITH LEADING ZEROES INCLUDED, SEPARATED BY SPACES, AND WITH CARRIAGE RETURNS AND LINE FEEDS TO GIVE A NEAT TABULATION. THE LISTING ENDS WITH THE "IMPOSSIBLE" NUMBER 999999, WHICH SHOULD BE TRAPPED FOR BY THE PROGRAMME. TURN ON THE PUNCH BEFORE TYPING D; TURN IT OFF BEFORE THE TRAILER IS COMPLETELY PUNCHED.

13 THIS COMMAND CAUSES THE CORRECTIONS, NOT THE INTEGRAL, TO BE STORED IN MEMORY. IT PROVIDES AN ALTERNATIVE TO THE AC COMMAND FOR CORRECTING THE BASELINE OF A SPECTRUM.

14 DO NOT INCLUDE THE COMMANDS PW OR PR IN THE LINK LIST: DO NOT INCLUDE DISC ACCESS COMMANDS (E.G. VW, KP) IN THE LINK LIST FOR PW OR PR.

15 THE COMMANDS KG, VW, PW, PR, LS, LH AND KP REQUIRE A DISC FILE NAME TO BE SPECIFIED. THE CURRENT FILE NAME IS FIRST PRINTED, AND THE PROGRAMME THEN WAITS FOR A NEW NAME (CONSISTING OF UP TO SIX CHARACTERS, AND TERMINATED BY A RETURN IF LESS THAN SIX) TO BE ENTERED. TYPE ONLY A RETURN TO INDICATE THAT THE CURRENT NAME IS TO BE USED AGAIN.

16 BEFORE TYPING KG SET VALUES OF NE, KN, D1, D2, THE VIEWING MODE AND MEMORY ALLOCATION. TO THE QUESTION "TITLE:" REPLY WITH UP TO ONE LINE OF DESCRIPTION OF THE REACTION, CONDITIONS, ETC, ENDING WITH A RETURN. THIS MESSAGE IS STORED ON DISC ALONG WITH THE MEASUREMENT PARAMETERS, AND MAY BE RECALLED BY THE LS COMMAND. INSTEAD OF ENTERING A TITLE YOU MAY TYPE CTRL/D TO PRINT THE LAST TITLE USED. THEN TYPE A RETURN TO USE THIS TITLE AGAIN, OR A LINE FEED TO ENTER A NEW ONE.
ALTHOUGH THE VALUE OF D1 HAS NO EFFECT ON DATA ACQUISITION, AND D2 HAS NO EFFECT IN THE XT (EXTERNAL TIMING) MODE, IT IS USEFUL TO ENTER THESE VALUES BEFORE STARTING A RUN SO THAT THEY WILL BE STORED ON DISC ALONG WITH THE OTHER PARAMETERS AND AVAILABLE FOR FUTURE REFERENCE, AND FOR USE BY THE LH COMMAND.

17 IF THE ANSWER TO "REPLACE?" IS Y, THE ORIGINAL SPECTRA (FIDS) ARE DELETED FROM THE DISC, AND THE PROCESSED SPECTRA ARE GIVEN THE SAME FILE NAME. OTHERWISE A NEW FILE NAME MUST BE ENTERED.

18 USE THE PW COMMAND FOR NORMAL PROCESSING WHICH CHANGES THE SPECTRUM (E.G. EXPONENTIAL MULTIPLICATION, FOURIER TRANSFORMATION, PHASE CORRECTION). USE THE PR COMMAND FOR ACCESSING DATA IN A WAY WHICH DOES NOT CHANGE IT (E.G. PLOTTING, LISTING PEAKS).

19 THESE ROUTINES CALCULATE AND PRINT AN INTEGRAL OF THE ENTIRE EXPANDED REGION, TAKING AS THE BASELINE LEVEL THE AVERAGE OF ONE-EIGHTH OF THE DISPLAYED POINTS ON EITHER OR BOTH SIDES OF THE REGION. "L" USES ONLY THE LEFT-HAND SIDE, "R" USES ONLY THE RIGHT-HAND SIDE, AND "A" CONSIDERS THE BASELINE TO BE A SLOPING LINE DRAWN THROUGH BOTH AVERAGES. THE ROUTINES ARE INTENDED FOR GIVING QUICK NUMERICAL INTEGRALS OF INDIVIDUAL PEAKS OR GROUPS OF PEAKS WITHOUT ANY NEED FOR PREVIOUS BASELINE CORRECTION.

20 THE PEAK MUST HAVE BEEN PREVIOUSLY SELECTED WITH THE SK OR CU COMMAND. THE PRESENT ROUTINE CALCULATES THE RATE CONSTANT ONLY FOR A PEAK WHOSE HEIGHT IS DECREASING WITH TIME. IF THE ROUTINE FAILS TO FIND THE PEAK IN THE SECOND SPECTRUM OF THE GROUP BECAUSE THE SPECTRA ARE OFFSET BY FIELD DRIFT THROUGH OPERATING WITH THE SPECTROMETER UNLOCKED, ENTER A VALUE OF FD EQUAL TO THE NUMBER OF CURSOR POINTS THE SECOND SPECTRUM HAS MOVED RELATIVE TO THE FIRST.

21 TO "SAVE?" ANSWER Y TO PUT PA AND PB EQUAL TO THESE VALUES

22 THIS IS EQUIVALENT TO A 180 DEGREE "A" PHASE CORRECTION.

23 IF, WHEN AC IS TYPED, THE SPECTRUM APPEARS WITH ITS HEIGHT OR SLOPE ALREADY CHANGED, TYPE Q AND THEN AC AGAIN.

APPENDIX 2

The determination of second-order rate constants for the chlorination reactions of metal acetylacetonates

$$\underset{(a-x)}{M(acacH)_3} + \underset{(a-x)}{RNCl} \xrightarrow{k} \underset{(x)}{M(acacH)_2(acacCl)} + \underset{(x)}{RNH} \qquad (i)$$

If the reaction (i) is carried out under second-order conditions with $[M(acacH)_3] = [RNCl] = a$, and x is the extent of reaction or the concentration of product $[M(acacH)_2(acacCl)]$ or RNH produced at time t. Then the rate of change of x with time (dx/dt) is given by:

$$(dx/dt) = k(a-x)^2 \qquad (ii)$$

Integrating (ii) gives:

$$x/(a-x)a = kt \qquad (iii)$$

As the height of a ^1H NMR resonance at any time t = (h_t) is directly related to the concentration (c) of the species present at time t by the equation:

$$h_t = c_t.p \qquad (iv)$$

where c is given by (a-x) and p is a proportionality constant. Thus by extrapolation to time zero of h_t (when x = 0), p can be calculated from the relationship

$$p = h_{t=0}/a \qquad (v)$$

From (iv): $(a-x) = h_t/p$

and $x = (a - h_t/p)$ (vi)

Hence, substituting (vi) into (iii) we obtain:

$$(a - h_t/p)/(h_t/p)a = kt \qquad (vii)$$

or $$(pa - h_t)/h_t a = kt \qquad (viii)$$

Rearranging (viii) gives:

$$1 - (p.a/h_t) = -kat \qquad (ix)$$

thus: $$1 + kat = (pa)/h_t \qquad (x)$$

and dividing throughout by pa gives:

$$1/h_t = 1/pa + (k/p)t \qquad (xi)$$

Therefore a plot of $1/h_t$ versus t will yield a straight line for a second-order reaction of slope k/p. Division of the slope by p will then give k the second-order rate constant in units of $dm^3 mol^{-1} s^{-1}$.

APPENDIX 3

Chemically Induced Dynamic Nuclear Polarization (CIDNP)

The phenomenon of CIDNP, or more correctly adiabatic nuclear polarization, occurs during a reaction when free-radical pairs are created or annihilated. Near-degeneracies exist for certain electronic energy levels of the free-radicals concerned, nuclear hyperfine interactions can mix these levels, and transitions within these electronic energy levels result from the motion of the radical pair during their creation or annihilation. The result of this energy level-crossing phenomenon is a polarization of the nuclear energy level populations, which is manifested as large emissive or absorptive signal enhancement (up to 600 fold or more) in the NMR spectrum of the species involved.

CIDNP is well documented[87-90] and can be used to investigate the kinetics of free-radical reactions in solution by FTNMR spectroscopy.[91] As the nuclear spin polarization created by CIDNP decays over a period of $5T_1$ (5 times the longitudinal spin lattive relaxation time of the free-radical species), 90° pulse angles have to be employed during these kinetic investigations. This is to ensure that any spin polarization created up to the time of sampling (or pulsing) due to the ensuing chemical reaction is destroyed by the pulse. By this method, meaningful signal intensities can be recorded throughout the course of the reaction.

Furthermore CIDNP spin polarization can only be produced in a laboratory magnetic field. Thus, if two reactants are mixed externally to an NMR magnetic field no polarization will occur. This can be shown by pulsing the sample (in an FTNMR experiment) at the time of introduction of the mixed sample into the spectrometer magnet. However, CIDNP effects will be observed upon magnetic equilibration of the reacting sample. This type of zero-field mixing experiment can be very useful in showing the presence of CIDNP effects and confirming the presence of a free-radical reaction.

APPENDIX 3

Chemically Induced Dynamic Nuclear Polarization (CIDNP)

The phenomenon of CIDNP, or more correctly adiabatic nuclear polarization, occurs during a reaction when free-radical pairs are created or annihilated. Near-degeneracies exist for certain electronic energy levels of the free-radicals concerned, nuclear hyperfine interactions can mix these levels, and transitions within these electronic energy levels result from the motion of the radical pair during their creation or annihilation. The result of this energy level-crossing phenomenon is a polarization of the nuclear energy level populations, which is manifested as large emissive or absorptive signal enhancement (up to 600 fold or more) in the NMR spectrum of the species involved.

CIDNP is well documented[87-90] and can be used to investigate the kinetics of free-radical reactions in solution by FTNMR spectroscopy.[91] As the nuclear spin polarization created by CIDNP decays over a period of $5T_1$ (5 times the longitudinal spin lattive relaxation time of the free-radical species), 90^{o} pulse angles have to be employed during these kinetic investigations. This is to ensure that any spin polarization created up to the time of sampling (or pulsing) due to the ensuing chemical reaction is destroyed by the pulse. By this method, meaningful signal intensities can be recorded throughout the course of the reaction.

Furthermore CIDNP spin polarization can only be produced in a laboratory magnetic field. Thus, if two reactants are mixed externally to an NMR magnetic field no polarization will occur. This can be shown by pulsing the sample (in an FTNMR experiment) at the time of introduction of the mixed sample into the spectrometer magnet. However, CIDNP effects will be observed upon magnetic equilibration of the reacting sample. This type of zero-field mixing experiment can be very useful in showing the presence of CIDNP effects and confirming the presence of a free-radical reaction.

APPENDIX 3

Chemically Induced Dynamic Nuclear Polarization (CIDNP)

The phenomenon of CIDNP, or more correctly adiabatic nuclear polarization, occurs during a reaction when free-radical pairs are created or annihilated. Near-degeneracies exist for certain electronic energy levels of the free-radicals concerned, nuclear hyperfine interactions can mix these levels, and transitions within these electronic energy levels result from the motion of the radical pair during their creation or annihilation. The result of this energy level-crossing phenomenon is a polarization of the nuclear energy level populations, which is manifested as large emissive or absorptive signal enhancement (up to 600 fold or more) in the NMR spectrum of the species involved.

CIDNP is well documented[87-90] and can be used to investigate the kinetics of free-radical reactions in solution by FTNMR spectroscopy.[91] As the nuclear spin polarization created by CIDNP decays over a period of $5T_1$ (5 times the longitudinal spin lattive relaxation time of the free-radical species), 90^{o} pulse angles have to be employed during these kinetic investigations. This is to ensure that any spin polarization created up to the time of sampling (or pulsing) due to the ensuing chemical reaction is destroyed by the pulse. By this method, meaningful signal intensities can be recorded throughout the course of the reaction.

Furthermore CIDNP spin polarization can only be produced in a laboratory magnetic field. Thus, if two reactants are mixed externally to an NMR magnetic field no polarization will occur. This can be shown by pulsing the sample (in an FTNMR experiment) at the time of introduction of the mixed sample into the spectrometer magnet. However, CIDNP effects will be observed upon magnetic equilibration of the reacting sample. This type of zero-field mixing experiment can be very useful in showing the presence of CIDNP effects and confirming the presence of a free-radical reaction.

APPENDIX 4

The determination of second- and first-order rate constants for the reactions of neutral multidentate ligands with the $[Al^{III}(DMSO)_6]^{3+}$ ion

The reaction of the tridentate ligand 2, 2':6',2" terpyridine (terpy) with the $[Al^{III}(DMSO)_6]^{3+}$ ion can be written in four stages as follows:-

$$[MS_6^b]^{3+} + L\text{-}L\text{-}L \xrightleftharpoons{K_o} [MS_6^b]^{3+},\ L\text{-}L\text{-}L \qquad (i)$$

$$[MS_6^b]^{3+},\ L\text{-}L\text{-}L \xrightleftharpoons[k_1]{k_1} [MS_5^b\text{—}L\text{-}L\text{-}L]^{3+} + S^f \qquad (ii)$$

$$[MS_5^b\text{—}L\text{-}L\text{-}L]^{3+} + S^f \xrightarrow{k_2} [MS_4^b\begin{smallmatrix}L\\)\\L\text{—}L\end{smallmatrix}]^{3+} + 2S^f \qquad (iii)$$

$$[MS_4^b\begin{smallmatrix}L\\)\\L\text{—}L\end{smallmatrix}]^{3+} + 2S^f \xrightarrow{k_3} [MS_3\begin{smallmatrix}L)\\L\\L'\end{smallmatrix}]^{3+} + 3S^f \qquad (iv)$$

where M = Al^{III}, S^b = bound DMSO, S^f = free DMSO and L-L-L = terpy.

A. Reactions (i) to (ii) can be written as an overall first bond formation reaction as follows:-

$$\underset{(a-x)}{[MS_6^b]^{3+}} + \underset{(a-x)}{L\text{-}L\text{-}L} \xrightarrow{k_f} \underset{(x)}{[MS_5^b\text{—}L\text{-}L\text{-}L]^{3+}} + \underset{(x)}{S^f} \qquad (v)$$

and applies to the formation reactions of pyridine, tert-butylamine and the first bond formation reactions of bipy and terpy. Thus under second-order conditions with $[MS_6^b] = [L\text{-}L\text{-}L] = a$ mol dm^3, and x as the extent of reaction or the concentration of product at time t, then the rate of production of x with time (dx/dt) is given by:-

$$(dx/dt) = k_f(a-x)^2 \qquad (vi)$$

Integrating (vi) gives $x/(a-x)a = k_f t$ (vii)

where k_f is the second-order rate constant for formation of the complex in units of $dm^3\ mol^{-1}\ s^{-1}$.

As the height of a ^1H NMR resonance at any time t throughout a chemical reaction is directly related to the concentration (c) of the species present at time t by the equation:-

$$h_t = c.p \qquad (viii)$$

where c is given by (a-x) or x, and p is a proportionality constant.

Thus the height of the observed bound DMSO resonance at any time t (h_t^b) for reaction (v) is given by:-

$$h_t^b = [6(a-x) + 5x]p \qquad (ix)$$

Similarly the height of the observed free DMSO resonance at any time t (h_t^f) for reaction (v) is given by:-

$$h_t^f = xp \qquad (x)$$

from (ix) and (x) $h_t^b + h_t^f = 6ap$

and $p = (h_t^b + h_t^f)/6a \qquad (xi)$

Thus $x = h_t^f/p$ from (x), and $a = (h_t^b + h_t^f)/6p$ from (xi)

Therefore $(a-x) = (h_t^b - 5h_t^f)/6p \qquad (xii)$

Substituting values of x, (a-x) and a into (vii) gives:-

$$(h_t^f)/(h_t^b - 5h_t^f) = ak_f t/6 \qquad (xiii)$$

Thus a plot of $(h_t^f)/(h_t^b - 5h_t^f)$ versus t will yield a slope of $ak_f/6$, where k_f is the second-order rate constant for reaction (v).

B. Reaction (iii) however is a first order process, and if $k_f >> k_2$ (reactions (v) and (iii)), as is the case in the reactions of bipy and terpy discussed in Chapter 4, then k_2 can be measured directly as follows:-

$$\underset{(a-x)}{[MS_6^b - L\text{-}L\text{-}L]^{3+}} + \underset{(a)}{S^f} \xrightarrow{k_2} \underset{(x)}{[MS_4^b \begin{smallmatrix} L \\ L-L \end{smallmatrix}]^{3+}} + \underset{(x)}{2S^f} \qquad (iii)$$

For reaction (iii) $dx/dt = k_2(a-x)$ and integration gives:-

$$(a-x)/a = e^{-k_2 t} \qquad (xiv)$$

From the arguments of section A

$$h_t^b = [5(a-x) + 4x]p \qquad (xv)$$

and $$h_t^f = (a+x)p \qquad (xvi)$$

Thus from (xvi) $x = (h_t^f/p) - a$ and $(a-x) = 2a - (h_t^f/p)$

and from (xv) and (xvi) $p = (h_t^b + h_t^f)/6a$

Therefore substituting values of p into (a -x) gives

$$(a-x) = (2ah_t^b - 4ah_t^f)/(h_t^b + h_t^f)$$

$$\text{or} \qquad (a-x)/a = 2[(h_t^b - 2h_t^f)/(h_t^b + h_t^f)] \qquad \text{(xvii)}$$

Thus substituting (xvii) into (xiv) and taking logs gives

$$\ln 2 + \ln[(h_t^b - 2h_t^f)/(h_t^b + h_t^f)] = -k_2 t \qquad \text{(xviii)}$$

Hence a plot of $\ln[(h_t^b - 2h_t^f)/(h_t^b + h_t^f)]$ versus t will yield a straight line plot for reaction (iii) of slope $-k_2$, where k_2 is the first-order rate constant for reaction (iii) with units of s^{-1}.

C. Reaction (iv) is also a first order process, thus if $k_2 \gg k_3$ for the reaction of terpy with the $[Al^{III}(DMSO)_6]^{3+}$ ion (reactions (iii) and (iv)), k_3 can be measured directly as follows:-

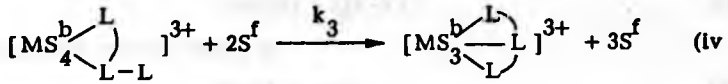

$$[MS_4^b(L)(L\text{-}L)]^{3+} + 2S^f \xrightarrow{k_3} [MS_3^b(L)_3]^{3+} + 3S^f \qquad \text{(iv)}$$

(a -x) (2a) (x) (x)

From section B it can be seen that for reaction (iv) $(dx/dt) = k_3(a-x)$, the integrated rate equation being

$$(a-x)/a = e^{-k_3 t} \qquad \text{(xix)}$$

By comparison with section B it can also be seen that

$$h_t^b = [4(a-x) + 3x]p = 4(a-x)p \qquad \text{(xx)}$$

$$\text{and } h_t^f = (2a-x)p \qquad \text{(xxi)}$$

Thus $p = (h_t^b + h_t^f)/6a$ and $x = (h_t^f/p) - 2a$

So $(a-x) = a - [(h_t^f/p) - 2a] = 3a - (h_t^f/p)$ (xxii)

Substituting values of p into (xxii) gives

$$(a-x) = 3a - [6ah_t^f/(h_t^b + h_t^f)] \qquad \text{(xxiii)}$$

Therefore $(a-x)/a = 3(h_t^b - h_t^f)/(h_t^b + h_t^f)$ (xxiv)

Thus substituting (xxiv) into (xix) and taking logs gives:-

$$\ln 3 + \ln[(h_t^b - h_t^f)/(h_t^b + h_t^f)] = -k_3 t \qquad \text{(xxv)}$$

Hence a plot of $\ln[(h_t^b - h_t^f)/(h_t^b + h_t^f)]$ versus time (t) will yield a straight line plot for reaction (iv) of slope $-k_3$, where k_3 is the first-order rate constant for reaction (iv) with units of s^{-1}.

APPENDIX 5

The determination of second-order rate constants for the reaction of 1, 10-phenanthroline with the $[Al^{III}(DMSO)_6]^{3+}$ ion.

The reaction of 1, 10-phenanthroline (phen) with the $[Al^{III}(DMSO)_6]^{3+}$ ion can be written as follows:-

$$[MS_6^b]^{3+} + L{-}L \xrightarrow{k_1} [MS_4^b\begin{smallmatrix}L\\L\end{smallmatrix}]^{3+} + 2S^f \qquad (i)$$

$$(a-x) \qquad (a-x) \qquad (x) \qquad (x)$$

where M = Al^{III}, S = DMSO, L-L = phen and a = the initial concentration of $[MS_6]^{3+}$ and L-L.

Under second-order conditions the rate of production of x with time (dx/dt) is given by:-

$$(dx/dt) = k_1(a-x)^2 \qquad (ii)$$

the integrated form of which is:-

$$x/a(a-x) = k_1 t \qquad (iii)$$

$$\text{or} \quad 1/(a-x) - 1/a = k_1 t \qquad (iv)$$

In reaction (i) let us consider the two DMSO's expelled from the Al^{III} inner sphere.

Let $h'_t = (h^b_t - 4/6\, h^b_{t=0})$ where h^b_t = height of the bound DMSO resonance at time t (see Appendix 4).

Also let p be a proportionality constant such that:-

$$ap = 2/6\, h^b_{t=0} \qquad (v)$$

for the two DMSO's expelled from the Al^{III} inner sphere during reaction (i). Thus p converts peak heights directly into concentrations, and from (v) is given by the relationship:-

$$p = 2h^b_{t=0}/6a \qquad (vi)$$

Thus the extent of reaction (x) in terms of peak heights is given by:-

$$xp = ap - h'_t$$

$$\text{or} \quad (a-x) = h'_t/p \qquad (vii)$$

where p is given by equation (vi).

As from equation (iv), a plot of 1/(a-x) versus time (t) will give a straight line of slope = $k_1/dm^3\ mol^{-1}\ s^{-1}$ for reaction (i). Then from equations (vii), (vi) and the definition of h'_t it can be seen that a plot of $1/[(h^b_t - 4/6\, h^b_{t=0})/(2h^b_{t=0}/6a)]$ versus time t will yield a straight line plot for reaction (i) of slope = $k_1/dm^3\ mol^{-1}\ s^{-1}$.

APPENDIX 5

The determination of second-order rate constants for the reaction of 1, 10-phenanthroline with the $[Al^{III}(DMSO)_6]^{3+}$ ion.

The reaction of 1, 10-phenanthroline (phen) with the $[Al^{III}(DMSO)_6]^{3+}$ ion can be written as follows:-

$$[MS_6^b]^{3+} + L{-}L \xrightarrow{k_1} [MS_4^b\begin{smallmatrix}L\\L\end{smallmatrix}]^{3+} + 2S^f \qquad (i)$$

$$(a-x) \qquad (a-x) \qquad (x) \qquad (x)$$

where M = Al^{III}, S = DMSO, L–L = phen and a = the initial concentration of $[MS_6]^{3+}$ and L-L.

Under second-order conditions the rate of production of x with time (dx/dt) is given by:-

$$(dx/dt) = k_1(a-x)^2 \qquad (ii)$$

the integrated form of which is:-

$$x/a(a-x) = k_1 t \qquad (iii)$$

$$\text{or} \qquad 1/(a-x) - 1/a = k_1 t \qquad (iv)$$

In reaction (i) let us consider the two DMSO's expelled from the Al^{III} inner sphere.

Let $h'_t = (h^b_t - 4/6\, h^b_{t=0})$ where h^b_t = height of the bound DMSO resonance at time t (see Appendix 4).

Also let p be a proportionality constant such that:-

$$ap = 2/6\, h^b_{t=0} \qquad (v)$$

for the two DMSO's expelled from the Al^{III} inner sphere during reaction (i). Thus p converts peak heights directly into concentrations, and from (v) is given by the relationship:-

$$p = 2h^b_{t=0}/6a \qquad (vi)$$

Thus the extent of reaction (x) in terms of peak heights is given by:-

$$xp = ap - h'_t$$

$$\text{or} \qquad (a-x) = h'_t/p \qquad (vii)$$

where p is given by equation (vi).

As from equation (iv), a plot of 1/(a-x) versus time (t) will give a straight line of slope = $k_1/dm^3\ mol^{-1}\ s^{-1}$ for reaction (i). Then from equations (vii), (vi) and the definition of h'_t it can be seen that a plot of $1/[(h^b_t - 4/6\, h^b_{t=0})/(2h^b_{t=0}/6a)]$ versus time t will yield a straight line plot for reaction (i) of slope = $k_1/dm^3\ mol^{-1}\ s^{-1}$.

REFERENCES

1. H. Hartridge, F.J.W. Roughton, Proc. Royal Soc., 1923, 104, 376-394.
2. B. Chance, J. Franklin Inst., 1940, 229, 455-476, 613-640, 737-766.
3. Q.H. Gibson, Discuss. Faraday Soc., 1954, 17, 137-139.
   Q.H. Gibson, E. Antonini, Biochem. J., 1960, 77, 328-341.
   Q.H. Gibson, C. Greenwood, Biochem. J., 1963, 86, 541-554.
   Q.H. Gibson, F.J.W. Roughton, Proc. Royal Soc. B., 1955, 310-334.
4. E.F. Caldin, 'Fast Reactions in Solution', 1964, Oxford-Blackwell.
5. 'Methods in Enzymology', vol. XVI, ed. K. Kustin, 1969, London - Academic.
6. K. Kustin, 'Fast Reactions', 1969, New York - Academic.
7. F.J.W. Roughton, B. Chance, 'Technique of Organic Chemistry', vol. VIII, part 2, ed. S.L. Friess, E.S. Lewis, A. Weissberger, 1963, New York - Interscience.
   B. Chance, 'Technique of Organic Chemistry', vol. VI, part 2, ed. G.G. Hammes, 1974, New York - Interscience.
8. E.F. Caldin, J.E. Crooks, A. Queen, J. Phys. E. (Scientific Instruments), 1973, 6, 930-932.
   G.K. Strother, E. Ackerman, Biochim. Biophys. Acta, 1961, 47, 317-326.
   P. Douzou, Biochimie, 1971, 53, 17-23.
   D.J. Benton, Ph.D. Thesis, University of Warwick, 1972.
9. 'Rapid Mixing and Sampling Techniques in Biochemistry', ed. B. Chance, R.H. Eisenhardt, Q.H. Gibson, K. Lonberg-Holme, 1964, London - Academic.
10. D. Michael, D. O'Donnell, N.H. Rees, Rev. Sci. Instruments, 1974, 45, 256-260.
11. J. Meier, G. Schwarzenbach, Helv. Chim. Acta, 1957, 40, 907-917.
12. G. Rechnitz, B. Fleet, Analyt. Chem., 1970, 42, 690-693.
13. R.H. Prince, Trans. Faraday Soc., 1958, 54, 838-848.
14. R.F. Chen, A.N. Schechter, R.L. Berger, Analyt. Biochem., 1969, 29, 68-75.
15. R.O.C. Norman, B.C. Gilbert, Adv. Phys. Org. Chem., 1967, 5, 53-119.

16. E. Saito, B.H.J. Bielski, J. Amer. Chem. Soc., 1961, 83, 4467-4468.
17. E. Saito, B.H.J. Bielski, J. Phys. Chem., 1962, 66, 2266-2268.
18. G. Czapski, J. Phys. Chem., 1971, 75, 2957-2967.
19. A. Samuni, G. Czapski, J. Phys. Chem., 1970, 74, 4592-4594.
20. R.O.C. Norman, P.R. West, J. Chem. Soc. B., 1969, 389-399.
21. R.L. Berger, L.C. Stoddart, Rev. Sci. Instrum., 1965, 36, 78-84.
22. R.L. Berger, B. Balko, Rev. Sci. Instrum., 1968, 39, 498-503.
23. M. Anson, P.M. Bayley, J. Phys. E.(Scientific Instruments), 1974, 7, 481-486.
24. M. Anson, P.M. Bayley, Biopolymers, 1974, 13, 401-405.
25. D.M. Goodall, M.T. Cross, Rev. Sci. Instrum., 1975, 46, 391-397.
26. S.E. Rudolph, L.F. Charbonneau, S.G. Smith, J. Amer. Chem. Soc., 1973, 95, 7083-7093.
27. S.E. Brady, J.P. Maher, J. Bromfield, K. Stewart, M. Ford, J. Phys. E.(Scientific Instruments), 1976, 9, 19-24.
28. R.L. Berger, B. Balko, H.F. Chapman, Rev. Sci. Instrum., 1968, 39, 486-493, 493-498.
29. J.E. Erman, G.G. Hammes, Rev. Sci. Instrum., 1966, 37, 746-753.
30. S.G. Smith, J. Billet, J. Amer. Chem. Soc., 1967, 89, 6948-6953.
31. J.O. Lephardt, G. Vileins, Applied Spectroscopy, 1975, 29, 221-225.
32. N.F. Chamberlain, 'The Practice of NMR Spectroscopy', 1974, New York - Plenum Press.
33. C.S. Johnson, Adv. in Magnetic Reson., 1965, 1, 33-102.
34. J.L. Sudmeier, J.J. Pesek, Inorg. Chem., 1971, 10, 860-863.
35. J. Grimaldi, J. Baldo, C. McMurray, B.D. Sykes, J. Amer. Chem. Soc., 1972, 94, 7641-7645.
36. J.J. Grimaldi, B.D. Sykes, J. Biol. Chem., 1975, 250, 1618-1624.
37. J.A. Richards, D.H. Evans, Analyt. Chem., 1975, 47, 964-966.
38. A.J. Brown, D.A. Couch, O.W. Howarth, P. Moore, J. Magnet. Reson., 1976, 21, 503-505.
39. C.A. Fyfe, M. Cocivera, S.W.H. Damji, T.A. Hostetter, D. Sproat, J. O'Brien, J. Magnet. Reson., 1976, 23, 377-384.

40. C.A. Fyfe, L. van Veen, J. Amer. Chem. Soc., 1977, 99, 3366-3371.

41. C.A. Fyfe, W.E. Sanford, C.S. Yannoni, J. Amer. Chem. Soc., 1976, 98, 7101-7102.

42. M. Cocivera, K.W. Woo, Tet. Letters, 1976, 36, 3109-3112.

43. M. Cocivera, C.A. Fyfe, A. Effio, S. Valsh, A. Chen, J. Amer. Chem. Soc., 1976, 98, 1573-1578.

44. M. Cocivera, A. Chen, E. Holger, J. Amer. Chem. Soc., 1976, 98, 7362-7366.

45. M. Cocivera, K.W. Woo, J. Amer. Chem. Soc., 1976, 98, 7366-7371.

46. C.A. Fyfe, M. Cocivera, S.W.H. Damji, J. Chem. Soc. Chem. Comm., 1973, 743-744.

47. C.A. Fyfe, M. Cocivera, S.W.H. Damji, J. Amer. Chem. Soc., 1975, 97, 5707-5713.

48. C.A. Fyfe, S.W.H. Damji, C.D. Malkiewich, A.R. Norris, J. Amer. Chem. Soc., 1976, 98, 6983-6988.

49. M.J.T. Robinson, S.M. Rosenfeld, Tet. Letters, 1975, 17, 1431-1434.

50. J.J. Grimaldi, B.D. Sykes, J. Amer. Chem. Soc., 1975, 97, 273-276.

51. D.A. Couch, O.W. Howarth, P. Moore, J. Phys. E.(Scientific Instruments), 1975, 8, 831-833.

52. D.A. Couch, O.W. Howarth, P. Moore, J. Chem. Soc. Chem. Comm., 1975, 822-823.

53. R. Thompson, G. Gordon, J. Sci. Instrum., 1964, 41, 480-481.

54. D. McClean, R.L. Tranter, J. Phys. E.(Scientific Instruments), 1971, 4, 455-459.

55. E.F. Caldin, V. Gold, 'Proton Transfer Reactions', ch. 6, 1975, London - Chapman and Hall.

56. S. Thomas, W.L. Reynolds, J. Chem. Phys., 1966, 44, 3148-3149.

57. B.E. Bryant, W.C. Fernelius, Inorg. Synthesis, 1957, 5, 105-113.

58. J.P. Frackler, Prog. Inorg. Chem., 1966, 7, 361-425.

59. J.P. Collman, 'Transition Metal Chemistry', 1966, 2, 35-45, ed. R.L. Carlin, New York - Marcel Decker.

60. K.C. Joshi, V.N. Pathak, Coordn. Chem. Revs., 1977, 22, 37-122.
61. J.J. Fortman, R.E. Sievers, Coordn. Chem. Revs., 1971, 6, 331-375.
62. R.H. Holm, M.J. O'Connor, Prog. Inorg. Chem., 1971, 14, 241-401.
63. J.P. Collman, R.L. Marshall, W.L. Young, Chem. Ind., 1962, 1380-1382.
64. M. Calvin, K.W. Wilson, J. Amer. Chem. Soc., 1945, 67, 2003-2007.
65. D.M.G. Lloyd, D.R. Marshall, Chem. Ind., 1964, 1760-1761.
66. R.H. Holm, F.A. Cotton, J. Amer. Chem. Soc., 1958, 80, 5658-5663.
67. P.R. Singh, R. Sahai, Aust. J.Chem., 1967, 20, 639-648.
68. P.R. Singh, R. Sahai, Aust. J. Chem., 1967, 20, 649-655.
69. R.W. Kluiber, J. Amer. Chem. Soc., 1961, 83, 3030-3032.
70. P.R. Singh, R. Sahai, Inorg. Chem. Acta, 1968, 2, 102-106.
71. J.P. Collman, R.L. Marshall, W.L. Young, S.D. Goldby, Inorg. Chem., 1962, 1, 704-710.
72. J.P. Collman, M. Yamada, J. Org. Chem., 1963, 28, 3017-3021.
73. J.P. Collman, R.L. Marshall, W.L. Young, C.T. Sears, J. Org. Chem., 1963, 28, 1449-1455.
74. F. Dewhurst, P.K.J. Shah, J. Chem. Soc.(C), 1970, 1737-1740.
75. B.E. Bryant, W.C. Fernelius, Inorg. Synthesis, 1946, 2, 17 and 25.
76. B.E. Bryant, W.C. Fernelius, Inorg. Synthesis, 1957, 5, 130 and 188.
77. F.P. Dwyer, A.M. Sargeson, J. Amer. Chem. Soc., 1953, 75, 984-985.
78. M. Tanaka, T. Shono, K, Shinra, Bull. Chem. Soc. Japan, 1969, 42, 3190-3194.
79. P.G. Frith, K.A. McLauchlan, Nuclear Mag. Res., 1974, 3, 378-405.
80. S. Koda, S. Ooi, H. Kuroya, K. Isobe, Y. Nakamura, S. Kawaguchi, J. Chem. Soc.Chem. Comm., 1971, 1321-1322.
81. R.E. Cramer, S.W. Cramer, K.F. Cramer, M.A. Chudyk, Inorg. Chem., 1977, 16, 219-223.
82. G.S. Vigee, C.L. Watkins, Inorg. Chem., 1977, 16, 709-711.
83. K. Kuroda, K. Yoshitani, K. Kunigita, K. Kamiiba, K. Watanabe, Bull. Chem. Soc. Japan, 1976, 49, 2445-2450.

84. G.N. Salaita, L.A. Al-Odeh, J. Inorg. Nucl. Chem., 1973, 35, 2116-2118.

85. H.C. Brown, Y. Okamoto, J. Amer. Chem. Soc., 1958, 80, 4979-4987.

86. O. Exner, Collection Czechoslov. Chem. Comm., 1966, 31, 65-89.

87. G.L. Closs, Adv. Magnetic Reson., 1974, 7, 157-229.

88. A.R. Lepley, G.L. Closs, "Chemically Induced Magnetic Polarization", 1973, Wiley-Interscience, N.Y.

89. R. Kaptein, J. Amer. Chem. Soc., 1972, 94, 6251-6262, 6262-6269.

90. P.G. Frith, K.A. McLauchlan, Nucl. Magnetic Reson., 1974, 3, 378-405.

91. C.F. Poranski, S.A. Sojka, W.B. Moniz, J. Amer. Chem. Soc., 1976, 98, 1337-1341.

92. J.C. Morrow, E.B. Parker, Acta Cryst.(B), 1973, 29, 1145-1146.

93. R.B. von Dreele, R.C. Fray, J.Amer. Chem. Soc., 1971, 93, 4936-4937.

94. V. Amirthalingam, V.M. Padmanabham, J. Shankar, Acta Cryst., 1960, 13, 201-204.

95. K. Dymock, G.J. Palenik, Acta Cryst.(B), 1974, 30, 1364-1366.

96. R.W. Kluiber, J. Amer. Chem. Soc., 1960, 82, 4839-4842.

97. Q. Fernando, Adv. Inorg. Radiochem., 1965, 7, 185-261.

98. R.O.C. Norman, R. Taylor, 'Reaction Mechanisms in Organic Chemistry', monograph 3, 'Electrophilic Substitution in Benzenoid Compounds', ch. 5, 1965, Elsevier - London.

99. D.J. Hewkin, R.H. Prince, Coordn. Chem. Revs., 1970, 5, 45-73.

100. K. Kustin, J. Swinehart, Prog. Inorg. Chem., 1970, 13, 107-158.

101. R.G. Wilkins, 'The Study of Kinetics and Mechanism of Reactions of Transition Metal Complexes', 1974, Allyn and Bacon, Inc., Boston.

102. A. Fratiello, Prog. Inorg. Chem., 1972, 17, 57-92.

103. I.O. Sutherland, Ann. Rep. NMR Spectroscopy, 1971, 4, 71-235.

104. A.J. Brown, O.W. Howarth, P. Moore, W.J.E. Parr, J. Chem. Soc. Chem. Comm., 1977, 586 - 587.

105. F.A. Cotton, R. Francis, J. Amer. Chem. Soc., 1960, 82, 2986-2991.

106. G.S. Vigee, P. Ng, J. Inorg. Nucl. Chem., 1971, 33, 2477-2489.

107. D.M.W. Buck, P. Moore, J. Chem. Soc.Dalton, 1973, 1602-1604.

108. D.M.W. Buck, P. Moore, J. Chem. Soc. Chem. Comm., 1974, 60-61.

109. J. Selbin, W.E. Bull, L.H. Holmes, J. Inorg. Nucl. Chem., 1961, 16, 219-224.

110. G.R. Cayley, D.W. Margerum, J. Chem. Soc. Chem. Comm., 1974, 1002-1004.

111. D.B. Rorabacher, Inorg. Chem., 1966, 5, 1891-1899.

112. T.S. Turan, Inorg. Chem., 1974, 13, 1584-1590.

113. R.B. Jordan, Inorg. Chem., 1976, 15, 748-750.

114. C.H. Langford, J.P.K. Tong, Acc. Chem. Res., 1977, 10, 258-264.

115. J.F. Coetzee, D.M. Gilles, Inorg. Chem., 1976, 15, 405-408.

116. J.F. Coetzee, C.G. Karakatsanis, Inorg. Chem., 1976, 15, 3112-3114.

117. W.L. Reynolds, Prog. Inorg. Chem., 1970, 12, 1-99.

118. K. Kustin, R.F. Pasternack, E.M. Weinstock, J. Amer. Chem. Soc., 1966, 88, 4610-4615.

119. S. Harada, Y. Okuue, H. Kan, T. Yasunaga, Bull. Chem. Soc. Japan, 1974, 47, 769-770.

120. H. Tomiyasu, G. Gordon, Inorg. Chem., 1976, 15, 870-874.

121. Y. Ukei, M. Tanaka, Inorg. Chem., 1976, 15, 964-967.

122. R.H. Voss, R.B. Jordan, J. Amer. Chem. Soc., 1976, 98, 2173-2177.

123. M.J. Carter, J.K. Beattie, Inorg. Chem., 1970, 9, 1233-1238.

124. H. Ogino, N. Tanaka, Chem. Letters, 1975, 687-689.

125. S.Y.J. Ng, C.S. Garner, Inorg. Chim. Acta, 1971, 5, 365-371.

126. R.J. Watts, J.S. Harrington, J. van Houten, J. Amer. Chem. Soc., 1977, 99, 2179-2184.

127. W.R. McWhinnie, J.D. Miller, Adv. Inorg. Chem. Radiochem., 1969, 12, 135-215.

128. J.W. Akitt, Ann. Rep. NMR Spectroscopy, 1972, 5A, 465-555.

129. J.D. Munro, P.L. Pauson, J. Chem. Soc., 1961, 3475-3479, 3479-3483, 3484-3486.

130. G.R. John, L.A.P. Kane-Maguire, J. Organometal. Chem., 1976, 120, C45-C48.

131. D.A. Sweigart, M. Gower, L.A.P. Kane-Maguire, J. Organometal. Chem., 1976, 108, C15-C17.

132. D.A. Sweigart, L.A.P. Kane-Maguire, J. Chem. Soc. Chem. Comm., 1976, 13-14.

133. A. Salzer, Inorg. Chim. Acta, 1976, 18, L31-32.

134. P. Hackett, G. Jaouen, Inorg. Chim. Acta, 1975, 12, L19-20.

135. D.A. Sweigart, C.N. Wilker, J. Chem. Soc. Chem. Comm., 1977, 304-305.

136. R.J. Angelici, Acc. Chem. Res., 1972, 5, 335-341.

137. G. Schiavon, C. Paradisi, C. Boanini, Inorg. Chim. Acta, 1975, 14, L5-L6; L.A.P. Kane-Maguire, personal communication.

138. K.M. Al-Kathumi, L.A.P. Kane-Maguire, J. Chem. Soc. Dalton, 1973, 1683-1685.

139. R.B. King, M.B. Bisnette, Inorg. Chem., 1964, 3, 785-790; R.B. King, A. Fronzaglia, Inorg. Chem., 1966, 5, 1837-1846.

140. L.J. Russell, P. Powell, private communication.

141. J.W. Cooper, 1974, 'T1PRGM The Automated Measurement of Spin-Lattice Relaxation Times'. Published by the Nicolet Instrument Corporation.

142. M.L. Maddox, S.L. Stafford, H.D. Kaesz, Adv. Organometallic Chem., 1965, 3, 99 and 151.

143. J.E. Mahler, R. Pettit, J. Amer. Chem. Soc., 1963, 85, 3955-3959, 3959-3963.

144. D.A. Brown, S.K. Chawla, W.K. Glass, Inorg. Chim. Acta, 1976, 19, L31-32.

145. J.J. Delpuech, M.R. Khaddar, A.A. Peguy, P.R. Rubini, J. Chem. Soc. Chem. Comm., 1974, 145-155.

146. J.J. Delpuech, M.R. Khaddar, A.A. Peguy, P.R. Rubini, J. Amer. Chem. Soc., 1975, 97, 3373-3379.

129. J.D. Munro, P.L. Pauson, J. Chem. Soc., 1961, 3475-3479, 3479-3483, 3484-3486.

130. G.R. John, L.A.P. Kane-Maguire, J. Organometal. Chem., 1976, 120, C45-C48.

131. D.A. Sweigart, M. Gower, L.A.P. Kane-Maguire, J. Organometal. Chem., 1976, 108, C15-C17.

132. D.A. Sweigart, L.A.P. Kane-Maguire, J. Chem. Soc. Chem. Comm., 1976, 13-14.

133. A. Salzer, Inorg. Chim. Acta, 1976, 18, L31-32.

134. P. Hackett, G. Jaouen, Inorg. Chim. Acta, 1975, 12, L19-20.

135. D.A. Sweigart, C.N. Wilker, J. Chem. Soc. Chem. Comm., 1977, 304-305.

136. R.J. Angelici, Acc. Chem. Res., 1972, 5, 335-341.

137. G. Schiavon, C. Paradisi, C. Boanini, Inorg. Chim. Acta, 1975, 14, L5-L6; L.A.P. Kane-Maguire, personal communication.

138. K.M. Al-Kathumi, L.A.P. Kane-Maguire, J. Chem. Soc. Dalton, 1973, 1683-1685.

139. R.B. King, M.B. Bisnette, Inorg. Chem., 1964, 3, 785-790; R.B. King, A. Fronzaglia, Inorg. Chem., 1966, 5, 1837-1846.

140. L.J. Russell, P. Powell, private communication.

141. J.W. Cooper, 1974, 'T1PRGM The Automated Measurement of Spin-Lattice Relaxation Times'. Published by the Nicolet Instrument Corporation.

142. M.L. Maddox, S.L. Stafford, H.D. Kaesz, Adv. Organometallic Chem., 1965, 3, 99 and 151.

143. J.E. Mahler, R. Pettit, J. Amer. Chem. Soc., 1963, 85, 3955-3959, 3959-3963.

144. D.A. Brown, S.K. Chawla, W.K. Glass, Inorg. Chim. Acta, 1976, 19, L31-32.

145. J.J. Delpuech, M.R. Khaddar, A.A. Peguy, P.R. Rubini, J. Chem. Soc. Chem. Comm., 1974, 145-155.

146. J.J. Delpuech, M.R. Khaddar, A.A. Peguy, P.R. Rubini, J. Amer. Chem. Soc., 1975, 97, 3373-3379.